# Tailored ligands for hybrid materials from colloidal inks

Dissertation
zur Erlangung des Grades
des Doktors der Naturwissenschaften
der Naturwissenschaftlich-Technischen Fakultät
der Universität des Saarlandes

von

Beate Reiser

Angefertigt am
INM – Leibniz–Institut für Neue Materialien

Saarbrücken
01/2018

| | |
|---|---|
| Tag des Kolloquiums: | 09.05.2018 |
| Dekan: | Prof. Dr. Guido Kickelbick |
| Berichterstatter: | Prof. Dr. Tobias Kraus |
| | Prof. Dr. Gerhard Wenz |
| Vorsitz: | Prof. Dr. Christopher Kay |
| Akad. Mitarbeiter: | Dr. Bernd Morgenstern |

# *Danksagung*

Zuerst möchte ich Prof. Eduard Arzt dafür danken, dass er mir die Möglichkeit geboten hat meine Doktorarbeit an diesem renommierten Institut anzufertigen und dass er mich dabei fortlaufend unterstützt hat, unter anderem in der Rolle meines Doktorvaters zu Beginn meiner Arbeit.

Anschließend übernahm Prof. Tobias Kraus, der von Anfang an mein wissenschaftlicher Betreuer am INM war, die Rolle meines Doktorvaters. Ihm möchte ich an dieser Stelle einen besonderen Dank aussprechen, denn er hatte stets Vertrauen in mich und meine Arbeit, nahm sich immer Zeit für wissenschaftliche Diskussionen, unterstützte mich wann immer ich Hilfe brauchte und darum bat, ermöglichte mir einen Forschungsaufenthalt in an der *University of Melbourne*, sowie zahlreiche Dienstreisen zu spannenden wissenschaftlichen Konferenzen und Messen und bewies große Ausdauer darin meine wissenschaftlichen Schreibstil, oftmals in vielen Iterationen, zu verbessern, wofür ich zutiefst dankbar bin.

Auch Prof. Gerhard Wenz möchte ich an dieser Stelle für die wertvollen wissenschaftlichen Diskussionen während meiner experimentellen Arbeit, die er in seiner Funktion als wissenschaftlicher Begleiter verfolgt hat und für die Übernahme der Rolle als Zweitgutachter dieser Arbeit danken.

Professor Paul Mulvaney und seiner Forschungsgruppe an der *University of Melbourne* bin ich ebenfalls zu tiefem Dank verpflichtet, denn sie ermöglichten mir nicht nur den 2-monatigen Aufenthalt in ihrer Gruppe, sondern nahmen mich dort mit großer Gastfreundlichkeit auf. Dadurch konnte ich in der Zeit nicht nur unschätzbar wertvolle Erkenntnisse über Kolloide, *Quantum Dots* und Solarzellen gewinnen, sondern hatte auch eine unvergesslich schöne Zeit.

Diese Doktorarbeit war Teil eines größeren, im "NanoMatFutur" Programm des Bundesministeriums für Bildung und Forschung (BMBF) geförderten Projekts: „NanoSPEKT". Daher möchte ich hier auch meinen Dank an das BMBF für die großzügige Förderung zum Ausdruck bringen.

An dieser Stelle möchte ich auch dem gesamten Projektteam um deren Leiterin Dr. Lola Gonzalez-Garcia, die mich dankenswerterweise auch wissenschaftlich unterstützt hat, für die großartige und erfolgreiche Zusammenarbeit danken.

Zusammenarbeit war auch der Schlüssel zum experimentellen Erfolg dieser interdisziplinären Arbeit. Im Folgenden möchte ich ein paar Personen nennen, die durch ihre Unterstützung einen wichtigen Beitrag zu meiner Arbeit geleistet haben: Anika Kleeman, Lars-Arne Meyer, Nicole Schiff und Kathrin Alt haben gute Arbeit bei der Herstellung des Gold-*precursors* (Tetrachlorogoldsäure) für all meine Synthesen geleistet; Corinna Saar, Nadine Poitiers, Andrea Pyttlik und Anna Heib (meine HIWI-Helfer) haben mich tatkräftig bei der routinemäßigen Synthese und Charakterisierungen von Nanopartikeln unterstützt. Größenteils wurden diese zwar für andere kleine Projekte, die nicht Teil dieser Arbeit waren, verwendet, ihre Arbeit war dadurch aber nicht weniger wichtig für mich, denn sie erlaubte mir mehr Zeit in die Themen dieser Arbeit zu investieren. Nicht nur bei Synthesearbeiten, sondern auch bei der Charakterisierung der hergestellten Nanoobjekte hatte ich das große Glück auf ein großartiges „Helferteam" zurückgreifen zu können. Einige wichtige und „häufig frequentierte" Helfer möchte ich auch hier namentlich nennen: Lola Gonzalez-Garcia, Thomas Kister (TEM); Lola Gonzalez-Garcia, Johannes Maurer, Daniel Brodoceanu (SEM); Dominik Gerstner, Johannes Maurer (SAXS); Ioannis Kanelidis (Raman Spektroskopie); Lola Gonzalez-Garcia (Leitfähigkeitsmessungen); und Robert Drumm (TGA). Euch und all den Anderen die mir während der Zeit am INM mit Rat und Tat zur Seite gestanden haben nochmal größten Dank. Dazu gehören natürlich auch die Mitarbeiter der Analytik Servicegruppen, die Verwaltung und die Werkstatt.

Auch bei der schriftlichen Ausarbeitung der Arbeit hatte ich einige Helfer. Tobias Kraus, Michael Reiser und Lola Gonzalez-Garcia gaben mir wichtiges *feedback* zum strukturellen und logischen Aufbau der Arbeit; Kevin Lossner überprüfte die Arbeit auf sprachliche Korrektheit. Vielen Dank dafür, ohne eure Hilfe wäre es vermutlich schwer nachzuvollziehen, was ich in der Arbeit eigentlich zum Ausdruck bringen will.

Ein gutes Arbeitsklima trägt bekanntlich auch zur Produktivität bei, daher auch vielen Dank an die gesamte „Strukturbildungsgruppe" für die schöne Zeit im und außerhalb des Labors. Ich hoffe der Zusammenhalt, die gute Stimmung und die gegenseitige Hilfsbereitschaft in der Gruppe bleibt euch noch lange so erhalten wie ich es während der letzten 4 Jahre erleben durfte.

Ein großer Dank gilt natürlich auch meine Familie, die mich während der Entstehung dieser Arbeit immer unterstützt hat. Mein Mann und selbsternanntes *„support team"* ist natürlich besonders hervorzuheben. Vielen Dank für deine unglaubliche Unterstützung, dein großes Verständnis für lange Labortage und teils arbeitsreiche Wochenenden, den tollen Arbeitsausgleich in der freien Zeit „und Alles" ;)

"Chemistry and nanotechnology are now forever united through nanochemistry. And despite the successes in advanced materials and biomedical technologies society has witnessed, it feels like we are only just getting started."

**(Geoffrey A. Ozin)**

---

in "Nanochemistry on my mind",
**CHEMICAL & ENGINEERING NEWS (2016)**

# Table of Contents

Table of Contents

# Statement on contribution

The ideas for the publications were largely developed in collaboration between the author and her supervisor Tobias Kraus and the project leader Lola González-García. Studies previously conducted and developed by Dominik Gerstner in collaboration with Tobias Kraus were included into two of the manuscripts that constitute this thesis (Publication 2 & 3). These manuscripts are justified within themselves without the studies developed by Dominik Gerstner, however, the inclusion of these studies improved the scholarly value. Experiments for this thesis were planned and executed solely by the author, unless stated otherwise. The following clarifies the individual contributions in detail.

Nanoparticle syntheses and surface chemistry modifications were executed by the author. Exceptions are some of the nanowires used for Small Angle X-ray Scattering (SAXS) studies (Publication 2), that were synthesized by Ioannis Kanelidis and Johannes Maurer and the spherical oleylamine-capped gold nanoparticles used as a negative-example for fiber-spinning (Publication 3), that were synthesized by Thomas Kister.

All analyses were planned, prepared, and performed by the author with the following exceptions: SAXS measurements were conducted by Dominik Gerstner and Johannes Maurer (Publication 2 & 3). The ICP-MS analysis of sulfur was planned in collaboration with Claudia Fink-Straube and executed by Yulia Silina (Publication 1). TGA measurements were conducted by Robert Drumm (Publication 1). Raman spectroscopy measurements were performed by Ioannis Kanelidis (Publication 1). Conductivity measurements were implemented by Lola González-García (Publication 1). Electron microscopy images (SEM, TEM) were taken by Lola González-García and Thomas Kister (Publication 1, 2 & 3), AFM images were taken by Arzu Colak (Publication 3). FIB-cuts were performed by Oscar Torrents-Abad (Publication 3). Surface tension and viscosity measurements were supported by Thomas Kister and Thiago Martins-Amaral (Publication 1). Andrea Pyttlik helped with optical microscopy images to determine AuNW fiber thicknesses (Publication 3).

All collected raw data, except for the SAXS data (Publication 2 & 3), was analyzed and interpreted and the Figures were composed and drawn by the author. SAXS data was analyzed and interpreted by Dominik Gerstner, who also drew the graphs presenting the analyzed data. The final Figures used in the manuscripts were composed by the author.

The presented manuscripts and the dissertation were conceived and written by the author using only the cited sources. All manuscripts presented in this dissertation were previously published in peer-reviewed journals and are reproduced in section 3 of this thesis.

# Zusammenfassung

Anorganische Nanoobjekte mit organischen Ligandenhüllen bilden eine interessante Klasse nanoskalig strukturierter Materialien, wenn sie zu größeren Einheiten zusammengesetzt werden - die Hybridmaterialien. Das Fehlen einfacher Produktionsprozesse verhindert bislang deren industrielle Nutzung. Ein vielversprechender Ansatz für einen einfachen Produktionsprozess von Hybridmaterialien ist deren Herstellung aus kolloidalen Tinten. Hierzu muss allerdings die Kontrolle über die gezielte Nanoobjektanordnung während des Verarbeitungsprozesses verbessert werden. Die Ligandenhüllen spielen dabei eine entscheidende Rolle, da sie die Anordnungseigenschaften der Nanoobjekte stark beeinflussen.

Um die kolloidale und supramolekulare Chemie der Ligandenhülle besser zu verstehen wurden ligandenstabilisierte, stäbchenförmige Nanoobjekte synthetisiert, modifiziert und deren Anordnungsverhalten in Verbindung mit dem Dispergiermittel aufgeklärt. Auf der Basis dieser Erkenntnisse wurden erfolgreich zwei unterschiedliche Hybridmaterialien aus Tinten hergestellt. Zum einen wurden Gold-Nanostäbe mit einer leitfähigen Polymer-Ligandhülle beschichtet, die gleichzeitig gute kolloidale Stabilität der Nanostäbe in Tinten und elektrische Leitfähigkeit der Hybridstrukturen direkt nach dem Trocknen der Tinte ermöglicht. Zum anderen wurde das Zusammenspiel der Ligandenhüllen ultradünner Goldnanodrähte mit dem Dispergiermedium ausgenutzt, um die Drähte zu hierarchischen Hybridfasern zu spinnen.

# Abstract

Inorganic nano-objects with organic shells form an interesting class of nanostructured materials when they are assembled into larger units - hybrid materials. The industrial use of materials produced via this bottom-up route is impeded by the lack of simple production processes. A promising process is their production from colloidal inks; however, the targeted control of the nano-objects' superstructure formation must be improved. Here interfaces and the organic shells are crucial, as they strongly affect the assembly characteristics of the hybrid nano-objects.

Here, the colloidal and supramolecular chemistry of the ligand shell is studied. Ligand-stabilized wire-like and rod-like nano-objects were synthesized, modified, and their assembly behavior in conjunction with the dispersant medium was elucidated. After that, two different hybrid materials were produced using an ink-based approach. First, gold nanorods were coated with a conjugated polymer ligand shell that enabled both good colloidal stability and electrical conductivity of the hybrid structures directly after drying of the ink without sintering. Second, ultrathin gold nanowires were spun into hierarchical fibers, exploiting the interaction of their ligand shells with the surrounding dispersant medium.

# 1 Motivation

Inorganic nano-objects, with their unique properties are interesting building blocks. Nowadays nano-objects are already applied in end-user products. For instance, spherical $TiO_2$ and $SiO_2$ nano-objects are used in paint, sunscreen, and even in food applications.[1] Future market-relevant applications of nano-objects are seen in their functional assemblies.[2] Therefore, robust and efficient bulk methods to assemble "nano-monomers" are required.[3] There are various challenges to be overcome before materials from nano-objects can be produced on an industrial scale. Scalability and reproducibility issues during the synthesis of nano-objects,[4] and more importantly, the lack of simple methods for their assembly with a high degree of structural control currently do not allow the cost-efficient production of nano-object superstructures.[5]

The structure of the assembled nano-objects can influence the properties of the material obtained. Hence, it is interesting to control the positions of the nano-objects within a material.[6] Established methods that allow the precise positioning of nano-objects typically manipulate the position of single nano-monomers sequentially.[7,8] These methods enable precise structural control, yet they are very time-consuming and usually require complicated, expensive equipment. Bulk methods which allow for the simultaneous, structurally controlled assembly of nano-objects with simple equipment are required for industrial scale material production.[5,9]

Solvent-based processes that exploit colloidal self-assembly are suitable approaches because they require only basic equipment and manipulate all dispersed nano-objects at once.[10,11] Therefore, nano-objects are processed from inks which are solvent-based formulations containing dispersible nano-objects. Inkjet printing is a well-known ink-based processing technique to deposit nano-object derived superstructures. This relatively straightforward approach is considered a very attractive and promising route towards market-relevant products, for instance in the field of printed electronics.[12] It can be used to produce radio frequency identification (RFID) antennas and printed circuits on packaging material.[13] Another less straightforward idea may be to profit from decades of experience in the solution processing of polymers, for instance fiber-spinning,[14] and aim for polymer analogue processing of colloidal inks.

For both processing methods, colloidal interactions need to be carefully controlled, because they determine ink stability and the assembly behavior of the nano-objects contained. Ligand-stabilized nano-objects are a good option for optimizing this behavior, because the ligand shell which forms the interface between the nano-object and the solvent can be adapted to tailor colloidal interactions independently of the nano-object core. Thus, almost any colloidal properties can be given to a selected core material by utilizing valuable know-how from organic and supramolecular chemistry.

Unfortunately, the current understanding of how especially non-polar ligand shells and their interactions with their surrounding medium can control assembly is rather limited. To identify an appropriate ligand which allows stabilization of a particular nano-object during processing and, on the other hand, allows for the controlled destabilization of the suspension to form the final nanomaterials, the respective experiment has to be performed with the ligand of choice. The thereby gained understanding of the structural control over the assembly of nano-objects from inks is necessary to enable rational design of functional hybrid materials.[15,16]

Consequently, an important aim of this thesis is to study solvent-interactions with the ligand shell to enable rational design of colloidal interactions. The interaction of ligand shells with the solvent will be investigated in particular, because these interactions are important for the stability of the colloidal inks. This is, for instance, very important for printing applications, because premature destabilization of the inks might clog the printing nozzle. The insights achieved will be exploited to produce two material embodiments which demonstrate material fabrication by processing colloidal inks.

One case elected for implementation as part of this thesis is the use of nano-metal inks for inkjet printing of conductive structures. There are already stable, printable nano-metal inks on the market. However, typically nano-objects in state-of-the-art inks carry bulky organic ligands which impede electron transport between the conductive metal cores. Thus a sintering step is required to remove the insulating ligand shells from the printed metal-organic hybrid structures to obtain the required percolating network of electrical conductor. This thesis aims to overcome this drawback of commercial inks by a clever design of the ligand shell. Tailoring the ligand shell such that, on one hand, the metal cores are colloidally stabilized in the ink and, on the other hand, the printed hybrid structures are already conductive without requiring removal of the ligand shell by sintering would simplify the

production of conductive structures and broaden the range of substrates to include materials which cannot withstand harsh sintering conditions. Therefore, a stable, water-based inkjet-compatible ink which can form sinter-free conductive structures should be produced as an example for simple material fabrication by processing a colloidal ink.

In the second case, the feasibility of transferring the technology of commercial polymer fiber spinning to ligand-stabilized nano-objects should be demonstrated. In principle, this should be achievable by injecting a stabilized dispersion of hybrid nano-objects of suitable shape into a poorly dispersing solvent. Here the advantage of the hybrid concept is the similarity to supramolecular self-assembly approaches. Organic ligands tethered to a nano-object may behave very similarly to self-assembled molecules which interact with the solvent.[17] Thus hybrid nano-objects may be understood in terms of supramolecular chemistry concepts and may form similar superstructures which can be tuned by appropriate solvent choice. This thesis should indicate whether this assumption is applicable. The feasibility to produce macroscopic hybrid materials with controlled structure from colloidal inks using a polymer analogous fiber spinning process should be demonstrated in a second step.

For both applications, gold nano-objects were chosen as model systems because of their chemical inertness and the availability of a multitude of synthesis protocols for gold nano-objects. For the conductive hybrid inks, gold nanorods synthesized via a standard wet-chemical synthesis protocol were selected. They are widely used for sensing applications, since their optical properties change in response to slight changes in their direct vicinity.[18] This property allows easy progress monitoring of, for instance, ligand exchange reactions by simple optical analytical techniques, such as UV-vis spectroscopy. Wet chemically synthesized ultrathin gold nanowires were the nano-objects of choice for solution spinning of fibers due to their polymers-like shape and their ease of synthesis using a simple, scalable wet-chemical protocol.[19]

# 2 State of the art

## 2.1 Hybrid materials

Hybrid materials are combinations of often complementary components. Unlike in composites, these components are mixed at a smaller scale in hybrid materials. According to stricter definitions, mixing occurs on the nanoscale or the molecular level.[20] By mixing two different components, such as a soft organic component with a more rigid inorganic one, new and interesting properties can emerge that are not achievable otherwise.[21] Small-scale mixing contributes to the homogeneity of the resulting material and enables fine-tuning of its properties.[22]

Even though researchers only recently started to study the field intensively and understand how these hybrid materials are built up on the nanoscale, hybrid materials have long been used because of beneficial processability or properties compared to single-component materials.[20] For instance, painters in the 19$^{th}$ century used mastic resin combined with inorganic pigments in oil paints to get beneficial rheological properties.[23] Inorganic polymer composites and hybrids also benefit from the versatile, simple polymer processing technology, which makes them easy to manufacture,[22] while the inorganic part lends them properties that are otherwise not achievable using only organic material.[1]

The structure into which the mixed components are assembled can contribute strongly to the material properties.[6] Hence tailor-made advanced hybrid materials require not only the right combination of components but also a controlled, tailored structure.[24] For instance, nature produces plenty of anisotropically structured, directional hybrid materials. Human bones are a typical example. This sophisticatedly structured collagen-hydroxyapatite hybrid material does not need the same fracture toughness in every direction. Thus, the structure is optimized to provide superior fracture toughness only in the directions needed.[25]

This kind of directionality cannot be found in randomly mixed hybrid materials, which are, on the other hand, easier to produce. This current trade-off between processing effort and functionality of hybrid materials exists because efficient structuring methods are currently lacking. According to Sanchez *et al.*[24], a holistic approach in which processing goes hand in hand with the chemistry of the components is required to be able to produce hybrid materials with tailored structure and functionality.

There are many ways to produce hybrid materials, which are described in detail elsewhere.[22] The so-called “building block approach” is the one chosen in this thesis for the fabrication of nano-object-based hybrid materials from colloidal inks, which is considered a particularly promising and simple method.[10] Since inorganic colloids are typically covered with a molecular layer of organic molecules, their assembly naturally leads to hybrid materials. Further on, colloids can be processed from solution, which is in line with the demand for simple, inexpensive processing techniques.[26] Therefore the following will focus on the fabrication of hybrid materials via this route, starting with a brief description of the chosen building blocks for the hybrid material fabrication: colloidal nano-objects.

## 2.2 Hybrid material building blocks: colloidal nano-objects

In nanoscience, the terminology used to describe the building blocks is not entirely clear and consistent in the literature. Therefore, the terminology used in this thesis will be described below. In accordance with the ISO/TS 8004-2 standard from 2015,[27] the size range of 1 to 100 nm is called the nanoscale. This particular size scale lies between typical length scales of single atoms and bulk materials and causes many of the interesting properties known for nanoparticles.[28] For a nanoparticle, all three dimensions must lie within the nanoscale, whereas the term nano-object is defined more broadly and relies only on one dimension of the nano-object being on the nanoscale. Hence, it includes nanospheres with three, nanorods- and wires with two, and nanoplates with one nanoscale dimension.[27] In addition, the widely used term “colloid” will be used when referring to a nano-object in dispersion, although the term is also sometimes used to describe to the dispersion itself.[29]

Nano-objects are attractive building blocks due to the unique properties of both the “nano-monomers” and their functional assemblies. The unique nano-object properties are caused by:

i. their large surface to volume ratio compared to bulk materials,
ii. the fact that at the nanoscale quantum confinement occurs, or
iii. their small sizes themselves.[30]

In detail, this means that

i. surface-related properties become predominant, especially in the case of nanoparticles with diameters below 10 nm. For example, approx. 50% of the atoms that constitute a 4 nm nanoparticle are at the surface.[31] This is beneficial, for instance, for their catalytic properties in relation with the material used. Furthermore, the contribution of the surface energy of a crystalline structure to the free energy of the system becomes increasingly dominant, which may lead to stabilization of different crystal structures on the nanoscale than in bulk.[32] These undercoordinated atoms, however, also give rise to a strong intrinsic tendency to minimize the surface/bulk atom ratio. Therefore ligands, which can passivate surface atoms, play a crucial role in stabilizing dispersions.

ii. The fact that the electrons of the nanoscale core material are confined lets us see the colorful effects of their surface plasmon resonances (SPR) in metals like gold and silver,[33] and size-dependent photoluminescence in quantum dots.[34] Those effects are interesting for many applications in (bio)sensing[35] or light-emitting diodes (LEDs).[36] Further on, the sensitive dependence of SPR- and photoluminescence signals towards the chemical environment of the nano-object[37–39] allows conclusions to be drawn on the nature of the ligand shell, which stabilizes the nano-object in dispersion, as well as on distances between nano-objects[40] and their orientation relative to each other.[41] Such insights are hard to gain otherwise.

iii. The reason for that is also the third unique nano-object characteristic mentioned above: their small size. Single objects are too small to be visible to the unaided eye. Technical imaging methods like electron microscopy or atomic force microscopy are required to make them visible. This poses several challenges, especially to analyzing the effect of a thin organic shell which surrounds the nano-object – the ligand shell, which is even harder to see – on their assembly. First of all, it is necessary to have a good idea of how the ligand shell looks, and secondly it is necessary to study colloidal behavior in dispersion. To date, the first aspect requires a combination of complementary analytical methods to get a good impression of what the ligand shell really looks like.[42,43] Monitoring their colloidal behavior in dispersion, on the other hand, often relies on indirect methods, which exploit the dependence of their interaction with electromagnetic radiation on their size, shape, chemical composition and the nature of their immediate vicinity.[44]

However, the small size of nano-objects also has advantages: even high-density materials such as metals can be dispersed in a solvent without immediate sedimentation. This fact makes

them workable from solution, meaning that simple printing- or polymer-processing principles can be applied for their assembly and deposition. Metal nano-objects, such as the ones used in this thesis, are, for instance, considered promising candidates for future printed circuitry.[45] Due to their small size, they might even be used for miniaturized devices and optically transparent materials.[30]

By building up functional materials from single nano-objects, the scale gets closer to components and features of materials used in our everyday life. This similarity of scale simplifies the incorporation of nanomaterials within existing technologies. It is thus a promising route towards the achievement of new applications for nano-objects,[26] which is where the greatest potential for future applications of nano-objects is seen.[2] In the particular case of inorganic nano-objects with organic shells, their assemblies form the desired hybrid materials. Mixing of both material types – organic and inorganic – at a very small scale is guaranteed. The dimensions of both components can be exquisitely controlled by the dimensions of the inorganic nano-object and its ligand shell respectively.

## 2.3 Solution processing of colloidal inks

In general, inks are defined as “a pigmented liquid or paste used especially for writing or printing”.[46] During colloidal self-assembly and in the context of this thesis, inks are understood as liquid formulations containing the dispersed precursors for the material to be produced via deposition of the ink. The “pigment” or precursor will be the metal nano-objects with ligand shells, which will be described in more detail in Section 2.5. It may further contain additives such as stabilizers or modifiers to adjust the fluid properties for a certain printing- or deposition technique.[47]

Both the bottom-up synthesis of nano-objects from atomically dispersed precursors and nanofabrication by self-assembly or process-driven assembly are examples of additive manufacturing steps, as depicted in Figure 2.3.1. Therefore the hybrid material fabrication via the controlled assembly of wet chemically synthesized colloidal nano-objects can theoretically be achieved without the generation of any waste.[48]

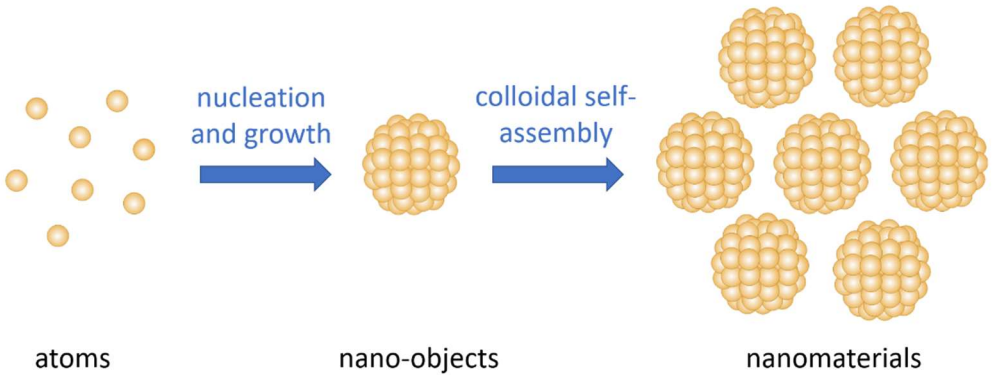


**Figure 2.3.1** Scheme of the bottom-up nano-object synthesis and the assembly of singe nano-objects into nanomaterials process of nanomterials. Ligands are neglected for the sake of clarity.

### 2.3.1 Gaining structural control through processing

As mentioned above, the ability to tailor the structure into which the hybrid material building blocks assemble is highly desirable because the structure can help to optimize material performance.[6] Classical techniques for structuring materials often use costly vacuum processes or complicated equipment. For instance, methods to precisely direct the position of building blocks may use atomic force microscopy (AFM) manipulation[7] and AFM nanoxerography.[8] However, these methods manipulate the nano-objects sequentially and are therefore very time-consuming. A less time-consuming method which has been applied is the use of pre-patterned templates to direct assembly.[49,50] Here colloidal inks were applied to fill the cavities of a template selectively with the nano-objects. It would, however, be desirable to obtain structural control without the need for templates.

The simple processing of inks usually requires only cheap, simple equipment, and high throughput processing is possible.[51–53] When using electrically conductive nano-object cores it is therefore a very promising technique for simple production methods of flexible electronic devices in the future.[54,55] Furthermore, complex printed structures can be achieved via inkjet printing, which allows a high degree of personalization because masks or templates are not required.[56] For good printing performance the inks need to be colloidally stable during printing.[45] This can be guaranteed by carefully controlling colloidal interactions.[57]

While inkjet printing yields structure by selective placement of the ink, the careful control over colloidal interactions can also lead to structural control on the single nano-object level, namely by colloidal self-assembly. Inspired by the high degree of control that supramolecular chemists gain over nanoscale assemblies by tuning non-covalent intermolecular

interactions,[58,59] an approach that selectively sets colloidal interaction forces might also be a very promising route towards simple bulk production of tailored hybrid materials.[60] To achieve assembly and disassembly of nano-objects and tune assembly in a purposeful way, all relevant interactions must be considered. Therefore the most important colloidal interactions will be described in Section 2.4.

In this context it would be desirable to tailor the processing parameters to optimize the structural control over the building blocks gained by colloidal self-assembly. As predicted by Sanchez *et al*.,[24] a holistic approach in which colloidal interactions and processing parameters contribute to the structural control will "open a land of opportunities to tailor-made advanced inorganic and hybrid materials".[24] To facilitate technical implementation, the production process would ideally be integratable with current processing technology.[26] In principal this should be possible for the fabrication of nanomaterials by colloidal self-assembly since printing techniques already use colloidal dispersions[61], and there are several liquid-based polymer processing techniques available that are optimized for material structuring and could be adapted. It would be highly interesting to demonstrate the applicability of such processing techniques to colloidal inks.

### 2.3.2 Advantages of anisotropic building blocks

Percolation and mechanical interdigitation are of particular interest in this thesis, since it focuses on electrically conductive and mechanically strong hybrid materials. In both cases, anisotropic cylindrical nano-objects are beneficial. Even if the typically stronger bound and electrically more conductive inorganic component is only randomly dispersed in an organic matrix, enhanced mechanical strength[62,63] and a lowered percolation threshold[64] can be obtained by increasing the aspect ratio of the inorganic component in the material. A lowered percolation threshold means that greater electrical conductivities can be achieved at lower volume fractions of the conducting material.[65] For example, solution-processed materials which use nanowires can provide improved directionality of electron transport while reducing the number of colloid-colloid interfaces for a certain conductive path compared to the respective material with spherical nano-objects.[4]

Little is known about the mechanical properties of materials obtained by colloidal self-assembly. These properties, however, are important for many industrially relevant applications.[26,66] Learning from hybrid materials or composite materials obtained by other

processing methods, cylindrical colloids should be beneficial for mechanically strong materials, because regardless of the nature of the organic-inorganic interface, the contact area is increased. If loads can be distributed efficiently along this enhanced contact area, the strength in fiber direction can be significantly increased. This effect is exploited in fiber-reinforced composites. Many of them are based on carbon nanotubes (CNTs) that reinforce elastic materials by the distribution of load along the CNTs.[62,63] Conceptually, many natural materials are also fiber-reinforced composites but with a much more sophisticated structure.[67] An optimized process achieves hierarchical assembly of anisotropic building blocks to delocalize strain and increase the fracture toughness in materials like bones.[25]

Directionality or structural optimization can also be introduced to man-made materials. Hucker *et al.*[68], for instance, invented and patented a hybrid fabric material which shows a structure of spaced electrically conductive fibers extending in one direction and electrically insulating fibers extending in another. The inventors propose their material for use in modern aircraft. The lightweight material should replace the traditional electric cabling used, for instance, for signal transduction. Tailored connectivity of anisotropic building blocks can, for instance, help to reduce the amount of electrically conductive or mechanically strengthening material to a minimum because it is only placed where needed. Serendipitously in case of anisotropic colloids, simply applicable external influences like electrostatic fields[69] or laminar flow fields[70] can trigger alignment in certain directions. This effect can be exploited to create tailored connectivity. Thereby the aspect ratio and degree of alignment of the nano-object are variables that allow tuning the materials properties.[4]

The effect of this kind of external forces, however, will be mostly reversible, which means that the nano-objects will resume a random orientation upon elimination of the external force. Hence to allow the stabilization of the structural order induced by electrostatic fields or shear flow it would be necessary to fix the processing-induced orientation somehow. This could, for instance, be achieved by inducing controlled agglomeration of the building blocks, hence by controlling colloidal self-assembly.

## 2.4 How to stabilize colloidal inks and control colloidal self-assembly

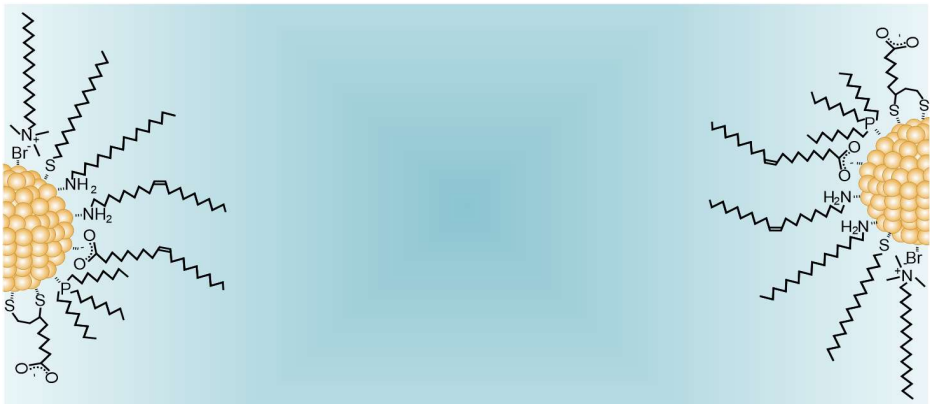

**Figure 2.4.1** Schematic representation of two adjacent a 1.6 nm (diameter) gold nanoparticles in dispersion. The skeletal formula of different ligands is drawn surrounding the nanoparticle core, indicating the ligand layer.

Stability is crucial for the processability of colloidal inks. Inkjet printers have a tiny nozzle which can easily be clogged by agglomerates and/or nano-object assemblies. Other ink-processing equipment also uses tubing to transport the ink and can be blocked by agglomerates or assemblies formed in prematurely destabilizing inks as well. This can severely damage processing equipment. On the other hand, if assembly is desired during the process, it should be known how to destabilize the ink in a controlled way to trigger nano-object assembly into tailored structures during processing. When aiming for selective control over nano-object assembly to form hybrid materials, it is necessary to start with a stable dispersion which can be destabilized in a controlled manner. In other words: one needs to control colloidal interactions.[60] Hence a comprehensive understanding of the forces acting on dispersed nano-objects like the ones shown in Figure 2.4.1 is required.

Various intermolecular interaction forces are acting on colloids and their length scales and magnitudes determine whether these may become a driving force for assembly or disassembly of nano-objects in dispersion.[3] The balance of all forces acting on colloidal nano-objects determines their behavior in dispersion.[71] If in sum the attractive forces dominate, assembly of the nano-objects will take place, whereas if the repulsive forces dominate, a stable dispersion is obtained. In stable colloidal dispersions of inorganic nano-objects, the core is typically surrounded by a stabilizing ligand layer, which will be described in detail in Section 2.5 (see also Figure 2.4.1). This layer is important because if during their Brownian motion in the dispersant bare nano-objects would get close enough to experience the purely

attractive interaction between their cores, they would agglomerate and eventually aggregate.[f1]

The following subsections will describe the most relevant interaction forces in further detail, namely van der Waals (v.d.W.), electrostatic, steric, and depletion interactions. There are core-core, core-ligand, and ligand-ligand interactions to be considered and which one of them dominates depends on various factors.

### 2.4.1 DLVO forces

#### *Van der Waals forces*

Van der Waals forces describe interactions between atoms, molecules and nano-objects but of bulk materials too as a consequence of electromagnetic fluctuations caused by the constant movement of positive and negative charges within these objects or because of permanent dipole moments.[3,72] Depending on the type of interaction, they can be further subdivided into Keesom,[73] Debye,[73] or London dispersion[74] interactions. They describe interactions between two permanent dipoles, an induced dipole with a permanent one or two induced dipoles respectively.

Generally, all kinds of v.d.W. forces are relatively short-ranged. They are always attractive in case of interaction between specimen of the same material.[75] For instance, core-core interaction forces between dispersed nano-objects of the same material are always attractive. The magnitude of the attractive force ($F$) between them depends on the geometry of the interacting objects. Using a geometrical factor ($G_f$) v.d.W. forces can be described by

$$F = -G_f \frac{A}{6}\frac{1}{a^2} \qquad \text{(eq. 2.4.1.1)}$$

where $a$ denotes the distance between the interacting objects and $A$ the Hamaker constant.[76] Detailed formulas for relevant geometries of nano-objects can be found elsewhere.[77,78]

The magnitude of the interaction force further depends on the nature of the interacting material and can be estimated using listed values of $A$ (for interaction in vacuum).[79] Although

[f1] Definitions of agglomeration and aggregation vary strongly in the pertinent literature.[166–168] In the context of this thesis, agglomeration will be defined as a firm, random assembly of nano-objects still surrounded by their ligand shells and which can be separated again upon sufficient energy input, for instance by sonication. Aggregation describes agglomerated nano-objects which are not fully covered by their ligand-shells and start to fuse with other nano-objects in the positions not covered by ligands due to Ostwald ripening. Thus aggregated nano-objects cannot be separated and re-dispersed.

*A* is dependent on the dispersing medium,[77] the value in vacuum serves as a convenient estimate. For metals, values are around one order of magnitude higher than that of $CH_2$ units often present in ligands, which have typical values on the order of $A \approx 5 \times 10^{-20}$ J.[3,77] This means that at equal distance, v.d.W. interactions between metal cores of nano-objects would be around one order of magnitude stronger than those between their organic ligand shells. However, the ligand shells naturally approach closer, because they are on the outside of the colloid. The spacing of the nano-object cores is set by the steric demand of the ligand shell. When the ligand shells are bulky and thus cause a large core-core distance when their shells touch, it may well be that v.d.W. interactions between neighboring ligand shells surpass those of the metallic cores. The organic ligand shells can get much closer, and the interaction force strongly decreases with increasing distance.[3] For instance, Murphy and coworkers[80] have ascribed the dominant role during assembly of gold nanocrystals capped by CTAB to the v.d.W. interactions between their interdigitating ligand shells.

### *Electrostatic forces*

Electrostatic interaction forces are caused by charged species attached either directly to the surface of the nano-object core or to the ligand chain and are attractive in the case of oppositely charged species but repulsive for species that are identically charged. Electrostatic forces are usually longer in range than v.d.W. forces. However, their range depends on the ionic strength of the dispersing medium. Colloids with permanently charged ligands can be stable over long periods. This is known from gold nanoparticles prepared with citrate ligands according to a synthesis reported by Turkevich *et al*.[81] and later refined by Frens.[82] To assure long-term stability of such electrostatically stabilized nano-objects, a few criteria have to be met. First, the ionic strength of the dispersing medium needs to be low, and second the pH needs to be within a certain range to ensure that the stabilizing charged groups do not get neutralized by protonation/deprotonation. While the pH sets the effective charge of the colloidal object, the ionic strength of the dispersing medium determines how long range electrostatic interactions are. In media of high ionic strength, the charge of an ion or a nano-object capped by charged ligands can be effectively screened by the electric double layer which builds up around the charge at a shorter distance, leading to a shorter Debye screening length.[2,76] Xu *et al.*[26] demonstrated that the Debye screening length can also be used to tune the distance between electrostatically stabilized nanoparticles within their assembly. Thus,

they demonstrate how selective control of this interparticle force can lead to control over the self-assembled material.

#### *The combination of van der Waals and electrostatic forces*

Both electrostatic and v.d.W. interactions are combined in the Derjaguin Landau Verwey Overbeek (DLVO) theory to explain colloidal interaction.[83,84] It has been successfully used for decades for predicting the behavior and stability of many colloidal systems and is thus a very important theory for all colloidal sciences.[76,85,86] This underlines the importance of these two kinds of interaction forces. Nevertheless, there are limitations to its applicability, which are partly due to interaction forces that are not taken into account, often called non-DLVO interactions,[76,87] and partly due to assumptions made in the theory, which are not always valid.[15]

### 2.4.2 Non-DLVO forces

Non-DLVO interactions include repulsive steric interactions occurring between bulky ligand shells,[3] entropically driven depletion forces,[3,88] chemical bonds between ligand shells[3] and all kinds of external forces.[76] **Steric interactions** e.g. between bound thiolated polyethylene glycol (PEG-SH) chains can also help to stabilize nano-objects in high ionic strength aqueous media,[2,89] but they can also stabilize colloids in solvents with low dielectric constants. Stabilization occurs because long ligand chains minimize entropy when they are compressed by the ligand chains of approaching nano-objects. Thus the entropy loss counteracts the increasing v.d.W. attraction between cores of the nano-object and can stabilize it in dispersion, when the forces are well-balanced.[3,89]

Compression of bound ligand layers can also become favorable when the entropy of the system is increased thereby. This happens when the entropic gain due to the increased volume accessible to the solute molecules surpasses the entropic losses due to ligand compression. A high concentration of solute molecule can lead to this situation, which causes an attractive interaction between the nano-objects. This attractive interaction is called **depletion interaction**.[90] It was, for instance, exploited by Badaire *et al.*[3,91] to direct the assembly of cylindrical nano-objects into an end-to-end superstructure.

### 2.4.3 Limitations of colloidal stability theories

Apart from forces not considered in DLVO theory and other colloidal stability theories,[92] the predictions of DLVO theory can differ considerably from the experimental results. This can be explained by the assumptions on which it is based. These assumptions include:

a) the shape of the colloid is simple, i.e. does not present any surface roughness;
b) all the interaction potentials considered are strictly additive;
c) both the colloid and its dispersing medium are continuous; and
d) solvent and other solute molecules are negligibly small compared to the colloid.[15]

While in the case of micrometer sized colloids these assumptions often lead to sufficiently accurate results, they are a source of incorrect estimates in the case of nanoparticles and other nano-objects which are only a few nanometers in size. Such small nanocrystals are typically faceted, and the ligands that are bound to the colloids, as well as the solvents, are in the same size range as the colloids themselves and can thus not be neglected.[15]

Newer theoretical considerations are working to overcome these limitations.[92–94] In particular, interactions between adjacent ligand layers[95] and ligand-solvent interactions[94,96] have shown a strong effect on colloidal stability and on nanoparticle growth as well. To understand that, it is important to understand better the packing of the ligand layer. This includes its packing density directly at the organic-inorganic interface[97] and whether the ligand chains pointing towards the dispersing medium are evenly spread or if ligand "bundling" occurs. Molecular dynamics (MD) simulations are capable of predicting such conformational details of the ligand layers[98] but it is still challenging and time-consuming to take interactions with solvent molecules into account. Furthermore, it would be beneficial to have an analytic technique that can give such detailed information on the ligand shell in solution to compare simulations with experimental results. Unfortunately, there is no simple technique to yield comprehensive information.[42] In particular, unusually shaped nano-objects, which could lead to interesting materials by self-assembly[99] and are therefore of particular interest, have hardly been studied to date. The following section will provide a closer look at the ligand shell for an impression of the difficulty in getting a complete picture of the colloid and its surrounding ligand shell. It also will provide an impression of how the ligand shell can influence the balance of interaction forces described above. Thus it will give insight into the ligand shell's capacity to actively control colloidal self-assembly.[94]

## 2.5 Ligand layer influence on colloidal stabilization and controlled destabilization

Colloidal stabilization is typically guaranteed by functional chemical groups attached to the surface of a nano-object. This can either simply consist of covalently bound charged surface groups – consider protonated or deprotonated hydroxy groups found on silica particles – or of ions or molecules adsorbed to the core. In this case the adsorbed species carries the stabilizing chemical functionality. To produce inorganic-organic hybrid materials by assembling colloids, organic molecules adsorbed to inorganic nano-objects are ideally suited. The organic shell which they create and which stabilizes nano-objects in dispersion can form the organic matrix surrounding the nano-objects after solvent removal. Hence a hybrid material is obtained upon solvent removal.

Thus the following will only focus on ligand layers made from organic molecules, which will be called “ligands”. Such ligands should contain at least one functional group that binds to the surface atoms of a nano-object core. Anchored to the core, the remaining part of the molecule can ensure electrostatic and/or steric stabilization by charged or sterically demanding groups.[100] Scheme 2.5.1 depicts the skeletal formula of typically used small organic molecules.

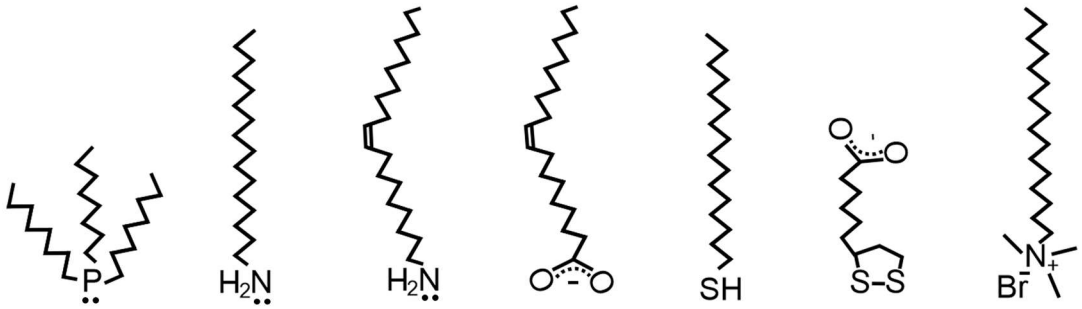


**Scheme 2.5.1** Skeletal formulas of commonly used ligands in the synthesis and stabilization of nano-objects.

In the simplest case, one kind of ligand adsorbs to all accessible binding sites of the nano-object, thereby forming the ligand layer. This layer comprises the interface between the core and the dispersing medium and is therefore very important for the formation of a stable, colloidal dispersion in a particular solvent.

Note that polymers are also suitable ligands. They can either be grafted to the nano-object, which means that they bind to the core with one anchoring group and exploit the steric

demand of the whole polymer chain for steric stabilization, or bind with multiple of their repeating units. The latter option binds the polymer closely to the core and consequentially reduces the degrees of freedom of the polymer chain and its potential for spacial extension away from the core. Hence, steric stabilization becomes less efficient, while the core ligand-binding strength is increased. Both aspects are important for the stability of colloidal dispersions, and will be further discussed in the sections to follow.

### 2.5.1 Nano-object-ligand bond

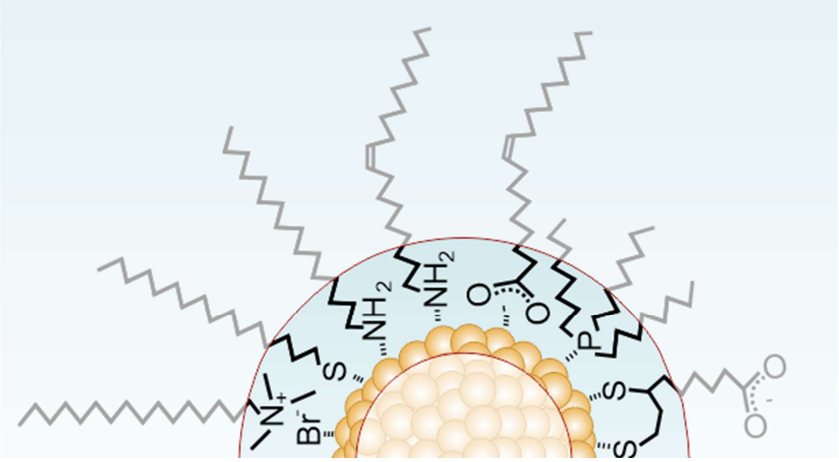


**Figure 2.5.1.1** Ligands binding to a gold nanoparticle with different anchoring groups. From left to right: Au-Br bond between gold and CTAB, Au-S bond between gold and hexadecanethiol, Au-S bond between gold and hexadecylamine, Au-N bond between gold and oleylamine, Au-$COO^-$ bond between gold and oleic acid, Au-P bond between gold and trioctylphosphine, and bivalent Au-S bond between gold and liponic acid.

The term “ligand” originates from the field of coordination chemistry. It describes molecules, atoms or ions which bind to a metal in solution. Similarly, in the field of colloidal chemistry it describes molecules, atoms or ions of organic molecules which bind to the surface atoms of a nano-object. Ligands are often bound to the nano-objects’ core via dative bonds in which a functional organic group with a lone pair of electrons overlaps with empty *d*-orbitals of the surface atoms of the nano-object (Figure 2.5.1.1).[42] Owen[101] proposed to classify ligands which form dative bonds further, either as X- or as L-type ligands. X-type bonds are formed by electrically neutral species such as amines (e.g. OAm), whereas L-type bonds are formed by ionic species (e.g. the bromide ions of cetyltrimethylammonium-bromide (CTAB)).[102] The most common ligands for metal nano-objects are either X- or L-type ligands, where the ligands act as Lewis bases and the nano-object as Lewis acids. Accordingly, Figure 2.5.1.1 shows only

these two kinds of ligands. A third type of ligand, the Z-type, acts as Lewis acid and plays a minor role for metal nano-objects.[101]

Pearson's hard soft acid base (HSAB) concept[103] is useful to estimate the strength of ligand-nano-object bonds. Nath *et al.*[104], for instance, tested the applicability of the principle by comparing the binding strength of very "soft" alkanethiol ligands and "harder" alkylamine ligands to very "soft" gold nanoparticles and "harder" silver nanoparticles and found that the alkanelthiols have a much higher affinity to gold cores than the alkylamines while both ligand types have similar affinities to the silver cores. In good agreement with the HSAB concept, their results suggest that gold nanoparticles are "softer" than silver nanoparticles.

Concepts established in coordination chemistry also explain the surface chemistry of nano-objects and allows us to understand the binding situation, which has major implications on nano-object stability. Nonetheless, nano-objects do differ in some ways from central ions capped by a ligand shell in coordination chemistry: for instance, certain crystal facets of a nano-object can be "harder" or "softer" as a result of the electronic distribution within the crystalline lattice.[42] Siddiqui[105] chose an empirical approach to study the binding strength of certain ligands to gold nanoclusters: he synthesized the same kind of nanoparticles with different ligands and did ligand replacement studies to obtain the following relative binding strengths:

"$SC_{12}H_{25} \gg H_2NC_{12}H_{25} > S(C_{12}H_{25})_2 > S(C_{10}H_{21})_2 > H_2NC_6H_{13} \gg [N(C_8H_{17})_4]Br \gg S(C_6H_{13})_2$",[105]

which he attributes to a combination of the strength of the dative bond with steric and inductive effects caused by the non-binding ligand part. Such studies are very time-consuming, but the information they yield is very valuable regarding the respective binding strengths of different ligands.

Weaker coordinating ligands may require excess free ligand in the colloidal dispersion to sufficiently cover the surface of the nano-object. This is, for instance, the case for CTAB capped gold nanorods (AuNR@CTAB).[106,107] Adding excess free CTAB, which can adsorb to free binding sites of the AuNR, ensures that the ligand layer stays dense enough to avoid aggregation.[45]

Weakly bound ligands can also be useful, because they enable ligand exchange reactions. While L- and Z-type ligands with long hydrocarbon chains provide the required control over

nanoparticle nucleation and growth to obtain monodisperse nano-objects of the desired shape,[42] they are often not suitable for the application. As a consequence, the ligand attached to the nano-object due to the synthesis needs to be replaced.[4,11] Gold nanorods, for instance, are widely used for biosensing, but the cytotoxicity of CTAB (the ligand of choice for synthesis) requires a ligand exchange before using the nanorods with living cells.[108] Further examples where ligand exchange reactions are useful to improve the properties of nano-objects are the quantum yield of nano-objects used in LEDs and the electrical conductivity of assemblies of nano-objects.[30,109]

When planning a ligand exchange reaction, it is useful to know how the ligand to be replaced is bound. Generally, ligand exchange reactions are possible via a dissociative or an associative pathway. The dissociative pathway relies on dynamic ligand attachment and detachment of weakly coordinating ligands. Due to this equilibrium, new ligands can adsorb at vacant binding sites. If the ligand to be exchanged is firmly attached, an associative ligand exchange pathway is required. Since the attached ligand is replaced by an incoming new ligand, this needs to be carefully tailored to fit steric[42] and electrostatic[107] needs to allow a smooth exchange. This means that the binding strength is not the only criterion for a suitable ligand but that there are lateral effects as well. If a new ligand causes detachment of neighboring ligands due to electrical repulsion or its steric demand, it may happen that nano-objects are not sufficiently stabilized against undesired aggregation during ligand exchange because the ligand shell is not dense enough.[110] Even if, given the time to create a dense shell of the new ligand, this ligand could successfully stabilize the colloid, this point will never be reached because the aggregation is irreversible. This has been reported, for instance, for ligand exchange reactions on AuNR@CTAB.[107]

Besides the type of bond, the number of binding sites per ligand can strongly influence the stability of the ligand-nano-object cohesion. The principle of multivalency is known from coordination chemistry,[111] where chelate ligands like ethylenediaminetetraacetic acid (EDTA) can interact with a central atom via its 6 interconnected binding sites. The interconnection makes the bond stronger than the sum of the corresponding 6 single bonds. Multivalency is also used to describe a similar stability enhancement effect in supramolecular chemistry.[112]

Liponic acid (shown in Figure 2.5.1.1) and its derivatives are commonly used multivalent ligands which form metal nano-object-ligand bonds.[113] Other examples are PEG-SH molecules

with multiple thiol binding moieties[114,115] and polymeric ligands with many repeating units each bearing a binding functionality.[116] All these cases provide superior ligand-nano-object binding strength compared to the respective monovalent ligand. While strong ligand binding is important for colloidal stability, it is not the only aspect influencing colloidal stability. The structure of the ligand shell also influence colloidal stablity.[117]

### 2.5.2 Ligand shell structure

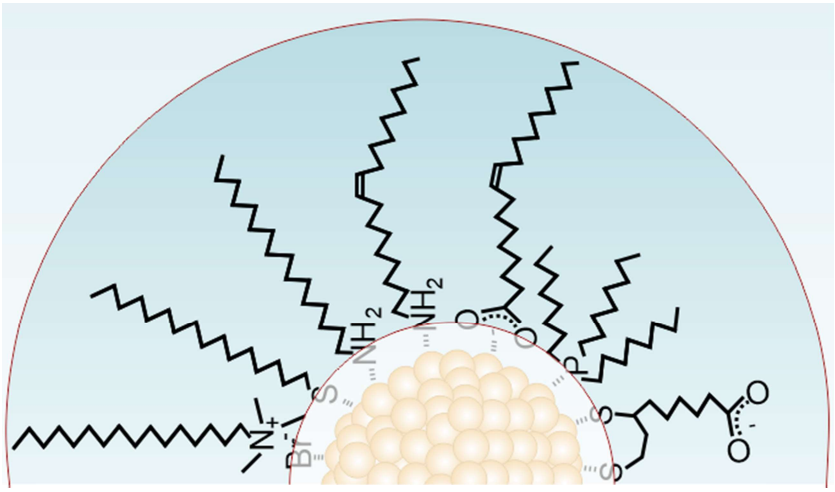

**Figure 2.5.2.1** Schematic representation of a ligand layer surrounding a small gold nanoparticle in dispersion. Ligands attached from left to right: CTAB, hexadecanethiol, hexadecyalamine, oleylamine, oleic acid, trioctylphosphine, and liponic acid.

The ligand shell forms the interface between the colloidal core and the dispersing medium. It determines, for instance, whether two adjacent nano-objects can coalesce or not and if and how fast certain small molecules like solvents or etchants can reach the core of the nano-objects. Therefore, the density of the part of the ligand shell highlighted in Figure 2.5.2.1. plays a decisive role. While a very dense ligand shell impedes etchants from reaching the core, a decreasing ligand shell density increases interaction with solvent molecules, which to a certain extent increases colloidal stability.[118] The ligand shell density is dependent on three main aspects, namely:

- the steric demand of the non-binding part of the ligand;
- the ligands surface grafting density ($\Gamma$); and
- the curvaure of the nano-object.

The first aspect is self-explanatory; the other two aspects and their influence on colloidal stabilization will be discussed below.

The ligand layer surrounding a nano-object often forms a self-assembled monolayer (SAM) of small molecules.[119,120] SAMs are well studied on flat surfaces, especially alkanethiols on Au (111) surface facets.[121] $\Gamma$ values known from these studies serve as a good first approximation for the $\Gamma$ values and the structure of the ligand shell of the respective ligands on nano-objects.

### *The influence of curvature*

Such approximations, however, become increasingly imprecise with decreasing nanoparticle diameter due to the nanoparticle curvature. Figure 2.5.2.2. shows how the curvature in two dimensions – corresponding to the curvature of a circle – increases with decreasing diameter. A 1.6 nm spherical nanoparticle with a coordination sphere of OAm, a ligand commonly used for nanoparticle synthesis,[122] which extends the diameter of the colloid to approximately 5.85 nm, is chosen as an example. The example is used to illustrate how the ligand layer of commonly used, non-bulky ligands naturally becomes sparse towards its outside. In this particular case the diameter of a hypothetical circle marking the footprint of the anchoring group (D) is 3.2 times smaller than the diameter of the hypothetical circle at the other end of the ligand (D'). The example shows the curvature only in one dimension, like it would be found on a nanorod or nanowire. In the case of a sphere, the effect would be enhanced by the same curvature in a second dimension.

This fact is one reason why AuNRs can grow preferentially along their tips.[123] The greater curvature at the AuNRs' hemispherical tips leads to a less dense CTAB layer. This lower ligand density facilitates the transport of gold atoms and ions to this position, and hence the nano-object can grow preferentially at this position.

The example shown in Figure 2.5.2.2 further illustrates that in case of a small nano-object core compared to the ligand layer thickness, there is plenty of space for gauche defects, intercalation of solvents, or other solutes into the coordination sphere, and for interdigitation of the ligand layers of adjacent nano-objects.[42,43]

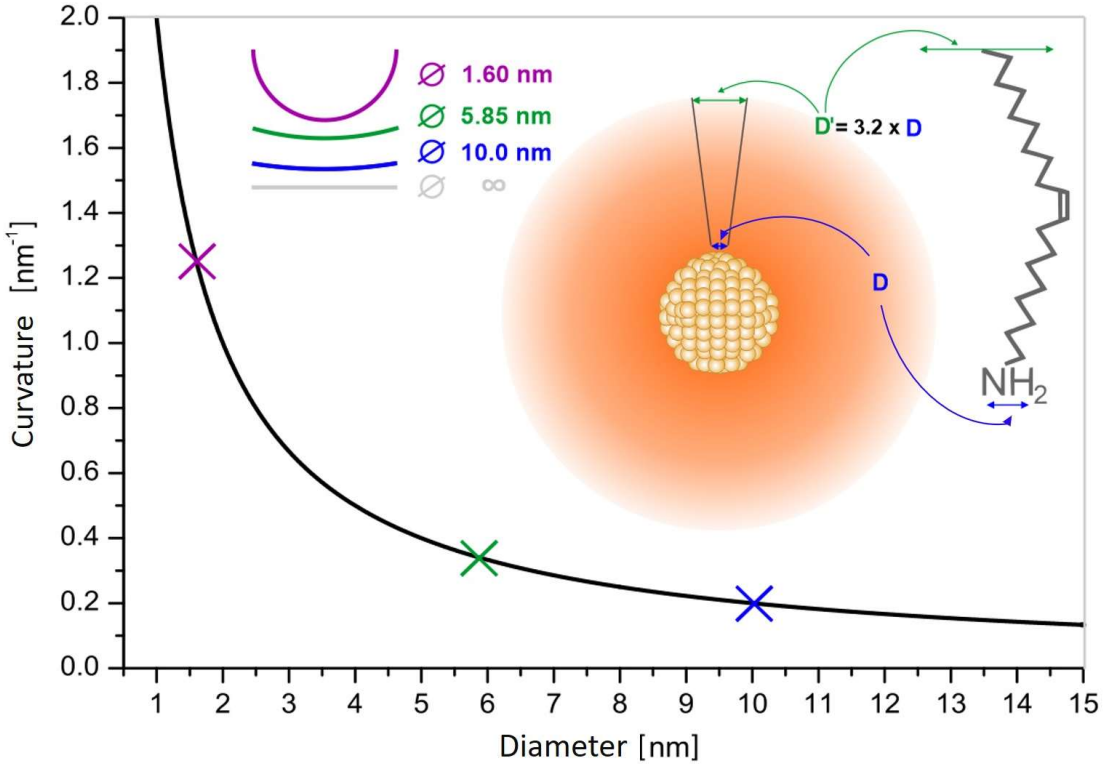


**Figure 2.5.2.2** Plot of the 2-dimensional (2D) nanoparticle curvature as a function of nanoparticle diameter. Insets: from left to right: schematic representation comparing the (2D) curvature of a 1.6 nm nanoparticle (purple) to a 5.85 nm nanoparticle (green), a 10 nm nanoparticle (blue) and a flat surface (grey); scheme of a 1.6 nm gold nanosphere, surrounded by a coordination sphere of oleylamine ligands (estimated diameter of the colloid including the ligand shell: 5.85 nm) illustrating the increased space available to the tail group of the ligand, compared to its headgroup.

This sparse outer part of the ligand layer is what differentiates ligand layers from SAMs on flat surfaces. It allows the intercalation of other molecules, but it can also induce a tighter packing of the molecular layer with increasing nano-object curvature. Leff *et al.*[124] reported that the ratio of sulfur atoms to gold surface atoms (S/Au) increased from 1/3 to 1/2 for long chain alkanethiol-capped gold nanoparticles with decreasing nanoparticle size. The 1/3 ratio is in good agreement with $\Gamma$ values for comparable alkanethiols on bulk Au (111) surfaces.[125] The same trend was seen for primary amine-capped gold nanoparticles, which generally form less dense ligand layers than alkanethiols.[126] Interestingly, the authors also observed an increase in stability of the Au-N bond in case of the formation of SAMs on strongly curved nanoparticles[126] compared to SAMs on flat Au substrates, on which they are only stable under certain conditions.[127] While the Au-S bond is thermodynamically stable on either curved or on flat surfaces, they found Au-N bonds to be kinetically stabilized. The energy barrier for destabilization was, however, high enough to render the nanoparticles stable in solvent over long periods, in contrast to the corresponding flat SAMs, which are only stable in vacuum.[126]

These results are counterintuitive because ligand crystallization is more likely in a plain SAM conformation, where weak v.d.W. bonds between $CH_2$ units can form and contribute to the stability of the SAM.[121] The authors attributed their findings to a finite size effect, which, however, does not explain the reason for this stability increase on a molecular level. Ligand assembly on a molecular level, in particular when taking its interaction with the dispersing medium into account, is still poorly understood.[42] Such knowledge would be highly desirable, because ligand layer interaction with the dispersing medium has proven useful to tune nano-object assembly behavior.[94]

### 2.5.3 Ligand-ligand and ligand-solvent interaction dependence on colloid geometry

As described in the previous section, ligand shell density influences interactions with the colloidal surroundings. Ligand shell interactions with solvent molecules or ligand shells of adjacent nano-objects, for instance, are important for colloidal dispersion- and assembly characteristics. Recent studies on small (i.e. highly curved nanoparticles) underline the influence of the solvent on colloidal behavior.[92–94] Since the ligand layer density is dependent on curvature, it is also dependent on the nano-object geometry, because this sets the curvature. Therefore, the colloidal assembly characteristics of nano-objects with non-spherical geometry are interesting.

The solvent influence on non-spherical nano-objects in particular has not yet been extensively studied. Chemically anisotropic modified AuNRs are a prominent example which has been investigated. Here the chemical anisotropy in the ligands shell is exploited rather than the shape itself.[128,129] The geometrical anisotropy, however, which enables the modification of AuNRs with a chemically anisotropic shell,[128] could also be used to guide the assembly of such anisotropic building blocks.

A simple comparison of the three basic shapes of colloidal nano-objects depicted in Figure 2.5.3.1 shows that their surface curvature is strongly dependent on the geometry: while spheres are curved in both dimensions, cylinders are only curved in one and platelets in no dimension.

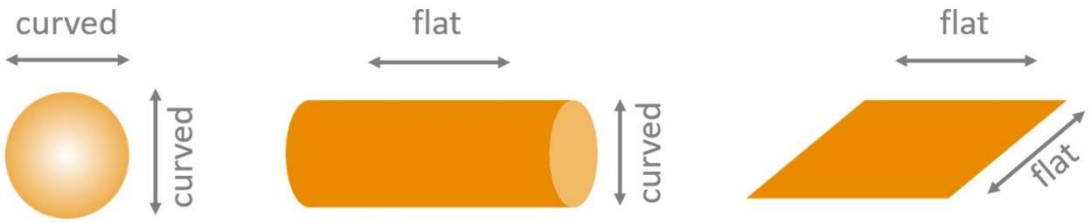


**Figure 2.5.3.1** Scheme comparing curvature of potential interaction sites of a sphere, a cylinder and a plate with another one of its kind.

It is apparent that only cylinders or wires combine curvature with enhanced contact area because their surface has a flat and a curved dimension.

While spheres allow a deeper ligand-ligand interdigitation in adjacent nano-objects, plates enable interactions of more ligands in the shell at the same time, because the contact area between two plates is much higher than that between two spheres. Cylinders or wires combine both effects: along their axial dimension they combine enhanced contact area with curvature. Thus these nano-objects can form line contacts with adjacent cylindrical nano-objects with moderately interpenetrating ligand layers, as depicted in Figure 2.5.3.2.

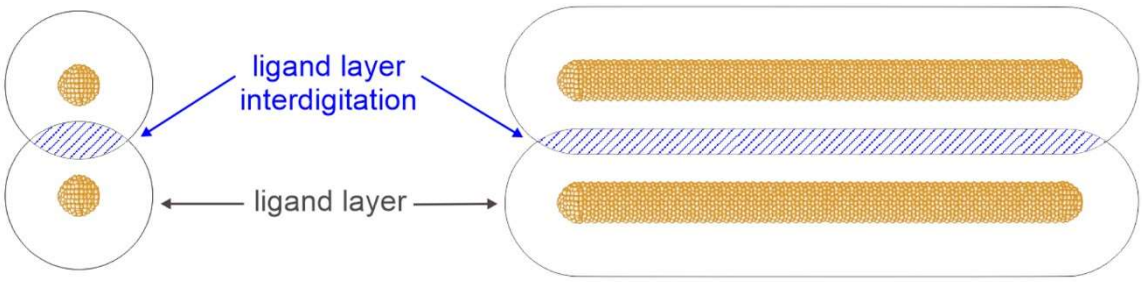


**Figure 2.5.3.2** Schematic comparison of the contact area generated by interpentration of ligand layers for two small gold nanospheres and two gold nano-cylinders.

Both effects, ligand interpenetration and enhanced ligand layer contact areas, can strengthen ligand-ligand interactions between the colloids. The more $CH_2$ units of a hydrocarbon tail can interact, the stronger the bond. Even though a single bond is weak (Binding energy: 0.07 eV per $CH_2$ unit, which is 30 times less than that of an Au-S bond),[121] the sum of all binding energies along the line of contact is large. This means that the bond between two wire-like colloids is stronger than one between two spherical colloids, and the longer the wire, the stronger the bond.

Not only the contact area for ligand-ligand interactions is influenced by the geometry of the nano-object, but the area accessible to solvent as well. Wu *et al.*[96] proposed that solvent

molecules interpenetrating into the ligand shell influence its structure and thus the colloidal behavior. The authors conducted their studies on small OAm-capped gold nanospheres.

On the basis of the above geometric considerations, it would be highly interesting to compare their results to that of a similar study on wire-like or other anisotropic colloids. Such studies might give further insight into the behavior of nano-objects in dispersion at the molecular level, which would be highly valuable for better understanding colloidal stabilization and self-assembly. To date, however, such studies are not available in literature.

Understanding how to direct assembly of such interesting building blocks by simple means, such as solvent exchange would be an important step towards rational design of materials from colloidal inks and describe a promising route towards the development of future functional hybrid materials.[130]

## 2.6 The three roles of the ligand shell for solution-processed hybrid materials

The production process to obtain hybrid materials from colloidal inks is very cost effective and can be implemented using simple coating or printing equipment.[10] It is crucial that the inks retain their colloidal stability during application. Furthermore, it would be interesting to be able to stimulate the colloids to assemble in a purposeful way. As described in Section 2.5, the organic ligands that surround the colloid play an important role in both nano-object stabilization and assembly, since they form the interface between the inorganic core and the dispersant. They also form the interface between two cores in the dry material, which is why the dry ligand shell properties also influence the properties of the hybrid material. Furthermore, ligands are also important before ink processing, namely during bottom-up synthesis of the colloid and in the performance of the hybrid material.[9]

In the following section, each point will be described separately in further detail, focusing on AuNRs and ultrathin gold nanowires (AuNWs):

### 2.6.1 Selective shape formation during nano-object synthesis

Nanomaterial synthesis is the first step of colloidal ink production. It determines shape and polydispersity of the colloidal objects in the ink. Metal nano-objects can be synthesized by wet chemical methods, which results in nano-objects that are already dispersed.

Typically, a dissolved molecular precursor is transformed into insoluble metal in the presence of ligands by heating or by chemical reduction.[131] A popular case is the seeded growth method. Here, nanocrystal nucleation and nanocrystal growth are performed as two separate steps.[132] Small seed nanocrystals are obtained quickly under harsh conditions, which are then added to a growth solution. The growth solution typically contains the molecular precursors under very mild reducing conditions. The separation of nucleation and growth suppresses uncontrolled nucleation in the growth solution and thus allows for improved control over nanoparticle size distributions and nano-object shapes.[132,133] Ligands can also help to control nano-object nucleation and trigger anisotropic growth.[134,135] Once attached to nano-objects, they can control growth kinetics as a function of ligand density, so that growth processes occur preferentially along certain crystal facets.[136] Sometimes the structure-directing effect of ligands – which are often also surfactants – is attributed to their self-assembly into micelles, which act as soft templates.[137] Fine-tuning of the micellar shape, and thereby the shape of the nano-object, is enabled by external stimuli like pH.[138]

The wet chemical synthesis of AuNRs by seeded growth uses CTAB as a structure-directing ligand.[139,140] This ligand, which is known to form a bilayer around the gold core, stabilizes the nanorods electrostatically in aqueous media.[141] Worm-like CTAB micelles are widely believed to steer their anisotropic growth,[137] and it is known that the pH during AuNW growth can influence the aspect ratio of the formed rods.[142] Other factors like the amount of surfactant, the addition of co-surfactant, impurities, silver ions and the shape of the seed particles also influence the reaction outcome, indicating a complex interplay between many components assisting anisotropic growth.[143] The exact mechanism for symmetry breaking and thus anisotropic growth is still under debate.[144]

Protocols for the wet chemical synthesis of AuNRs are known since 1999;[139] the first reports on ultrathin gold nanowires are from 2007.[145] Thus, their growth is less extensively studied, but it seems to crucially depend on OAm as ligand: wet chemical synthesis protocols for ultrathin gold nanowires in organic media[19,145–150] always use this molecule as a ligand,

sometimes in combination with oleic acid (OAc), which is structurally very similar. While Halder *et al.*[145] proposed a synthesis mechanism based on oriented attachment of preformed small gold nanoparticles with unequally dense OAm layers on different crystal facets, Lu *et al.*[149] attributed the morphological anisotropy of the nano-objects to chain-like AuCl-OAm complexes that form due to aurophilic interactions. Others[147,150] propose the formation of OAm micelles as soft templates which are responsible for the growth of AuNWs. All these studies, however, rely on slightly different AuNW synthesis conditions. Varying temperatures, reducing agents, ligand concentrations, solvent molecules and the addition of a co-surfactant in one case make the studies hard to compare. Hence it may well be that all the authors are right in their particular case and that different wire formation mechanisms lead to the same characteristic shape.[151]

The synthesis of ultrathin gold nanowires adapted from Feng *et al.,*[19] which uses triisopropylsilane to reduce the gold precursor dissolved in a *n*-hexane/OAm mixture at room temperature, has been investigated in more detail by Loubat and coworkers.[152] They studied the synthesis *in situ* by small angle X-ray scattering (SAXS) and dismissed oriented attachment as a possible growth mechanism for this synthesis protocol. Instead, they point out similarities to the seeded growth of AuNRs described above and propose a micellar growth.

Generally – it is often not entirely clear how but – it is evident that ligands play a crucial role during the wet chemical synthesis of nano-objects.[151]

### 2.6.2 Targeted stabilization or destabilization of colloids for controlled assembly

The surface modification strategy and the resulting surface chemistry establishes the colloidal stability in a given solvent[3,153] and is therefore important for the processing of colloidal inks and for the assembly of colloidal monomers into functional materials.[5] Colloidal stability must be assured throughout processing to prevent the clogging of printing nozzles or ink-carrier tubing and thus ensure good ink shelf life.[45,136] On the other hand, if the controlled formation of hybrid materials is desired, it is necessary to enable destabilization and assembly in a controlled way.[16]

Core-core interactions cannot be switched between attraction and repulsion; they can only be screened more or less efficiently by ligand shells. Hence the controlled assembly is dominated by the ligand's properties, which can be influenced by external stimuli.[16,154] Klajn *et al.*[155] demonstrated that conformational changes in the ligand shell allow for reversible

switching between assembly and disassembly of nanoparticles. They introduced a ligand with an azobenzene moiety, that carries a *trans* double bond when irradiated with visible light and a *cis* double bond when exposed to UV light. As the double bond switches configuration, the dipole moment of the azobenzene moiety changes. This change influences the interaction forces between the colloids that carry this moiety sufficiently to switch between colloidal assembly and disassembly. Thereby Klajn *et al.*[155] proved that slight changes in the ligand shell, caused by external influences, are a suitable tool to control the assembly of colloidal nano-objects.

Anisotropic or wire-like colloids provide another possibility to direct assembly based on their shape, as described in Section 2.5.3. While isotropic particles are limited to basic packing rules for their self-assembly, the intrinsic shape anisotropy[156,157] and the resulting chemical anisotropy in the ligand shell[158] can determine superstructures that are formed from them[159] and lead to other interesting assembly structures and geometries.

Ultrathin gold nanowires, which are of particular interest for this thesis, are prone to form hexagonal superstructures (bundles) in which their ligand shells can interact efficiently. The bundles are formed in the reaction mixture subsequently to their anisotropic growth (carrying OAm bilayers),[152] and after washing (carrying single OAm layers).[8] Loubat *et al.*[152] concluded from the SAXS data that these randomly oriented bundles have the morphology of elongated fibers with typical diameters of 70 nm. Their data interpretation also let them infer that only 40% of the wires in dispersion were embedded in such bundles, whereas 60% of the wires remained dispersed. Apparently, the energy differences between the self-assembled state – wires in bundles, in which adjacent ligand shells can undergo ligand-ligand interactions with their neighbor wires – and the dispersed state – in which the ligand shells of AuNWs can undergo ligand-solvent interactions – are small. Hence, AuNWs are a good starting point for controlled colloidal self-assembly.

While the self-assembly into fiber-like bundles is very interesting for the fabrication of hybrid fibers, their controlled fabrication will still require major improvements. Using *n*-hexane as a dispersing medium, it seems to be impossible to obtain a colloidally stable ink. Premature bundling might clog tubing or other parts of the processing equipment. Ideally, one would start with dispersed nanowire monomers and trigger bundling – with improved yield – in a controlled way, while being able to control the orientation of the bundles.

### 2.6.3 Hybrid material properties

Ligands form the organic part of metal-organic hybrid materials created by colloidal self-assembly, and they strongly influence its properties. Here

- the degree of ligand interdigitation upon solvent removal,
- the ligand-ligand interaction strength,
- and the strength of the ligand-nano-object bond

set the cohesive strength between the inorganic nano-objects, and the bulk or volume of the ligand shell sets the gap between them.[43]

Regardless for which application the hybrid materials are designed, their mechanical properties are important for their technical use.[26] Nanoparticle membranes serve as a convenient model system to discuss the cohesion of a nanomaterial as a function of the ligands. Membranes produced by the self-assembly of dodecanethiol-capped spherical gold nano-objects possessed a tensile strength of 11 MPa.[160] Stronger interactions between interdigitating ligands could possibly increase membrane cohesion. Andryszewski *et al.*[161] showed that strong, self-supporting membranes can be created by introducing covalent connections between adjacent nanoparticles.

Ligands do not only determine the mechanical properties of a hybrid material but its electrical properties as well in case of electrically conductive cores such as gold. Most ligands suitable for synthesis or colloidal stabilization are electrically insulating.[42,162] Hence they present insulating barriers between the conductive material, and small gaps between the conductor can prevent electron transport completely.[163] A common approach to improve electrical conductivity is post-deposition ligand removal. This additional step of sintering can drastically increase electrical conductivity but often adversely affects mechanical material properties and leads to cracks because of the volume shrinkage.[4,164] Long sintering times and harsh conditions are hard to reconcile with high throughput roll-to-roll processing.[165] Hybrid materials which retain the soft organic ligand layer surrounding the nano-objects offer the possibility of flexibility and simple processing.[20] Modern concepts focus on ligands which are easy to remove or on electrically conductive ligands to overcome these challenges in solution-processed electronics. Many of these concepts, however, compromise on colloidal stability and/or the ease of processing.

## 2.7 References


(1) Hanemann, T.; Szabó, D. V. Polymer-Nanoparticle Composites: From Synthesis to Modern Applications. *Materials (Basel).* **2010**, *3*, 3468–3517.

(2) Schiffrin, D. J. Nanoparticles and Self-Organisation: The Emergence of Hierarchical Properties from the Nanoparticle Soup (I.e., the Small Is Getting Bigger). Concluding Remarks for Faraday Discussion: Nanoparticle Synthesis and Assembly. *Faraday Discuss.* **2015**, *181*, 481–487.

(3) Bishop, K. J. M.; Wilmer, C. E.; Soh, S.; Grzybowski, B. A. Nanoscale Forces and Their Uses in Self-Assembly. *Small* **2009**, *5*, 1600–1630.

(4) Kim, J.-Y.; Kotov, N. A. Charge Transport Dilemma of Solution-Processed Nanomaterials. *Chem. Mater.* **2014**, *26*, 134–152.

(5) Antonietti, M.; Ozin, G. A. Promises and Problems of Mesoscale Materials Chemistry or Why Meso? *Chem. - A Eur. J.* **2004**, *10*, 28–41.

(6) Judeinstein, P.; Sanchez, C. Hybrid Organic–inorganic Materials: A Land of Multidisciplinarity. *J. Mater. Chem.* **1996**, *6*, 511–525.

(7) Kim, S.; Shafiei, F.; Ratchford, D.; Li, X. Controlled AFM Manipulation of Small Nanoparticles and Assembly of Hybrid Nanostructures. *Nanotechnology* **2011**, *22*, 115301.

(8) Moutet, P.; Lacroix, L.-M.; Robert, A.; Impéror-Clerc, M.; Viau, G.; Ressier, L. Directed Assembly of Single Colloidal Gold Nanowires by AFM Nanoxerography. *Langmuir* **2015**, *31*, 4106–4112.

(9) Talapin, D. V.; Lee, J.-S.; Kovalenko, M. V.; Shevchenko, E. V. Prospects of Colloidal Nanocrystals for Electronic and Optoelectronic Applications. *Chem. Rev.* **2010**, *110*, 389–458.

(10) Vogel, N.; Retsch, M.; Fustin, C.-A.; Del Campo, A.; Jonas, U. Advances in Colloidal Assembly: The Design of Structure and Hierarchy in Two and Three Dimensions. *Chem. Rev.* **2015**, *115*, 6265–6311.

(11) Boles, M. A.; Engel, M.; Talapin, D. V. Self-Assembly of Colloidal Nanocrystals: From Intricate Structures to Functional Materials. *Chem. Rev.* **2016**, *116*, 11220–11289.

(12) Søndergaard, R. R.; Hösel, M.; Krebs, F. C. Roll-to-Roll Fabrication of Large Area Functional Organic Materials. *J. Polym. Sci. Part B Polym. Phys.* **2013**, *51*, 16–34.

(13) Perelaer, J.; Smith, P. J.; Mager, D.; Soltman, D.; Volkman, S. K.; Subramanian, V.; Korvink, J. G.; Schubert, U. S. Printed Electronics: The Challenges Involved in Printing Devices, Interconnects, and Contacts Based on Inorganic Materials. *J. Mater. Chem.* **2010**, *20*, 8446.

(14) Smith, P.; Lemstra, P. J.; Pijpers, J. P. L. Tensile Strength of Highly Oriented

Polyethylene. II. Effect of Molecular Weight Distribution. *J. Polym. Sci. Polym. Phys. Ed.* **1982**, *20*, 2229–2241.

(15) Silvera Batista, C. A.; Larson, R. G.; Kotov, N. A. Nonadditivity of Nanoparticle Interactions. *Science (80-. ).* **2015**, *350*, 1242477–1242477.

(16) Min, Y.; Akbulut, M.; Kristiansen, K.; Golan, Y.; Israelachvili, J. The Role of Interparticle and External Forces in Nanoparticle Assembly. *Nat. Mater.* **2008**, *7*, 527–538.

(17) Maeda, H.; Terashima, Y. Solvent-Dependent Supramolecular Assemblies of π-Conjugated Anion-Responsive Acyclic Oligopyrroles. *Chem. Commun.* **2011**, *47*, 7620.

(18) Zhu, J.; Li, J.; Zhao, J. Effect of Dielectric Coating on the Sensing Capability of Gold Nanorods Based on Plasmonic Band Widening. *J. Nanoparticle Res.* **2012**, *14*, 864.

(19) Feng, H.; Yang, Y.; You, Y.; Li, G.; Guo, J.; Yu, T.; Shen, Z.; Wu, T.; Xing, B. Simple and Rapid Synthesis of Ultrathin Gold Nanowires, Their Self-Assembly and Application in Surface-Enhanced Raman Scattering. *Chem. Commun. (Camb).* **2009**, 1984–1986.

(20) Kickelbick, G. Hybrid Materials – Past, Present and Future. *Hybrid Mater.* **2014**, *1*, 39–51.

(21) Costi, R.; Saunders, A. E.; Banin, U. Colloidal Hybrid Nanostructures: A New Type of Functional Materials. *Angew. Chemie Int. Ed.* **2010**, *49*, 4878–4897.

(22) Kickelbick, G. Introduction to Hybrid Materials. In *Hybrid Materials: Strategies, Syntheses, Characterization and Applications*; Kickelbick, G., Ed.; Wiley-VCH: Weinheim, Germany, 2007; pp. 1–48.

(23) de Viguerie, L.; Jaber, M.; Pasco, H.; Lalevée, J.; Morlet-Savary, F.; Ducouret, G.; Rigaud, B.; Pouget, T.; Sanchez, C.; Walter, P. A 19th Century “Ideal” Oil Paint Medium: A Complex Hybrid Organic-Inorganic Gel. *Angew. Chemie Int. Ed.* **2017**, *56*, 1619–1623.

(24) Sanchez, C.; Boissiere, C.; Cassaignon, S.; Chaneac, C.; Durupthy, O.; Faustini, M.; Grosso, D.; Laberty-Robert, C.; Nicole, L.; Portehault, D.; *et al.* Molecular Engineering of Functional Inorganic and Hybrid Materials. *Chem. Mater.* **2014**, *26*, 221–238.

(25) Wegst, U. G. K.; Bai, H.; Saiz, E.; Tomsia, A. P.; Ritchie, R. O. Bioinspired Structural Materials. *Nat. Mater.* **2014**, *14*, 23–36.

(26) Xu, L.; Ma, W.; Wang, L.; Xu, C.; Kuang, H.; Kotov, N. A. Nanoparticle Assemblies: Dimensional Transformation of Nanomaterials and Scalability. *Chem. Soc. Rev.* **2013**, *42*, 3114.

(27) International Organization for Standardization. Technical Specification ISO/TS 80004-2, Nanotechnologies — Vocabulary — Part 2: Nano-Objects, 2015.

(28) Daniel, M.-C.; Astruc, D. Gold Nanoparticles: Assembly, Supramolecular Chemistry, Quantum-Size-Related Properties, and Applications toward Biology, Catalysis, and Nanotechnology. *Chem. Rev.* **2004**, *104*, 293–346.

(29) Encyclopaedia Britannica https://www.britannica.com/science/colloid (accessed Aug 7, 2017).

(30) Goesmann, H.; Feldmann, C. Nanoparticulate Functional Materials. *Angew. Chemie Int. Ed.* **2010**, *49*, 1362–1395.

(31) Grassian, V. H. When Size Really Matters: Size-Dependent Properties and Surface Chemistry of Metal and Metal Oxide Nanoparticles in Gas and Liquid Phase Environments ? *J. Phys. Chem. C* **2008**, *112*, 18303–18313.

(32) Reyes-Coronado, D.; Rodríguez-Gattorno, G.; Espinosa-Pesqueira, M. E.; Cab, C.; de Coss, R.; Oskam, G. Phase-Pure TiO 2 Nanoparticles: Anatase, Brookite and Rutile. *Nanotechnology* **2008**, *19*, 145605.

(33) Ozbay, E. Plasmonics: Merging Photonics and Electronics at Nanoscale Dimensions. *Science (80-. ).* **2006**, *311*, 189–193.

(34) Norris, D. J.; Bawendi, M. G. Measurement and Assignment of the Size-Dependent Optical Spectrum in CdSe Quantum Dots. *Phys. Rev. B* **1996**, *53*, 16338–16346.

(35) Howes, P. D.; Chandrawati, R.; Stevens, M. M. Colloidal Nanoparticles as Advanced Biological Sensors. *Science (80-. ).* **2014**, *346*, 1247390–1247390.

(36) Caruge, J. M.; Halpert, J. E.; Wood, V.; Bulović, V.; Bawendi, M. G. Colloidal Quantum-Dot Light-Emitting Diodes with Metal-Oxide Charge Transport Layers. *Nat. Photonics* **2008**, *2*, 247–250.

(37) Zvaigzne, M.; Martynov, I.; Samokhvalov, P.; Mochalov, K.; Chistyakov, A. Influence of Surface Ligands on the Luminescent Properties of Cadmium Selenide Quantum Dots in a Polymethylmethacrylate Matrix. *Phys. Procedia* **2015**, *73*, 150–155.

(38) Liu, I.-S.; Lo, H.-H.; Chien, C.-T.; Lin, Y.-Y.; Chen, C.-W.; Chen, Y.-F.; Su, W.-F.; Liou, S.-C. Enhancing Photoluminescence Quenching and Photoelectric Properties of CdSe Quantum Dots with Hole Accepting Ligands. *J. Mater. Chem.* **2008**, *18*, 675.

(39) Peng, S.; McMahon, J. M.; Schatz, G. C.; Gray, S. K.; Sun, Y. Reversing the Size-Dependence of Surface Plasmon Resonances. *Proc. Natl. Acad. Sci.* **2010**, *107*, 14530–14534.

(40) Kadkhodazadeh, S.; de Lasson, J. R.; Beleggia, M.; Kneipp, H.; Wagner, J. B.; Kneipp, K. Scaling of the Surface Plasmon Resonance in Gold and Silver Dimers Probed by EELS. *J. Phys. Chem. C* **2014**, *118*, 5478–5485.

(41) Sajanlal, P. R.; Sreeprasad, T. S.; Samal, A. K.; Pradeep, T. Anisotropic Nanomaterials: Structure, Growth, Assembly, and Functions. *Nano Rev.* **2011**, *2*, 5883–5945.

(42) Boles, M. A.; Ling, D.; Hyeon, T.; Talapin, D. V. The Surface Science of Nanocrystals. *Nat. Mater.* **2016**, *15*, 141–153.

(43) Badia, A.; Cuccia, L.; Demers, L.; Morin, F.; Lennox, R. B. Structure and Dynamics in Alkanethiolate Monolayers Self-Assembled on Gold Nanoparticles: A DSC, FT-IR, and Deuterium NMR Study. *J. Am. Chem. Soc.* **1997**, *119*, 2682–2692.

(44) Mulvaney, P. Surface Plasmon Spectroscopy of Nanosized Metal Particles. *Langmuir* **1996**, *12*, 788–800.

(45) Kamyshny, A.; Magdassi, S. Conductive Nanomaterials for Printed Electronics. *Small* **2014**, *10*, 3515–3535.

(46) *American Heritage Dictionary of the English Language*; 4th ed.; Houghton Mifflin Harcourt Company, 2006.

(47) Derby, B. Inkjet Printing of Functional and Structural Materials: Fluid Property Requirements, Feature Stability, and Resolution. *Annu. Rev. Mater. Res.* **2010**, *40*, 395–414.

(48) Biswas, A.; Bayer, I. S.; Biris, A. S.; Wang, T.; Dervishi, E.; Faupel, F. Advances in Top–down and Bottom–up Surface Nanofabrication: Techniques, Applications & Future Prospects. *Adv. Colloid Interface Sci.* **2012**, *170*, 2–27.

(49) Tebbe, M.; Mayer, M.; Glatz, B. A.; Hanske, C.; Probst, P. T.; Müller, M. B.; Karg, M.; Chanana, M.; König, T. A. F.; Kuttner, C.; *et al.* Optically Anisotropic Substrates via Wrinkle-Assisted Convective Assembly of Gold Nanorods on Macroscopic Areas. *Faraday Discuss.* **2015**, *181*, 243–260.

(50) Kraus, T.; Malaquin, L.; Schmid, H.; Riess, W.; Spencer, N. D.; Wolf, H. Nanoparticle Printing with Single-Particle Resolution. *Nat. Nanotechnol.* **2007**, *2*, 570–576.

(51) Reuss, R. H.; Chalamala, B. R. Introduction to Solution-Deposited Inorganic Electronics. In *Solution Processing of Inorganic Materials*; Mitzi, D. B., Ed.; John Wiley & Sons Ltd, 2009; pp. 1–32.

(52) Chason, M.; Gamota, D. R.; Brazis, P. W.; Kalyanasundaram, K.; Zhang, J.; Lian, K. K.; Croswell, R. Toward Manufacturing Low-Cost, Large-Area Electronics. *MRS Bull.* **2006**, *31*, 471–475.

(53) Chabinyc, M. L.; Wong, W. S.; Arias, A. C.; Ready, S.; Lujan, R. A.; Daniel, J. H.; Krusor, B.; Apte, R. B.; Salleo, A.; Street, R. A. Printing Methods and Materials for Large-Area Electronic Devices. *Proc. IEEE* **2005**, *93*, 1491–1499.

(54) Woo, K.; Bae, C.; Jeong, Y.; Kim, D.; Moon, J. Inkjet-Printed Cu Source/drain Electrodes for Solution-Deposited Thin Film Transistors. *J. Mater. Chem.* **2010**, *20*, 3877–3882.

(55) Minari, T.; Kanehara, Y.; Liu, C.; Sakamoto, K.; Yasuda, T.; Yaguchi, A.; Tsukada, S.; Kashizaki, K.; Kanehara, M. Room-Temperature Printing of Organic Thin-Film Transistors with π-Junction Gold Nanoparticles. *Adv. Funct. Mater.* **2014**, *24*, 4886–

4892.

(56) Tekin, E.; Smith, P. J.; Schubert, U. S. Inkjet Printing as a Deposition and Patterning Tool for Polymers and Inorganic Particles. *Soft Matter* **2008**, *4*, 703.

(57) Grzelczak, M.; Vermant, J.; Furst, E. M.; Liz-Marzán, L. M. Directed Self-Assembly of Nanoparticles. *ACS Nano* **2010**, *4*, 3591–3605.

(58) Lehn, J.-M. *Supramolecular Chemistry*; Wiley-VCH Verlag GmbH & Co. KGaA: Weinheim, Germany, 1995.

(59) Stupp, S. I. Supramolecular Materials: Self-Organized Nanostructures. *Science (80-. ).* **1997**, *276*, 384–389.

(60) Rotello, V. M.; Boal, A. K.; Ilhan, F.; DeRouchey, J. E.; Thurn-Albrecht, T.; Russell, T. P. Self-Assembly of Nanoparticles into Structured Spherical and Network Aggregates. *Nature* **2000**, *404*, 746–748.

(61) Mulla, M. A.; Yow, H. N.; Zhang, H.; Cayre, O. J.; Biggs, S. Colloid Particles in Ink Formulations. In *Fundamentals of Inkjet Printing*; Wiley-VCH Verlag GmbH & Co. KGaA: Weinheim, Germany, 2015; pp. 141–168.

(62) Gorbatikh, L.; Wardle, B. L.; Lomov, S. V. Hierarchical Lightweight Composite Materials for Structural Applications. *MRS Bull.* **2016**, *41*, 672–677.

(63) Qian, D.; Dickey, E. C.; Andrews, R.; Rantell, T. Load Transfer and Deformation Mechanisms in Carbon Nanotube-Polystyrene Composites. *Appl. Phys. Lett.* **2000**, *76*, 2868–2870.

(64) Mutiso, R. M.; Sherrott, M. C.; Rathmell, A. R.; Wiley, B. J.; Winey, K. I. Integrating Simulations and Experiments To Predict Sheet Resistance and Optical Transmittance in Nanowire Films for Transparent Conductors. **2013**, 7654–7663.

(65) Kyrylyuk, A. V.; Hermant, M. C.; Schilling, T.; Klumperman, B.; Koning, C. E.; van der Schoot, P. Controlling Electrical Percolation in Multicomponent Carbon Nanotube Dispersions. *Nat. Nanotechnol.* **2011**, *6*, 364–369.

(66) Çolak, A.; Wei, J.; Arfaoui, I.; Pileni, M.-P. Coating Agent-Induced Mechanical Behavior of 3D Self-Assembled Nanocrystals. *Phys. Chem. Chem. Phys.* **2017**.

(67) Fratzl, P.; Weinkamer, R. Nature's Hierarchical Materials. *Prog. Mater. Sci.* **2007**, *52*, 1263–1334.

(68) Hucker, M. J.; Haq, S.; Dunleavy, M. US 20110122591 A1 "Hybrid Fabric Materials, and Structural Components Incorporating Same" priority Date 2008-07-08.

(69) Šutka, A.; Timusk, M.; Loot, A.; Joost, U.; Käämbre, T. Polarizable Nanowire Colloids for Power Free Naked Eye Optical Detection of Electrostatic Surface Charges. *Adv. Mater. Technol.* **2016**, *1*, 1600154.

(70) Trebbin, M.; Steinhauser, D.; Perlich, J.; Buffet, A.; Roth, S. V; Zimmermann, W.;

Thiele, J.; Förster, S. Anisotropic Particles Align Perpendicular to the Flow Direction in Narrow Microchannels. *Proc. Natl. Acad. Sci. U. S. A.* **2013**, *110*, 6706–6711.

(71) Nie, Z.; Petukhova, A.; Kumacheva, E. Properties and Emerging Applications of Self-Assembled Structures Made from Inorganic Nanoparticles. *Nat. Nanotechnol.* **2010**, *5*, 15–25.

(72) Hermann, J.; DiStasio, R. A.; Tkatchenko, A. First-Principles Models for van Der Waals Interactions in Molecules and Materials: Concepts, Theory, and Applications. *Chem. Rev.* **2017**, *117*, 4714–4758.

(73) Leite, F. L.; Bueno, C. C.; Da Róz, A. L.; Ziemath, E. C.; Oliveira, O. N. Theoretical Models for Surface Forces and Adhesion and Their Measurement Using Atomic Force Microscopy. *Int. J. Mol. Sci.* **2012**, *13*, 12773–12856.

(74) London, F. The General Theory of Molecular Forces. *Trans. Faraday Soc.* **1937**, 8–26.

(75) Hamaker, H. C. The London—van Der Waals Attraction between Spherical Particles. *Physica* **1937**, *4*, 1058–1072.

(76) *Colloid Stability; The Role of Surface Forces - Part II*; Tadros, T. F., Ed.; Wiley-VCH Verlag GmbH & Co. KGaA, 2007.

(77) Israelachvili, J. N. *Intermolecular and Surface Forces*; 3rd ed.; Elsevier, 2011.

(78) Tadmor, R. The London-van Der Waals Interaction Energy between Objects of Various Geometries. *J. Phys. Condens. Matter* **2001**, *13*, L195–L202.

(79) Bergström, L. Hamaker Constants of Inorganic Materials. *Adv. Colloid Interface Sci.* **1997**, *70*, 125–169.

(80) Sau, T. K.; Murphy, C. J. Self-Assembly Patterns Formed upon Solvent Evaporation of Aqueous Cetyltrimethylammonium Bromide-Coated Gold Nanoparticles of Various Shapes. *Langmuir* **2005**, *21*, 2923–2929.

(81) Turkevich, J.; Stevenson, P. C.; Hillier, J. A Study of the Nucleation and Growth Processes in the Synthesis of Colloidal Gold. *Discuss. Faraday Soc.* **1951**, *11*, 55.

(82) Frens, G. Controlled Nucleation for the Regulation of the Particle Size in Monodisperse Gold Suspensions. *Nat. Phys. Sci.* **1973**, *241*, 20–22.

(83) Derjaguin, B.; Landau, L. Theory of the Stability of Strongly Charged Lyophobic Sols and of the Adhesion of Strongly Charged Particles in Solutions of Electrolytes. *Prog. Surf. Sci.* **1993**, *43*, 30–59.

(84) Bishop, K. J. M. Nanoscale Self-Assembly: Seeing Is Understanding. *ACS Cent. Sci.* **2015**, *1*, 16–17.

(85) Bhardwaj, R.; Fang, X.; Somasundaran, P.; Attinger, D. Self-Assembly of Colloidal Particles from Evaporating Droplets: Role of DLVO Interactions and Proposition of

a Phase Diagram. *Langmuir* **2010**, *26*, 7833–7842.

(86) Behrens, S. H.; Christl, D. I.; Emmerzael, R.; Schurtenberger, P.; Borkovec, M. Charging and Aggregation Properties of Carboxyl Latex Particles: Experiments versus DLVO Theory. *Langmuir* **2000**, *16*, 2566–2575.

(87) Liang, Y.; Hilal, N.; Langston, P.; Starov, V. Interaction Forces between Colloidal Particles in Liquid: Theory and Experiment. *Adv. Colloid Interface Sci.* **2007**, *134–135*, 151–166.

(88) Asakura, S.; Oosawa, F. Interaction between Particles Suspended in Solutions of Macromolecules. *J. Polym. Sci.* **1958**, *33*, 183–192.

(89) Doty, R. C.; Tshikhudo, T. R.; Brust, M.; Fernig, D. G. Extremely Stable Water-Soluble Ag Nanoparticles. *Chem. Mater.* **2005**, *17*, 4630–4635.

(90) Mao, Y.; Cates, M. E.; Lekkerkerker, H. N. W. Depletion Force in Colloidal Systems. *Phys. A Stat. Mech. its Appl.* **1995**, *222*, 10–24.

(91) Badaire, S.; Cottin-Bizonne, C.; Stroock, A. D. Experimental Investigation of Selective Colloidal Interactions Controlled by Shape, Surface Roughness, and Steric Layers. *Langmuir* **2008**, *24*, 11451–11463.

(92) Milowska, K. Z.; Stolarczyk, J. K. Role of Ligand-Ligand vs. Core-Core Interactions in Gold Nanoclusters. *Phys. Chem. Chem. Phys.* **2016**, *18*, 12716–12724.

(93) Hajiw, S.; Schmitt, J.; Imperor-Clerc, M.; Pansu, B. Solvent-Driven Interactions between Hydrophobically-Coated Nanoparticles. *Soft Matter* **2015**, *11*, 3920–3926.

(94) Goubet, N.; Richardi, J.; Albouy, P.-A.; Pileni, M.-P. Which Forces Control Supracrystal Nucleation in Organic Media? *Adv. Funct. Mater.* **2011**, *21*, 2693–2704.

(95) Luedtke, W. D.; Landman, U. Structure, Dynamics, and Thermodynamics of Passivated Gold Nanocrystallites and Their Assemblies. *J. Phys. Chem.* **1996**, *100*, 13323–13329.

(96) Wu, B.-H.; Yang, H.-Y.; Huang, H.-Q.; Chen, G.-X.; Zheng, N.-F. Solvent Effect on the Synthesis of Monodisperse Amine-Capped Au Nanoparticles. *Chinese Chem. Lett.* **2013**, *24*, 457–462.

(97) Widmer-Cooper, A.; Geissler, P. L. Ligand-Mediated Interactions between Nanoscale Surfaces Depend Sensitively and Nonlinearly on Temperature, Facet Dimensions, and Ligand Coverage. *ACS Nano* **2016**, *10*, 1877–1887.

(98) Ghorai, P. K.; Glotzer, S. C. Molecular Dynamics Simulation Study of Self-Assembled Monolayers of Alkanethiol Surfactants on Spherical Gold Nanoparticles †. *J. Phys. Chem. C* **2007**, *111*, 15857–15862.

(99) Thorkelsson, K.; Bai, P.; Xu, T. Self-Assembly and Applications of Anisotropic Nanomaterials: A Review. *Nano Today* **2015**, *10*, 48–66.

(100) Zhao, P.; Li, N.; Astruc, D. State of the Art in Gold Nanoparticle Synthesis. *Coord. Chem. Rev.* **2013**, *257*, 638–665.

(101) Owen, J. The Coordination Chemistry of Nanocrystal Surfaces. *Science (80-. ).* **2015**, *347*, 615–616.

(102) Grzelczak, M.; Sanchez-Iglesias, A.; Rodriguez-Gonzalez, B.; Alvarez-Puebla, R.; Perez-Juste, J.; Liz-Marzan, L. M. Influence of Iodide Ions on the Growth of Gold Nanorods: Tuning Tip Curvature and Surface Plasmon Resonance. *Adv. Funct. Mater.* **2008**, *18*, 3780–3786.

(103) Pearson, R. G. Hard and Soft Acids and Bases. *J. Am. Chem. Soc.* **1963**, *85*, 3533–3539.

(104) Nath, S.; Ghosh, S. K.; Kundu, S.; Praharaj, S.; Panigrahi, S.; Pal, T. Is Gold Really Softer than Silver? HSAB Principle Revisited. *J. Nanoparticle Res.* **2006**, *8*, 111–116.

(105) Siddiqui, M. R. H. Protected Gold Nanoparticles with Thioethers and Amines As Surrogate Ligands. *J. Chem.* **2013**, *2013*, 1–4.

(106) Orendorff, C. J.; Alam, T. M.; Sasaki, D. Y.; Bunker, B. C.; Voigt, J. A. Phospholipid−Gold Nanorod Composites. *ACS Nano* **2009**, *3*, 971–983.

(107) Vigderman, L.; Manna, P.; Zubarev, E. R. Quantitative Replacement of Cetyl Trimethylammonium Bromide by Cationic Thiol Ligands on the Surface of Gold Nanorods and Their Extremely Large Uptake by Cancer Cells. *Angew. Chem. Int. Ed. Engl.* **2012**, *51*, 636–641.

(108) Takahashi, H.; Niidome, Y.; Niidome, T.; Kaneko, K.; Kawasaki, H.; Yamada, S. Modification of Gold Nanorods Using Phosphatidylcholine to Reduce Cytotoxicity. *Langmuir* **2006**, *22*, 2–5.

(109) Nag, A.; Kovalenko, M. V; Lee, J.; Liu, W.; Spokoyny, B.; Talapin, D. V. Metal-Free Inorganic Ligands for Colloidal Nanocrystals: S 2– , HS – , Se 2– , HSe – , Te 2– , HTe – , TeS 3 2– , OH – , and NH 2 – as Surface Ligands. *J. Am. Chem. Soc.* **2011**, *133*, 10612–10620.

(110) Indrasekara, A. S. D. S.; Wadams, R. C.; Fabris, L. Ligand Exchange on Gold Nanorods: Going Back to the Future. *Part. Part. Syst. Charact.* **2014**, *31*, 819–838.

(111) Schwarzenbach, G. Chelate Complex Formation as a Basis for Titration Processes. *Anal. Chim. Acta* **1952**, *7*, 141–155.

(112) Fasting, C.; Schalley, C. A.; Weber, M.; Seitz, O.; Hecht, S.; Koksch, B.; Dernedde, J.; Graf, C.; Knapp, E.-W.; Haag, R. Multivalency as a Chemical Organization and Action Principle. *Angew. Chemie Int. Ed.* **2012**, *51*, 10472–10498.

(113) Uyeda, H. T.; Medintz, I. L.; Jaiswal, J. K.; Simon, S. M.; Mattoussi, H. Synthesis of Compact Multidentate Ligands to Prepare Stable Hydrophilic Quantum Dot Fluorophores. *J. Am. Chem. Soc.* **2005**, *127*, 3870–3878.

(114) Stein, B.; Zopes, D.; Schmudde, M.; Schneider, R.; Mohsen, A.; Goroncy, C.; Mathur, S.; Graf, C. Kinetics of Aggregation and Growth Processes of PEG-Stabilised Mono- and Multivalent Gold Nanoparticles in Highly Concentrated Halide Solutions. *Faraday Discuss.* **2015**, *181*, 85–102.

(115) Zopes, D.; Stein, B.; Mathur, S.; Graf, C. Improved Stability of "Naked" Gold Nanoparticles Enabled by in Situ Coating with Mono and Multivalent Thiol PEG Ligands. *Langmuir* **2013**, *29*, 11217–11226.

(116) Grubbs, R. B. Roles of Polymer Ligands in Nanoparticle Stabilization. *Polym. Rev.* **2007**, *47*, 197–215.

(117) Schulz, F.; Vossmeyer, T.; Bastús, N. G.; Weller, H. Effect of the Spacer Structure on the Stability of Gold Nanoparticles Functionalized with Monodentate Thiolated Poly(ethylene Glycol) Ligands. *Langmuir* **2013**, *29*, 9897–9908.

(118) Kister, T. (INM - Leibniz Institute for New Materials, Structure Formation Group, Saarbrücken) Unpublished Results.

(119) Browne, K. P.; Grzybowski, B. A. Controlling the Properties of Self-Assembled Monolayers by Substrate Curvature. *Langmuir* **2011**, *27*, 1246–1250.

(120) Zhou, J.; Ralston, J.; Sedev, R.; Beattie, D. A. Functionalized Gold Nanoparticles: Synthesis, Structure and Colloid Stability. *J. Colloid Interface Sci.* **2009**, *331*, 251–262.

(121) Dubois, L. H.; Nuzzo, R. G. Synthesis, Structure, and Properties of Model Organic Surfaces. *Annu. Rev. Phys. Chem.* **1992**, *43*, 437–463.

(122) Mourdikoudis, S.; Liz-Marzán, L. M. Oleylamine in Nanoparticle Synthesis. *Chem. Mater.* **2013**, *25*, 1465–1476.

(123) Pérez-Juste, J.; Liz-Marzán, L. M.; Carnie, S.; Chan, D. Y. C.; Mulvaney, P. Electric-Field-Directed Growth of Gold Nanorods in Aqueous Surfactant Solutions. *Adv. Funct. Mater.* **2004**, *14*, 571–579.

(124) Leff, D. V.; Ohara, P. C.; Heath, J. R.; Gelbart, W. M. Thermodynamic Control of Gold Nanocrystal Size: Experiment and Theory. *J. Phys. Chem.* **1995**, *99*, 7036–7041.

(125) Camillone, N.; Chidsey, C. E. D.; Liu, G.; Scoles, G. Superlattice Structure at the Surface of a Monolayer of Octadecanethiol Self-assembled on Au(111). *J. Chem. Phys.* **1993**, *98*, 3503–3511.

(126) Leff, D. V.; Brandt, L.; Heath, J. R. Synthesis and Characterization of Hydrophobic, Organically-Soluble Gold Nanocrystals Functionalized with Primary Amines. *Langmuir* **1996**, *12*, 4723–4730.

(127) Xu, C.; Sun, L.; Kepley, L. J.; Crooks, R. M.; Ricco, A. J. Molecular Interactions between Organized, Surface-Confined Monolayers and Vapor-Phase Probe Molecules. 6. In-Situ FT-IR External Reflectance Spectroscopy of Monolayer Adsorption and Reaction Chemistry. *Anal. Chem.* **1993**, *65*, 2102–2107.

(128) Nie, Z.; Fava, D.; Rubinstein, M.; Kumacheva, E. “Supramolecular” Assembly of Gold Nanorods End-Terminated with Polymer “Pom-Poms”: Effect of Pom-Pom Structure on the Association Modes. *J. Am. Chem. Soc.* **2008**, *130*, 3683–3689.

(129) Grubbs, R. B. Nanoparticle Assembly: Solvent-Tuned Structures. *Nat. Mater.* **2007**, *6*, 553–555.

(130) Ozin, G. A.; Hou, K.; Lotsch, B. V; Cademartiri, L.; Puzzo, D. P.; Scotognella, F.; Ghadimi, A.; Thomson, J. Nanofabrication by Self-Assembly. *Mater. Today* **2009**, *12*, 12–23.

(131) Ling, D.; Hackett, M. J.; Hyeon, T. Surface Ligands in Synthesis, Modification, Assembly and Biomedical Applications of Nanoparticles. *Nano Today* **2014**, *9*, 457–477.

(132) Jana, N. R.; Gearheart, L.; Murphy, C. J. Seed-Mediated Growth Approach for Shape-Controlled Synthesis of Spheroidal and Rod-like Gold Nanoparticles Using a Surfactant Template. *Adv. Mater.* **2001**, *13*, 1389–1393.

(133) Polte, J. Fundamental Growth Principles of Colloidal Metal Nanoparticles – a New Perspective. *CrystEngComm* **2015**, *17*, 6809–6830.

(134) Tao, A. R.; Habas, S.; Yang, P. Shape Control of Colloidal Metal Nanocrystals. *Small* **2008**, *4*, 310–325.

(135) Bakshi, M. S. How Surfactants Control Crystal Growth of Nanomaterials. *Cryst. Growth Des.* **2016**, *16*, 1104–1133.

(136) Yin, Y.; Alivisatos, A. P. Colloidal Nanocrystal Synthesis and the Organic–inorganic Interface. *Nature* **2005**, *437*, 664–670.

(137) Cates, M. E.; Candau, S. J. Statics and Dynamics of Worm-like Surfactant Micelles. *J. Phys. Condens. Matter* **1990**, *2*, 6869–6892.

(138) Patel, V.; Dharaiya, N.; Ray, D.; Aswal, V. K.; Bahadur, P. pH Controlled Size/shape in CTAB Micelles with Solubilized Polar Additives: A Viscometry, Scattering and Spectral Evaluation. *Colloids Surfaces A Physicochem. Eng. Asp.* **2014**, *455*, 67–75.

(139) Lohse, S. E.; Murphy, C. J. The Quest for Shape Control: A History of Gold Nanorod Synthesis. *Chem. Mater.* **2013**, *25*, 1250–1261.

(140) Grzelczak, M.; Pérez-Juste, J.; Mulvaney, P.; Liz-Marzán, L. M. Shape Control in Gold Nanoparticle Synthesis. *Chem. Soc. Rev.* **2008**, *37*, 1783–1791.

(141) Gómez-Graña, S.; Hubert, F.; Testard, F.; Guerrero-Martínez, A.; Grillo, I.; Liz-Marzán, L. M.; Spalla, O. Surfactant (Bi)layers on Gold Nanorods. *Langmuir* **2012**, *28*, 1453–1459.

(142) Ye, X.; Zheng, C.; Chen, J.; Gao, Y.; Murray, C. B. Using Binary Surfactant Mixtures to Simultaneously Improve the Dimensional Tunability and Monodispersity in the Seeded Growth of Gold Nanorods. *Nano Lett.* **2013**, *13*, 765–771.

(143) Scarabelli, L.; Sánchez-Iglesias, A.; Pérez-Juste, J.; Liz-Marzán, L. M. A "Tips and Tricks" Practical Guide to the Synthesis of Gold Nanorods. *J. Phys. Chem. Lett.* **2015**, *6*, 4270–4279.

(144) Lohse, S. E.; Burrows, N. D.; Scarabelli, L.; Liz-Marzán, L. M.; Murphy, C. J. Anisotropic Noble Metal Nanocrystal Growth: The Role of Halides. *Chem. Mater.* **2014**, *26*, 34–43.

(145) Halder, A.; Ravishankar, N. Ultrafine Single-Crystalline Gold Nanowire Arrays by Oriented Attachment. *Adv. Mater.* **2007**, *19*, 1854–1858.

(146) Pazos-Pérez, N.; Baranov, D.; Irsen, S.; Hilgendorff, M.; Liz-Marzán, L. M.; Giersig, M. Synthesis of Flexible, Ultrathin Gold Nanowires in Organic Media. *Langmuir* **2008**, *24*, 9855–9860.

(147) Huo, Z.; Tsung, C.-K.; Huang, W.; Zhang, X.; Yang, P. Sub-Two Nanometer Single Crystal Au Nanowires. *Nano Lett.* **2008**, *8*, 2041–2044.

(148) Kura, H.; Ogawa, T. Synthesis and Growth Mechanism of Long Ultrafine Gold Nanowires with Uniform Diameter. *J. Appl. Phys.* **2010**, *107*, 74310.

(149) Lu, X.; Yavuz, M. S.; Tuan, H.-Y.; Korgel, B. A.; Xia, Y. Ultrathin Gold Nanowires Can Be Obtained by Reducing Polymeric Strands of Oleylamine−AuCl Complexes Formed via Aurophilic Interaction. *J. Am. Chem. Soc.* **2008**, *130*, 8900–8901.

(150) Wang, C.; Hu, Y.; Lieber, C. M.; Sun, S. Ultrathin Au Nanowires and Their Transport Properties. *J. Am. Chem. Soc.* **2008**, *130*, 8902–8903.

(151) Wang, C.; Sun, S. Facile Synthesis of Ultrathin and Single-Crystalline Au Nanowires. *Chem. - An Asian J.* **2009**, *4*, 1028–1034.

(152) Loubat, A.; Impéror-Clerc, M.; Pansu, B.; Meneau, F.; Raquet, B.; Viau, G.; Lacroix, L.-M. Growth and Self-Assembly of Ultrathin Au Nanowires into Expanded Hexagonal Superlattice Studied by in Situ SAXS. *Langmuir* **2014**, *30*, 4005–4012.

(153) Kamiya, H.; Iijima, M. Surface Modification and Characterization for Dispersion Stability of Inorganic Nanometer-Scaled Particles in Liquid Media. *Sci. Technol. Adv. Mater.* **2010**, *11*, 44304.

(154) Born, P.; Kraus, T. Ligand-Dominated Temperature Dependence of Agglomeration Kinetics and Morphology in Alkyl-Thiol-Coated Gold Nanoparticles. *Phys. Rev. E* **2013**, *87*, 62313.

(155) Klajn, R.; Bishop, K. J. M.; Grzybowski, B. A. Light-Controlled Self-Assembly of Reversible and Irreversible Nanoparticle Suprastructures. *Proc. Natl. Acad. Sci.* **2007**, *104*, 10305–10309.

(156) Cademartiri, L.; Bishop, K. J. M.; Snyder, P. W.; Ozin, G. A. Using Shape for Self-Assembly. *Philos. Trans. A. Math. Phys. Eng. Sci.* **2012**, *370*, 2824–2847.

(157) Jana, N. R. Shape Effect in Nanoparticle Self-Assembly. *Angew. Chemie Int. Ed.*

**2004**, *43*, 1536–1540.

(158) Liu, K.; Nie, Z.; Zhao, N.; Li, W.; Rubinstein, M.; Kumacheva, E. Step-Growth Polymerization of Inorganic Nanoparticles. *Science (80-. ).* **2010**, *329*, 197–200.

(159) Burrows, N. D.; Vartanian, A. M.; Abadeer, N. S.; Grzincic, E. M.; Jacob, L. M.; Lin, W.; Li, J.; Dennison, J. M.; Hinman, J. G.; Murphy, C. J. Anisotropic Nanoparticles and Anisotropic Surface Chemistry. *J. Phys. Chem. Lett.* **2016**, *7*, 632–641.

(160) Wang, Y.; Kanjanaboos, P.; Barry, E.; Mcbride, S.; Lin, X.-M.; Jaeger, H. M. Fracture and Failure of Nanoparticle Monolayers and Multilayers. *Nano Lett.* **2014**, *14*, 826–830.

(161) Andryszewski, T.; Iwan, M.; Hołdyński, M.; Fiałkowski, M. Synthesis of a Free-Standing Monolayer of Covalently Bonded Gold Nanoparticles. *Chem. Mater.* **2016**, *28*, 5304–5313.

(162) Wünscher, S.; Abbel, R.; Perelaer, J.; Schubert, U. S. Progress of Alternative Sintering Approaches of Inkjet-Printed Metal Inks and Their Application for Manufacturing of Flexible Electronic Devices. *J. Mater. Chem. C* **2014**, *2*, 10232–10261.

(163) Perelaer, J.; Abbel, R.; Wünscher, S.; Jani, R.; van Lammeren, T.; Schubert, U. S. Roll-to-Roll Compatible Sintering of Inkjet Printed Features by Photonic and Microwave Exposure: From Non-Conductive Ink to 40% Bulk Silver Conductivity in Less Than 15 Seconds. *Adv. Mater.* **2012**, *24*, 2620–2625.

(164) Voitekhovich, S. V.; Talapin, D. V.; Klinke, C.; Kornowski, A.; Weller, H. CdS Nanoparticles Capped with 1-Substituted 5-Thiotetrazoles: Synthesis, Characterization, and Thermolysis of the Surfactant. *Chem. Mater.* **2008**, *20*, 4545–4547.

(165) Park, J.; Kang, H. J.; Shin, K.-H.; Kang, H. Fast Sintering of Silver Nanoparticle and Flake Layers by Infrared Module Assistance in Large Area Roll-to-Roll Gravure Printing System. *Sci. Rep.* **2016**, *6*, 34470.

(166) Nichols, G.; Byard, S.; Bloxham, M. J.; Botterill, J.; Dawson, N. J.; Dennis, A.; Diart, V.; North, N. C.; Sherwood, J. D. A Review of the Terms Agglomerate and Aggregate with a Recommendation for Nomenclature Used in Powder and Particle Characterization. *J. Pharm. Sci.* **2002**, *91*, 2103–2109.

(167) BS 2955: 1993: Glossary of Terms Relating to Particle Technology. British Standards Institution, London, UK.

(168) ISO 14887: 2000 (E). Sample Preparation- Dispersing Procedures for Powders in Liquids. British Standards Institution, London, UK.

# 3 Results and discussion

All results of this thesis are published in peer-reviewed scientific journals. The publications contain discussions of the results in context of the respective topic they describe. Section 4 will put all results and discussions from this section in context of this thesis.

Section 3.1 - 3.6 reproduces the following 3 publicatons along ith the respective Supporting Information

1. **Reiser, B.**; González-García, L.; Kanelidis, I.; Maurer, J. H. M.; Kraus, T. Gold Nanorods with Conjugated Polymer Ligands: Sintering-Free Conductive Inks for Printed Electronics. *Chem. Sci.* **2016**, *7*, 4190–4196;
2. **Reiser, B**.; Gerstner, D.; González-García, L.; Maurer, J. H. M.; Kanelidis, I.; Kraus, T. Multivalent Bonds in Self-Assembled Bundles of Ultrathin Gold Nanowires. *Phys. Chem. Chem. Phys.* **2016**;
3. **Reiser, B.**; Gerstner, D.; Gonzalez-Garcia, L.; Maurer, J. H. M.; Kanelidis, I.; Kraus, T. Spinning Hierarchical Gold Nanowire Microfibers by Shear Alignment and Intermolecular Self-Assembly. *ACS Nano* **2017**;

with permission of all authors and the respective pulisher.

The contributions of all the authors is discussed on page 3 in the Statement on Contribution.

## 3.1 Publication 1: Gold nanorods with conjugated polymer ligands: sintering-free conductive inks for printed electronics

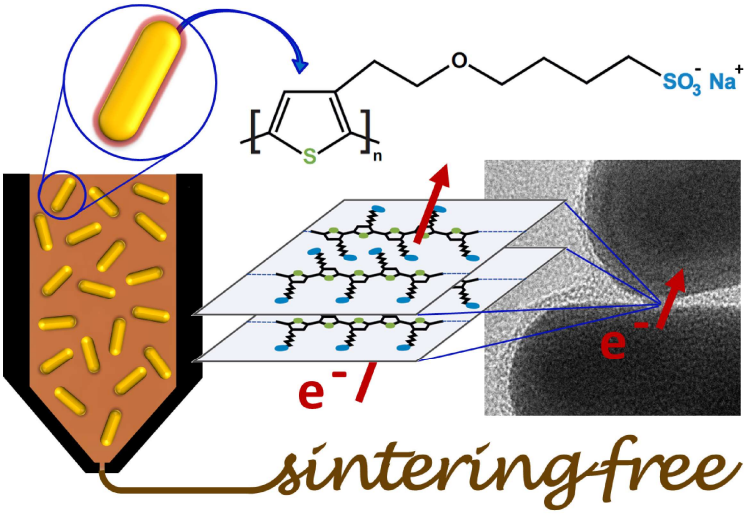


**Reiser, B.**; González-García, L.; Kanelidis, I.; Maurer, J. H. M.; Kraus, T. Gold Nanorods with Conjugated Polymer Ligands: Sintering-Free Conductive Inks for Printed Electronics. *Chem. Sci.* **2016**, *7*, 4190–4196.

Reprinted with permission of all authors. Copyright (2016) Royal Society of Chemistry.[f2]

[f2] Note that Figure, Table and equation numbers as well as section names and numbers have been adapted to ensure consistent labeling and numbering throughout the whole thesis. Some Figures have been rearranged and resized to better fit the format of the thesis.

### 3.1.1 Abstract

Metal-based nanoparticle inks for printed electronics usually require sintering to improve the poor electron transport at particle-particle interfaces. The ligands required for colloidal stability act as insulating barriers and must be removed in a post-deposition sintering step. This complicates the fabrication process and makes it incompatible with many flexible substrates. Here, we bind a conjugated, electrically conductive polymer on gold nanorods (AuNRs) as a ligand. The polymer, poly[2-(3-thienyl)-ethyloxy-4-butylsulfonate)] (PTEBS), provides colloidal stability and good electron transport properties to stable, sintering-free inks. We confirm that the polymer binds strongly through a multidentate binding motif and provides superior colloidal stability in polar solvents over months by IR and Raman spectrometry and zeta potential measurements. We demonstrate that the developed ligand exchange protocol is directly applicable to other polythiophenes such as poly(3,4-ethylenedioxythiophene) polystyrene sulfonate (PEDOT:PSS). Films of AuNRs coated with above polymers reached conductivities directly after deposition comparable to conventional metal inks after ligand removal and retained their conductivity for at least one year when stored under ambient conditions.

### 3.1.2 State of the art

The accelerating market of printed electronics requires inks that are suitable for large-area, high-throughput and low-cost production of lightweight and flexible conductive materials. Relevant market drivers are touchscreen panels, memory components, organic photovoltaic, radio frequency identification (RFID) tags and optoelectronic devices.[1] Preferable deposition methods are solution-based processes such as inkjet printing using inks containing metal or conductive metal oxide colloids.[2–4]

Successful printing requires suitable inks. The performance of nanoparticle-based inks depends on their colloidal stability under the conditions that occur during printing.[1,5] Conventionally, bulky organic molecules are used as ligands to ensure colloidal stability; they provide steric stabilization to the nanoparticles. After deposition, these ligands impede the contact between the particles and limit electronic conduction. Organic molecules represent insulating barriers; post-deposition treatments to remove them after drying are required. Thermal sintering at high temperatures and with long residence times is hard to reconcile with polymer substrates and roll-to-roll printing processes.[6] Alternative post-treatment methods with reduced time and thermal budgets include plasma, laser, infrared (IR), microwave and intense pulsed light treatments.[1,7–10] Some of them can remove organic ligands and improve electrical transport in less than a minute, but the resulting volume shrinkage can rupture the material.

Sintering-free inks avoid these challenges altogether. Grouchko *et al.* developed a self-sintering metal nanoparticle ink with a non-volatile destabilizing agent.[11] Upon solvent evaporation, the concentration of this destabilizing agent increases and detaches the ligand from the particles. Detachment leads to metal-metal contacts, but the ink with its rapidly decreasing colloidal stability is hard to handle.

Here, we introduce a sintering-free nanoparticle ink in which conjugated polymer ligands lend the particles

- chemical stability due to strong multidentate binding to the metal surface,
- colloidal stability and compatibility in different relevant solvents, and
- good electron transport properties in dry state.

Kanehara and coworkers synthesized tailored phtalocyanine ligands and demonstrated that aromatic systems can provide mobile electrons in the ligand shells.[2,12] We adapted this idea with polymer-coated particles and created hybrid particles with increased colloidal stability using commercially available conjugated polymers such as poly[2-(3-thienyl)-ethyloxy-4butylsulfonate)] (PTEBS) 40-70 kDa. To ensure that the π-electrons couple to the metal surface, polythiophene derivatives were used; they bring the π-system in close proximity to the gold because they contain a sulfur heteroatom in the aromatic ring. Polymer chains with more than 100 repetition units, molecular weights of more than 20 kDa and highly polar side chains can provide colloidal stability in polar solvents.

We demonstrate the effectiveness of polythiophene ligands in nanoparticle inks based on gold nanorods (AuNRs). AuNRs are anisotropic nanoparticles that show lower percolation thresholds than spherical particles and thus provide large conductivities at low volume fractions.[13] The rods can be synthetized using a well-established protocol that yields narrow size distributions and negligible shape impurities.[14] After synthesis, AuNRs are capped by a cetyltrimethylammonium bromide (CTAB) double layer (AuNR@CTAB).[15] The ligand plays a crucial role in the anisotropic particle growth[14,16,17] but leads to poor colloidal stability unless the AuNRs are kept in excess CTAB.[16]

Most existing strategies for the stabilization of AuNRs are based on large, non-conductive polymers that provide stability even if the CTAB has not been exchanged completely.[17–20] The poor colloidal stability of AuNR@CTAB system renders ligand exchange with small molecules challenging.[16,18] The few successful exchange protocols that exist for small ligands[17,21] require

unusual and non-conductive ligands or multi-step ligand exchange protocols. The rods' anisotropy presents an additional challenge: surface properties of the different crystal planes presented on the rod are not equivalent. It is possible to specifically exchange ligands only at the tips of the rods.[22–24] For nanoparticle inks, ligand exchange protocols have to be chosen such that a homogeneous ligand shell forms unless anisotropic particle interactions during ink processing are desirable.

Here we describe a facile and straightforward ligand exchange procedure to modify AuNR@CTAB with PTEBS. We prove the complete exchange of the ligand and discuss the binding site and arrangement of the polymer chains on the surface of the AuNRs. The resulting colloidal dispersion was stable in water and in a mixture of polar solvents over months. We formulated inks and used them to deposit conductive patterns that immediately reached conductivities in the range of annealed metal inks. The protocol is also readily applicable to other polythiophenes, and we demonstrate its compatibility with poly(3,4-ethylenedioxythiophene) polystyrene sulfonate (PEDOT: PSS), a polymer mixture commonly used in organic electronics.

### 3.1.3 Results and discussion

#### *Nanorod synthesis and ligand exchange*

AuNRs were synthesized using a published protocol.[25] Transmission electron microscopy (TEM) images of the as-synthesized AuNR@CTAB are shown in Figure 3.1.3.1a and 3.1.3.1b. The mean length and width were 115 and 25 nm respectively, both with 6% relative standard deviation (Figure 3.1.3.1c). As-synthesized AuNR@CTAB exhibited maxima of longitudinal localized surface plasmon resonance (L-LSPR) and transversal resonance (T-LSPR) at 909 and 508 nm, respectively (Figure 3.1.3.1d).

Figure 3.1.3.2a schematically depicts the ligand exchange procedure. Washed AuNR@CTAB (excess CTAB below 100 µM)[26] were incubated with a solution of PTEBS in water. After the ligand exchange, the remaining free (new and old) ligands were separated from the nanorods by centrifugation. The ligand exchange protocol was optimized to provide full coverage of the surface of the studied particles. We determined that a polymer addition to the dispersion equivalent to at least 7 mg/m$^2$ (polymer mass/particle surface area) was required to obtain colloidally stable AuNR@PTEBS. We recommend a polymer to surface area ratio equivalent to 10 mg/m$^2$ and 8 h incubation for optimal stability. Details on the ligand exchange protocol and its optimization are described in section 3.2.1.

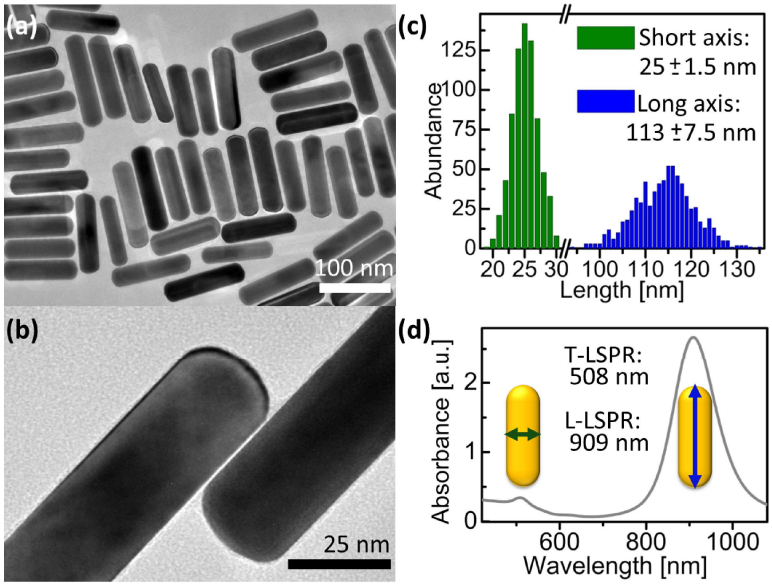


**Figure 3.1.3.1** As-synthesized AuNR@CTAB. (a,b) TEM images. (c) Particle size distribution from 726 AuNRs measured by TEM. (d) UV-vis/NIR spectrum.

### *Surface chemistry characterization*

Figure 3.1.3.2b illustrates the surface of a nanorod before and after modification. The constitutional formulas of CTAB and PTEBS suggest that the nanorods' surface charge should reverse during a ligand exchange process. The observed change in zeta potential from +25 mV to -40 mV confirms a successful ligand exchange.

The UV-vis spectrum of the AuNR@PTEBS showed a blueshift in both LSPR maxima compared to AuNR@CTAB (Figure 3.1.3.2c), indicating an increased dielectric constant in the direct vicinity of the nanorods.[27] We attribute the strong shift to the π-electrons of the conductive polymer that couple with the conduction band of gold. Subtraction of the AuNR@CTAB spectrum from the AuNR@PTEBS spectrum revealed the characteristic absorption band of PTEBS at $\lambda_{max}$ = 415 nm (Figure 3.1.3.2c, inset) from the polymer attached to the gold surface.

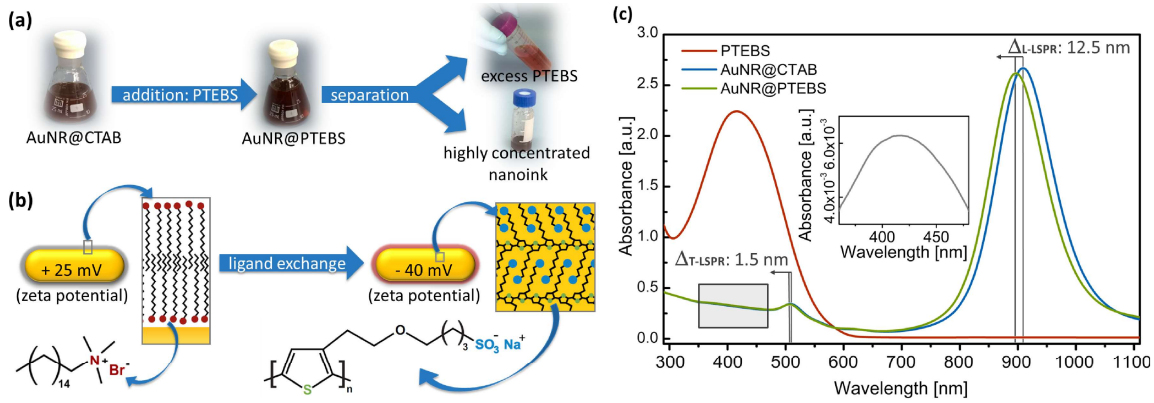


**Figure 3.1.3.2** (a) Ligand exchange process: photographs of dispersions before and after ligand exchange. (b) Schematic depiction of the AuNRs surface chemistry before and after ligand exchange. (c) UV-vis/NIR spectra of pure PTEBS, AuNR@CTAB, and AuNR@PTEBS. Inset: difference between the UV-vis spectra of AuNR@PTEBS and AuNR@CTAB.

The completeness of the ligand exchange was confirmed by IR spectroscopy. Figure 3.1.3.3a compares the fingerprint regions of pure PTEBS, AuNR@CTAB and AuNR@PTEBS. Pure polymer exhibited characteristic vibration bands of the sulfonate group[28] ($\nu_s$: 1042 $cm^{-1}$; $\nu_a$: 1175 $cm^{-1}$) in the side chain. The original rods, AuNR@CTAB, exhibited two prominent peaks at 910 and 960 $cm^{-1}$. After ligand exchange, AuNR@PTEBS showed only the vibrations of the sulfonate group. The signals in the region of the two prominent peaks from CTAB were negligible, confirming that CTAB has been removed and replaced by PTEBS on the surface of the AuNRs.

Raman spectroscopy was used to determine the PTEBS-Au binding motifs (Figure 3.1.3.3b). The signal of the Au-bromide bond of AuNR@CTAB occurred at a Raman shift of 182 $cm^{-1}$ as reported in literature.[20,26] Modified AuNRs did not show this but two other peaks at 172 and 278 $cm^{-1}$. The broad peak at 278 $cm^{-1}$ is in the region where Au-S bonds are typically found.[20] To clarify whether the peak at 172 $cm^{-1}$ originated from the aromatic ring or from the side chain of PTEBS, AuNR@CTAB were plasma-cleaned until the Au-bromide bond was no longer visible in the Raman spectra. The cleaned surface was dipped into pure thiophene. The resulting spectra (Figure S3.2.2.4) evidenced that both peaks found for AuNR@PTEBS arise from thiophene rings adsorbed onto gold. We conclude that PTEBS binds to the AuNRs with its conductive backbone as a multidentate ligand.

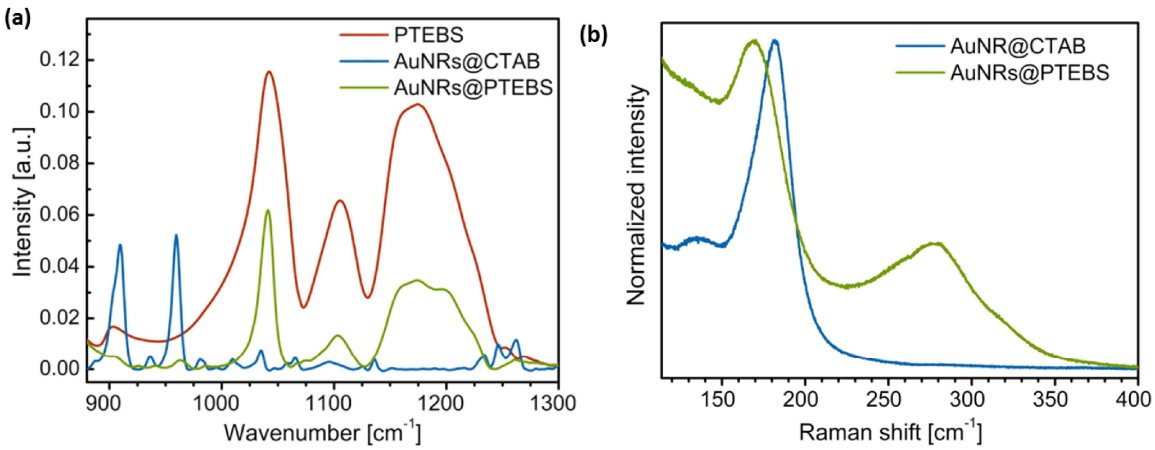


**Figure 3.1.3.3** (a) IR spectra of PTEBS, AuNR@CTAB, and AuNR@PTEBS. (b) Raman spectra of AuNR@CTAB and AuNR@PTEBS ($\lambda_{exc}$ = 782 nm) normalized to the maximum intensity.

TEM images of AuNR@PTEBS showed dry ligand shells with thicknesses that varied between 0.7 nm and 2.1 nm (Figure 3.1.3.4a). Thermogravimetric analysis (TGA) on thoroughly washed AuNR@PTEBS resulted in 2.9% mass loss after heating to 800 °C. We converted this value to an average shell thickness using a geometrical model described in section 3.2.1 (Table S3.2.1.1). The packing density of the polymer was estimated for the packing depicted in Figure 3.1.3.4b with

- the distance of two neighboring polymer chains (a = 0.90 nm)[28],
- the π-stacking distance (b = 0.38 nm)[29], and
- the size of one monomer unit (c = 0.39 nm)[29].

The dry density of perfectly packed PTEBS on the AuNR surface was 7.5 monomers/nm³ (3.5 g/cm³) according to this model. This corresponds to a volumetric shrinkage upon ligand removal of 16.1% and an average dry ligand shell thickness of 0.9 nm, in the range of thicknesses observed in TEM.

Conjugated polymers can bind to a surface face-on or edge-on (Figure 3.1.3.4c).[30] The binding type affects the electronic properties of the coated particle: the edge-on configuration creates spacing between the conjugated polymer backbone and the metal surface. D. Tanaka *et al.* and Y. Abe *et al.* demonstrated that the spacing between the metal surface and a π-electron system affects electronic coupling.[31,32] Hence, face-on adsorption of the polymer onto the AuNRs is beneficial for the conductivity of particle-particle interfaces. Our Raman study shows that PTEBS binds face-on with its conductive backbone and not with its side chains. This is in

accordance with results previously reported for poly-(3-hexylthiophene) (P3HT), a polymer with the same backbone, that adsorbs face-on on Au (111) surface.[33] According to the TGA data, each AuNR is surrounded by an average of three polymer layers that bind to the gold and to each other through π-stacking interactions.

We estimated the binding strength of the multidentate ligand from the amount of desorbed polymer measured by inductively coupled plasma mass spectrometry (ICP-MS). A dilute particle dispersion was thoroughly purified to remove free polymer and the closed vessel was shaken at room temperature for one week to reach equilibrium. All particles were then removed by centrifugation. We found 1.1 ± 0.02 ppm of sulphur in the freshly purified, particle-containing sample and 0.4% of it (4.9 ± 0.07 ppb) in the supernatant of the centrifuged sample, demonstrating strong binding of the polymer.

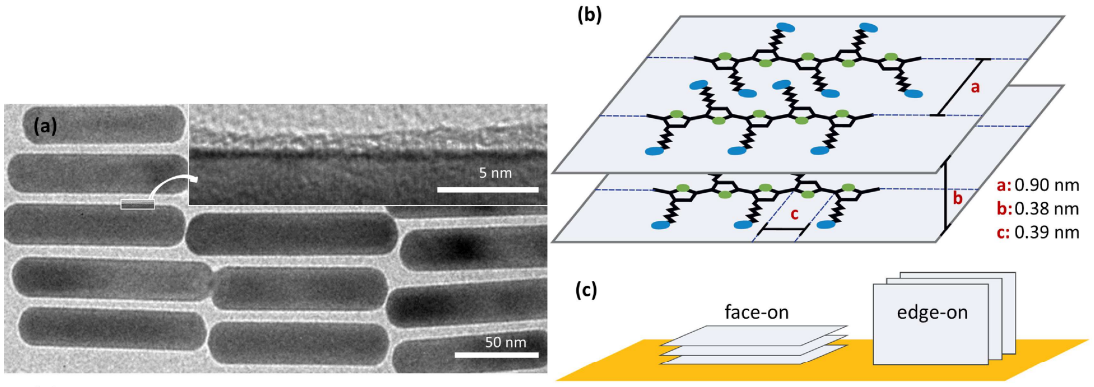


**Figure 3.1.3.4** (a) TEM images of AuNR@PTEBS at low and high magnification. (b) Scheme of the polymer chains packing for crystalline PTEBS: a is the distance between 2 polymer chains, b is the π-stacking distance; c is the length of one monomer unit. (c) Two binding types for polymers packed as depicted in (b).

### *Colloidal stability*

Inkjet inks are typically formulated in a mixture of solvents, often water-alcohol mixtures are most convenient.[5] The poor colloidal stability of AuNR@CTAB in such mixtures limits their use in printed electronics. The rods aggregate even in pure water unless excess CTAB is added, and small amounts of short-chain alcohols or acetone precipitate them.[16] We compared the colloidal stability of AuNR@CTAB to that of AuNR@PTEBS by centrifuging them, seperating the supernatant, and adding different solvents to redisperse them after washing. It was easy to fully redisperse AuNR@PTEBS in short-chain alcohols and in acetone. In a second experiment we introduced rods into solvent mixtures by first dispersing AuNRs in water and adding the 2nd solvent subsequently to a final ratio of 75/25 solvent/water (v/v). Figure

3.1.3.5a shows that the AuNR@CTAB dispersions responded to the addition of methanol and acetone with a color change that was visible to the naked eye after seconds. The corresponding blueshift and the decrease in intensity in the L-LSPR band (Figure 3.1.3.5a) are due to side-by-side assembly of the nanorods (Figure 3.1.3.5c).[34] Aggregates of AuNR@CTAB in methanol and acetone precipitated irreversibly after minutes. The same experiments with AuNR@PTEBS yielded stable dispersions (Figure 3.1.3.5b) with a slight red-shift in the L-LSPR bands that is due to the change of refractive index (RI) caused by the second solvent.

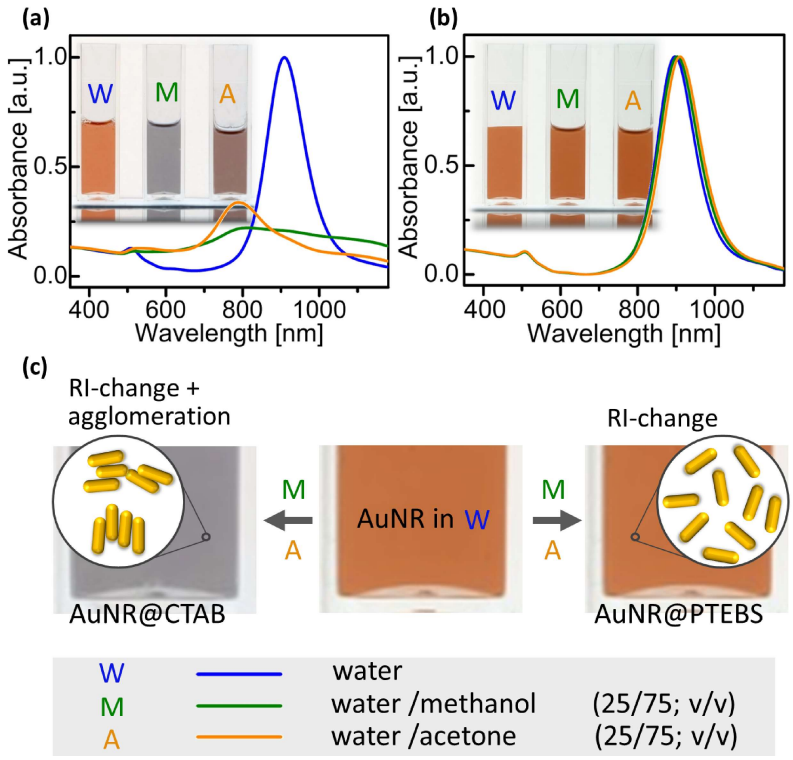


**Figure 3.1.3.5** UV-vis/NIR spectra and photographs of dispersions of (a) AuNR@CTAB and (b) AuNR@PTEBS recorded directly after the addition of 75% of water, methanol and acetone, respectively. (c) Schematic depiction of the AuNR´s sensitivity towards their assembly and towards the chemical composition of their surrounding media.

We formulated inks from AuNR@PTEBS in water, short chain alcohols, acetone, and their mixtures. Their shelf lifes depended on the polarity of the solvent, as expected for electrosterically stabilized colloids with a zeta potential of 40 mV. Inks in pure acetone or alkohols remained stable for 1-2 weeks. Increasing water content increased stability, and a fully aqueous ink with 100 mg/mL (12 wt %) was stable under shaking for at least 10 months.

### *Conductivity of deposited inks*

The electron transport properties of the modified AuNRs were measured in films deposited from concentrated inks. We compared the results to the properties of AuNRs coated with a non-conductive polymer, O-[2-(3-mercaptopropionylamino)ethyl]-O'-methylpolyethylene glycol (AuNR@PEG-SH), molecular weight 20 kDa.[20] Dense lines of AuNR with a thickness of 1 ± 0.2 µm, determined by profilometry, were deposited onto sputtered gold electrodes through masks (Figure 3.1.3.6a and 3.1.3.6b) with inks that contained 25 mg/mL (3 wt%) AuNRs in water/methanol (25/75; v/v). No post-treatment was performed after drying at room temperature (see detailed deposition parameters in section 3.2.1). Their conductivity was calculated from measured current-voltage (I-V) curves (Figure 3.1.3.6c). Note that, in Figure 3.1.3.6c, current is normalized to the thickness of each line so that the resistivity of the material is equal to the inverse of the slope. AuNR@PTEBS lines were conductive without any further treatment; they exhibited a resistivity of 7.0 x $10^{-6}$ Ω·m, equivalent to a sheet resistance of 276 mΩ/sq/mil, with a relative standard deviation of 15%. The resistivity of as-deposited lines of AuNR@PEG-SH was above the limits of our measurement (330 Ω·m), as expected for inks containing a non-conductive polymer ligand.

A 30 min exposure to a $H_2$/Ar-plasma removed the organic ligands from the AuNR@PEG-SH film to below the detection limits of Raman spectroscopy, and the film became conductive. The structure of the nanorods was largely retained during the treatment (Figure 3.1.3.6b), but the ligand shell removal caused volume shrinkage. The resistivity of the plasma-annealed AuNR line was 4.5 x $10^{-6}$ Ω·m (177 mΩ/sq/mil). This is about one order of magnitude above the resistivities reported for fully sintered, nanoparticle-based inks where individual particles cannot be distinguished anymore.[35]

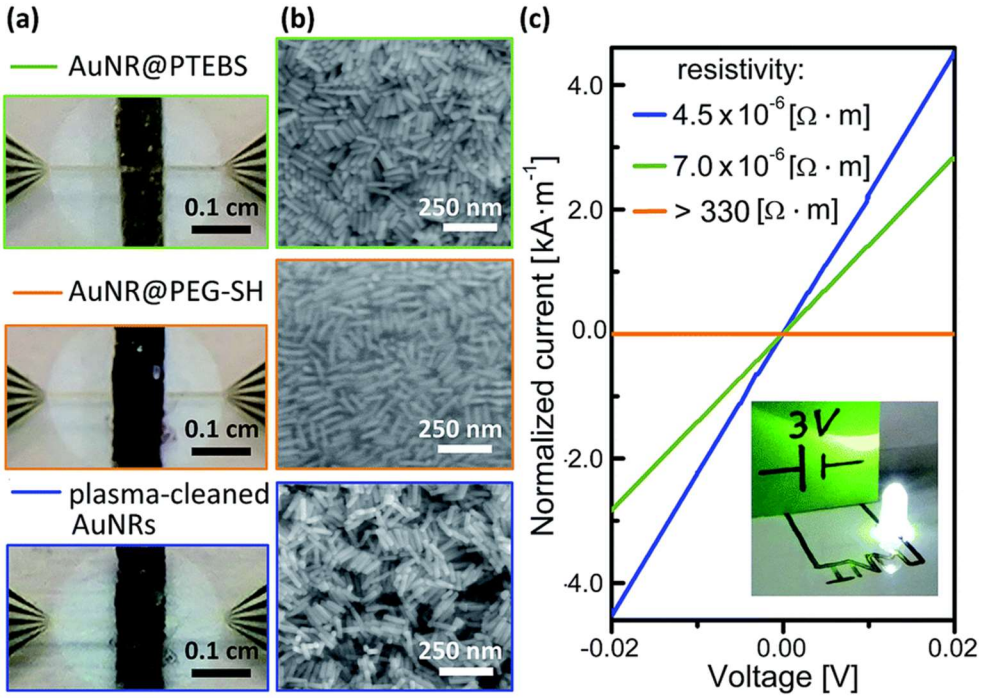


**Figure 3.1.3.6** (a) Photographs and (b) SEM images of AuNR lines prepared for electrical testing. (c) I-V curves with current normalized to film thickness; inset: circuit drawn on glossy paper using a fountain pen loaded with AuNR@PTEBS ink.

The resistivity of the AuNR@PTEBS lines ($7.0 \times 10^{-6}$ Ω·m) is less than double that of the plasma-treated AuNR. This resistivity is about 250 times that of bulk gold and similar to that of nichrome.[36] It is considerably lower (about 10,000 times) than that of purely organic conductive polymers and mixtures such as poly(3,4-ethylenedioxy-thiophene) with polystyrene sulfonate (PEDOT:PSS).[37]

The sinter-free formulation can be applied like a regular ink: we loaded a fountain pen with AuNR@PTEBS at 25 mg/mL (2.6 wt%) in an isopropanol/water 10/90 (v/v) mixture and drew a circuit on glossy paper (Figure 3.1.3.6c, inset). The pattern dried within minutes and was conductive enough to power a light-emitting diode (LED).

### *Applicability to other polymers*

We assessed the versatility of the developed ligand exchange protocol using a structurally different polymer: PEDOT:PSS. This polymer fulfills the requirements for ligands listed above. No changes in the ligand exchange procedure were required to successfully coat AuNRs with PEDOT:PSS.

The resulting AuNR@PEDOT:PSS dispersions possessed a negative zeta potential (-45 mV) similar to that of AuNR@PTEBS and blueshifted LSPRs. They formed stable inks in short-chain

alcohols and in acetone. The resistivity of deposited lines of AuNR@PEDOT:PSS was 9.9 x $10^{-7}$ Ω·m (39 mΩ/sq/mil), 5 times lower than the resistivity of plasma-annealed AuNRs and 7 times lower than the line of AuNR@PTEBS. We believe that the soft PEDOT:PSS shell increases the effective contact area between nanorods. Further experiments have to be performed to clarify the exact mechanism of inter-particle charge transfer.

Long-term stability is a critical property for printed electronics, and PEDOT:PSS is acidic enough to corrode metals.[38] We performed long-term experiments and stored samples under ambient conditions. Lines of both AuNR@PTEBS and AuNR@PEDOT:PSS retained their electrical performance for at least 1 year. No visible signs of degradation occurred.

### *Ink requirements for printing*

Printing requires inks with good colloidal stability and suitable rheological properties. Agglomeration leads to inhomogeneous deposition and equipment damage,[5] inappropriate fluid properties and wetting behavior drastically reduce printing quality.[39]

Our particles are colloidally stable in a wide range of formulations. As an example, we investigated the rheological properties of a formulation that is suitable for inkjet printing, AuNR@PEDOT:PSS, 100 mg/mL (12 wt%) in isopropanol/water (10/90; v/v) and found a

- density ($\rho$) of 1.2 ± 0.02 mg/mL,
- viscosity ($\eta$) of 1.46 ± 0.15 cP, and
- surface tension ($\gamma$) of 54.1 ± 1.1 mN/m.

Commercial piezoelectric printing heads (for example the equipment sold by Microdrop technologies, Germany) often require at least 0.4 cP. The Ohnesorge (*Oh*) number (eq. 3.1.3.1) characterizes fluids in ink jet printing:

$$\mathrm{Oh} = \frac{\eta}{\sqrt{\gamma \rho a}} \qquad \text{(eq. 3.1.3.1)}$$

where a is a characteristic length, usually the nozzle diameter. Stable printing is possible[39] for *Oh* = 0.1-1.0, which implies a upper limit of the nozzle diameter of 3.3 µm for our ink suitable for very high resolution printing. It is straightforward to tune the viscosity; for example, adding 1 mg/mL of excess PEDOT:PSS (i.e. 0.1 wt% to the liquid ink) increased the viscosity to 4.6 cP, made it suitable for larger low-cost nozzles, and retained the conductivity of the printed lines.

### 3.1.4 Conclusion

In summary, thiophene-based conjugated polymers with polar side chains prove to be highly suitable ligands for AuNRs in electronic applications. We developed a simple and straightforward protocol to obtain concentrated, stable colloidal inks suitable for printing. IR and Raman spectroscopy confirmed the complete exchange of CTAB on the AuNRs. PTEBS binds in a face-on configuration with 3 layers of polymer π–stacked on the gold surface in average, a configuration that facilitates electron transport through particle-particle interfaces. Deposited, untreated films reached conductivities comparable to plasma-annealed AuNRs and no signs of degradation were observed after storing them for one year under ambient conditions.

The ligand exchange protocol is also applicable to other polythiophenes as we demonstrated by preparing AuNR@PEDOT:PSS inks. Printed films of AuNR@PEDOT:PSS reached conductivities that surpassed that of AuNR@PTEBS films.

We expect the developed ligand exchange protocol to be applicable to polythiophene derivatives beyond the two examples presented here. The concept is not limited to AuNRs: other conductive or semi-conductive nanoparticles can be coated with conductive polymer ligands to increase inter-particle charge transfer. Nanoparticle based materials in many applications can profit from this concept. Sintering-free conductive particle packings are a step towards conductive composites of nanoparticles in insulating polymer matrices.

### 3.1.5 References

(1) Perelaer, J.; Smith, P. J.; Mager, D.; Soltman, D.; Volkman, S. K.; Subramanian, V.; Korvink, J. G.; Schubert, U. S. Printed Electronics: The Challenges Involved in Printing Devices, Interconnects, and Contacts Based on Inorganic Materials. J. Mater. Chem. 2010, 20, 8446–8453.

(2) Minari, T.; Kanehara, Y.; Liu, C.; Sakamoto, K.; Yasuda, T.; Yaguchi, A.; Tsukada, S.; Kashizaki, K.; Kanehara, M. Room-Temperature Printing of Organic Thin-Film Transistors with π-Junction Gold Nanoparticles. Adv. Funct. Mater. 2014, 24, 4886–4892.

(3) Woo, K.; Bae, C.; Jeong, Y.; Kim, D.; Moon, J. Inkjet-Printed Cu Source/drain Electrodes for Solution-Deposited Thin Film Transistors. J. Mater. Chem. 2010, 20, 3877–3882.

(4) Jou, J.-H.; Hwang, P.-Y.; Wang, W.-B.; Lin, C.-W.; Jou, Y.-C.; Chen, Y.-L.; Shyue, J.-J.; Shen, S.-M.; Chen, S.-Z. High-Efficiency Low Color Temperature Organic Light Emitting Diodes with Solution-Processed Emissive Layer. Org. Electron. 2012, 13, 899–904.

(5) Kamyshny, A.; Magdassi, S. Conductive Nanomaterials for Printed Electronics. Small 2014, 10, 3515–3535.

(6) Kang, H.; Sowade, E.; Baumann, R. R. Direct Intense Pulsed Light Sintering of Inkjet-Printed Copper Oxide Layers within Six Milliseconds. ACS Appl. Mater. Interfaces 2014, 6, 1682–1687.

(7) Perelaer, J.; Abbel, R.; Wünscher, S.; Jani, R.; van Lammeren, T.; Schubert, U. S. Roll-to-Roll Compatible Sintering of Inkjet Printed Features by Photonic and Microwave Exposure: From Non-Conductive Ink to 40% Bulk Silver Conductivity in Less Than 15 Seconds. Adv. Mater. 2012, 24, 2620–2625.

(8) Tobjörk, D.; Aarnio, H.; Pulkkinen, P.; Bollström, R.; Määttänen, A.; Ihalainen, P.; Mäkelä, T.; Peltonen, J.; Toivakka, M.; Tenhu, H.; et al. IR-Sintering of Ink-Jet Printed Metal-Nanoparticles on Paper. Thin Solid Films 2012, 520, 2949–2955.

(9) Wünscher, S.; Abbel, R.; Perelaer, J.; Schubert, U. S. Progress of Alternative Sintering Approaches of Inkjet-Printed Metal Inks and Their Application for Manufacturing of Flexible Electronic Devices. J. Mater. Chem. C 2014, 2, 10232–10261.

(10) Maurer, J. H. M.; González-García, L.; Reiser, B.; Kanelidis, I.; Kraus, T. Sintering of Ultrathin Gold Nanowires for Transparent Electronics. ACS Appl. Mater. Interfaces 2015, 7, 7838–7842.

(11) Grouchko, M.; Kamyshny, A.; Mihailescu, C. F.; Anghel, D. F.; Magdassi, S. Conductive Inks with a “Built-In” Mechanism That Enables Sintering at Room Temperature. ACS Nano 2011, 5, 3354–3359.

(12) Kanehara, M.; Takeya, J.; Uemura, T.; Murata, H.; Takimiya, K.; Sekine, H.; Teranishi, T. Electroconductive π-Junction Au Nanoparticles. Bull. Chem. Soc. Jpn. 2012, 85, 957–961.

(13) Mutiso, R. M.; Sherrott, M. C.; Rathmell, A. R.; Wiley, B. J.; Winey, K. I. Integrating Simulations and Experiments To Predict Sheet Resistance and Optical Transmittance in Nanowire Films for Transparent Conductors. 2013, 7654–7663.

(14) Grzelczak, M.; Pérez-Juste, J.; Mulvaney, P.; Liz-Marzán, L. M. Shape Control in Gold Nanoparticle Synthesis. Chem. Soc. Rev. 2008, 37, 1783–1791.

(15) Gomez-Grana, S.; Hubert, F. Surfactant (Bi) Layers on Gold Nanorods. Langmuir 2011, 28, 1453–1459.

(16) Vigderman, L.; Khanal, B. P.; Zubarev, E. R. Functional Gold Nanorods: Synthesis, Self-Assembly, and Sensing Applications. Adv. Mater. 2012, 24, 4811–4841.

(17) Vigderman, L.; Manna, P.; Zubarev, E. R. Quantitative Replacement of Cetyl Trimethylammonium Bromide by Cationic Thiol Ligands on the Surface of Gold Nanorods and Their Extremely Large Uptake by Cancer Cells. Angew. Chem. Int. Ed. Engl. 2012, 51, 636–641.

(18) Leonov, A. P.; Zheng, J.; Clogston, J. D.; Stern, S. T.; Patri, A. K.; Wei, A. Detoxification of Gold Nanorods by Treatment with Polystyrenesulfonate. ACS Nano 2008, 2, 2481–2488.

(19) Rostro-Kohanloo, B. C.; Bickford, L. R.; Payne, C. M.; Day, E. S.; Anderson, L. J. E.; Zhong, M.; Lee, S.; Mayer, K. M.; Zal, T.; Adam, L.; et al. The Stabilization and Targeting of Surfactant-Synthesized Gold Nanorods. Nanotechnology 2009, 20, 434005.

(20) Zhang, Z.; Lin, M. Fast Loading of PEG–SH on CTAB-Protected Gold Nanorods. RSC Adv. 2014, 4, 17760–17767.

(21) Wijaya, A.; Hamad-Schifferli, K. Ligand Customization and DNA Functionalization of Gold Nanorods via Round-Trip Phase Transfer Ligand Exchange. Langmuir 2008, 24, 9966–9969.

(22) Nie, Z.; Fava, D.; Rubinstein, M.; Kumacheva, E. “Supramolecular” assembly of Gold Nanorods End-Terminated with Polymer “pom-Poms”: Effect of Pom-Pom Structure on the Association Modes. J. Am. Chem. Soc. 2008, 130, 3683–3689.

(23) Zijlstra, P.; Paulo, P. M. R.; Yu, K.; Xu, Q.-H.; Orrit, M. Chemical Interface Damping in Single Gold Nanorods and Its near Elimination by Tip-Specific Functionalization. Angew. Chem. Int. Ed. Engl. 2012, 51, 8352–8355.

(24) Nie, Z.; Fava, D.; Kumacheva, E.; Zou, S.; Walker, G. C.; Rubinstein, M. Self-Assembly of Metal-Polymer Analogues of Amphiphilic Triblock Copolymers. Nat. Mater. 2007, 6, 609–614.

(25) Ye, X.; Zheng, C.; Chen, J.; Gao, Y.; Murray, C. B. Using Binary Surfactant Mixtures to Simultaneously Improve the Dimensional Tunability and Monodispersity in the Seeded Growth of Gold Nanorods. Nano Lett. 2013, 13, 765–771.

(26) Tebbe, M.; Kuttner, C.; Männel, M.; Fery, A.; Chanana, M. Colloidally Stable and Surfactant-Free Protein-Coated Gold Nanorods in Biological Media. ACS Appl. Mater. Interfaces 2015, 7, 5984–5991.

(27) Novo, C.; Funston, A. M.; Gooding, A. K.; Mulvaney, P. Electrochemical Charging of Single Gold Nanorods. J. Am. Chem. Soc. 2009, 131, 14664–14666.

(28) Zhang, S.; Pelligra, C. I.; Keskar, G.; Jiang, J.; Majewski, P. W.; Taylor, A. D.; Ismail-Beigi, S.; Pfefferle, L. D.; Osuji, C. O. Directed Self-Assembly of Hybrid Oxide/Polymer Core/Shell Nanowires with Transport Optimized Morphology for Photovoltaics. Adv. Mater. 2012, 24, 82–87.

(29) Colle, R.; Grosso, G.; Ronzani, A.; Zicovich-Wilson, C. M. Structure and X-Ray Spectrum of Crystalline poly(3-Hexylthiophene) from DFT-van Der Waals Calculations. Phys. status solidi 2011, 248, 1360–1368.

(30) Chen, M. S.; Niskala, J. R.; Unruh, D. A.; Chu, C. K.; Lee, O. P.; Fréchet, J. M. J. Control of Polymer-Packing Orientation in Thin Films through Synthetic Tailoring of Backbone Coplanarity. Chem. Mater. 2013, 25, 4088–4096.

(31) Tanaka, D.; Inuta, Y.; Sakamoto, M.; Furube, A.; Haruta, M.; So, Y.-G.; Kimoto, K.; Hamada, I.; Teranishi, T. Strongest π–metal Orbital Coupling in a Porphyrin/gold Cluster System. Chem. Sci. 2014, 5, 2007–2010.

(32) Abe, Y.; Kanehara, M.; Kanai, K. Electronic Structure of Phthalocyanine Derivative-Protected π-Junction Au Nanoparticles. Org. Electron. 2014, 15, 3465–3470.

(33) Liu, Y.-F.; Krug, K.; Lee, Y.-L. Self-Organization of Two-Dimensional poly(3-Hexylthiophene) Crystals on Au(111) Surfaces. Nanoscale 2013, 5, 7936–7941.

(34) Sajanlal, P. R.; Sreeprasad, T. S.; Samal, A. K.; Pradeep, T. Anisotropic Nanomaterials: Structure, Growth, Assembly, and Functions. Nano Rev. 2011, 2, 5883–5945.

(35) Määttänen, A.; Ihalainen, P.; Pulkkinen, P.; Wang, S.; Tenhu, H.; Peltonen, J. Inkjet-Printed Gold Electrodes on Paper: Characterization and Functionalization. ACS Appl. Mater. Interfaces 2012, 4, 955–964.

(36) Neelakanta, P. S. Handbook of Electromagnetic Materials: Monolithic and Composite Versions and Their Applications; 1st ed.; CRC Press, 1995.

(37) Mengistie, D. A.; Ibrahem, M. A.; Wang, P.; Chu, C. Highly Conductive PEDOT:PSS Treated with Formic Acid for ITO-Free Polymer Solar Cells. ACS Appl. Mater. Interfaces 2014, 6, 2292–2299.

(38) Glover, C. F.; McGettrick, J.; Williams, G.; Watson, T. M.; Bryant, D. A Scanning Kelvin Probe Investigation of the Interaction of PEDOT:PSS Films with Metal Surfaces and Potential Corrosion Protection Properties. J. Electrochem. Soc. 2015, 162, H799–H805.

(39) Derby, B. Inkjet Printing of Functional and Structural Materials: Fluid Property Requirements, Feature Stability, and Resolution. Annu. Rev. Mater. Res. 2010, 40, 395–414.

## 3.2 Supporting Information: Gold nanorods with conjugated polymer ligands: sintering-free conductive inks for printed electronics

### 3.2.1 Experimental section

#### *Materials*

All chemicals were used as received without further purification.

Poly[2-(3-thienyl)-ethyloxy-4-butylsulfonate] (PTEBS) (Mw = 40-70 kDa) was purchased from Solaris Chem Inc., (Quebec, Canada).

Poly(3,4-ethylenedioxythiophene) polystyrene sulfonate (PEDOT:PSS) (dry, re-dispersible pellets; resistance: 200-450 Ω/sq) was purchased from Sigma-Aldrich, (Steinheim, Germany).

O-[2-(3-mercaptopropionylamino)ethyl]-O'-methylpolyethylene glycol (PEG-SH) (Mw = 20 kDa) was purchased from Sigma-Aldrich, (Steinheim, Germany).

Thiophene (≥ 99%) was purchased from Sigma-Aldrich, (Steinheim, Germany).

Cetylammoniumbromide (≥ 99%) was purchased from Sigma-Aldrich, (Steinheim, Germany).

Other chemicals were analytical-grade reagents, and all solutions were prepared using Milli-Q water.

Sputtered gold electrodes were purchased from ABTECH Scientific, Inc. (South Carolina 29621, USA).

Silver paste (G3692) was purchased from Plano GmbH (Wetzlar, Germany).

#### *Characterization*

Widths and lengths of the AuNRs were evaluated through transmission electron microscopy (TEM) (JEM 2010, JEOL, Japan) operating at 200 kV. The mean lengths of the short and long axes were calculated by evaluating 726 AuNRs in TEM images. Volume and surface area were calculated using a cylinder with a hemisphere attached at each tip as a model (table S1). Zeta potentials were measured in triplicate on colloidal dispersions containing 1 mM KCl using a Nano ZSP Zetasizer (Malvern, Germany) at 25°C and the data were analyzed based on the Smoluchowski model. Optical characterization of the dispersions was performed with a UV-vis/NIR spectrophotometer (Cary 5000, Varian, CA, USA) in absorbance mode. Fourier transform infrared (FTIR) spectra were recorded in the ATR modus using a Tensor 27 spectrometer (Bruker, Germany). Raman spectra were recorded on a Raman Labram HR

Evolution spectrometer (Horiba Jobin Yvon, Germany) using a 782 nm near-IR laser diode. For thermogravimetric analysis (TGA), colloids were washed 3 times with Milli-Q water, dried in an $Al_2O_3$ crucible at room temperature, placed in a STA Jupiter 449 F 3 analyzer (Netzsch, Germany), and heated at 10 °C/min from 50 to 800 °C under an argon atmosphere. Ligand shell volume fractions and thicknesses were calculated from the organic mass fraction obtained by TGA (Table S3.2.1.1). Inductively coupled plasma mass spectrometry (ICP-MS) was used to determine the polymer distribution in a AuNR@PTEBS dispersion by comparing the sulfur content before and after removing the nanoparticles by centrifugation. The sulfur content (isotope m/z: 32) was measured on an ELEMENT XR mass spectrometer (Thermo Fisher, Germany) with 1250 W plasma power and external calibration with PTEBS standards ($R^2$: 0.998). Each sample was measured 30 times to calculate the mean value and the standard deviation. Electrical measurements were done with a 2450 Sourcemeter (Keithley Instruments, Ohio, USA); the relative standard deviation was calculated from the averages of 10 measurements on each of 4 samples. Scanning electron microscopy (SEM) images were recorded after film deposition on glass with a Quanta 400 ESEM (FEI, Germany). The thickness of the deposited AuNR patterns was measured with a Surfcom 1500SD3 profilometer (Zeiss, Germany). We removed non-conductive ligands by 30 min exposure to $H_2$/Ar (5/95 (v/v)) RF plasma (100 W) at 0.3 mbar gas pressure in a PICO plasma reactor (Diener electronic, Ebhausen, Germany). The surface tension of the inks was measured with the pendant drop method in an OCA 35 setup (Dataphysics, Germany) using the Young-Laplace equation. A digital camera was used to record the shape of the pendant drop. Mean values and the standard deviations were calculated from a minimum of 200 measured surface tension values. Dynamic viscosity of the ink at room temperature was measured in the rotation mode of a PHYSICA MCR 300 modular compact rheometer (Anton Paar, Germany). Mean values and the standard deviations were calculated from a minimum of 10 shear experiments.

**Table S3.2.1.1** Properties of AuNR@PTEBS.

| Au core | | | Ligand shell | | |
|---|---|---|---|---|---|
| 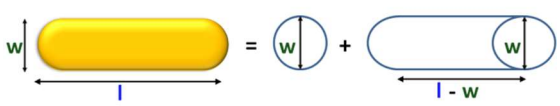 | | | 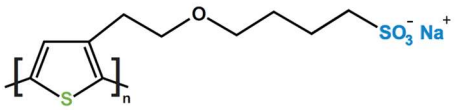 | | |
| **Length (TEM)** | 113 | nm | **Mass fraction (TGA)** | 2.9 | % |
| **Width (TEM)** | 25 | nm | **Volume fraction (calculated)** | 16.1 | % |
| **Density (literature[1])** | 19.3 | g/cm³ | **Density (literature[2,3])** | 3.5 | g/cm³ |
| **Volume (calculated)** | 51380 | nm³ | **Volume (calculated)** | 8300 | nm³ |
| **Surface area (calculated)** | 8875 | nm² | **Thickness (calculated)** | 0.9 | nm |

### *Nanoparticle synthesis and ligand exchange*

Gold nanorods (AuNR@CTAB) were prepared following a published protocol[4] and washed to ensure an excess CTAB concentration of below 80 µM (Note that literature[5] recommended concentrations below 100 µM, however we found that concentrations below 80 µM were preferable in our case). The washed AuNRs were immediately incubated with the new ligand at room temperature under vigorous stirring in order to prevent agglomeration due to the low CTAB concentration. After the incubation time (2-8 h), the AuNR@PTEBS were separated from the excess PTEBS by centrifugation. PTEBS remaining in the supernatant was quantified by UV-vis spectroscopy to estimate the amount of polymer adsorbed on the nanorods (Figure S3.2.1.2). The remaining concentration was used to calculate the PTEBS surface coverage of the AuNRs and thus, the polymer/surface ratio required to form a sufficiently dense polymer ligand layer. We found that AuNRs could be redispersed only for PTEBS ratios above 5.6 mg/m$^2$. Ratios below 6.7 mg/m$^2$ provided AuNRs that were stable but only for a few hours to a few days. Larger ratios yielded AuNRs that were stable for weeks. Figure S3.2.1.1 compares colloidal dispersions after ligand exchange with insufficient (left) and sufficient (right) PTEBS. We attribute the differences in colloidal stability to the ligand surface density. Table 2 shows PTEBS surface coverage calculated from the amount of PTEBS remaining in the supernatant. The values indicate an increase in coverage for up to a PTEBS/surface ratio of 9.0 mg/m², with saturation for greater values.

We also studied the incubation time required for ligand exchange using the blueshift in the AuNRs L-LSPR band. No change in the L-LSPR band occurred after 8 h regardless of the PTEBS

excess employed. In summary, we recommend a reaction time of 8 h and a PTEBS/surface ratio equivalent to 9-10 mg/m² to obtain complete ligand exchange reliably. For example, to obtain 10 mg/mL of AuNR@PTEBS, 5 mL of AuNR@CTAB in a concentration of 20 mg/mL (equivalent surface area of 0.886 $m^2$) was incubated with 5 mL of a 1.6 mg/mL of PTEBS solution.

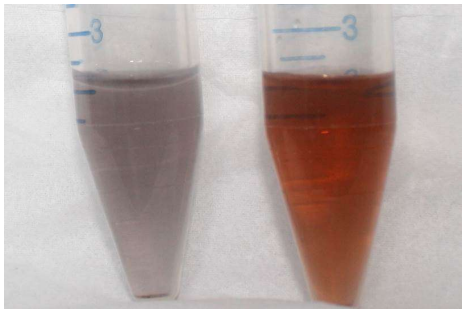

**Figure S3.2.1.1** Photograph of dispersions after redispersion in Milli-Q water subsequently to ligand exchange with a PTEBS/Au surface area ratio of left: 2.8 mg/m² and right: 11.3 mg/m².

### *Calibration of PTEBS concentration and measurements*

Aqueous solutions containing between 0.1 and 250 µg/mL of PTEBS were prepared and their integrated absorbance between 310 and 550 nm was measured. The peak area showed a linear dependence of the PTEBS concentration throughout the full concentration range (Figure S3.2.1.2). We used the PTEBS concentration decrease in the supernatant and the known amount of gold surface area in the reaction mixture to calculate PTEBS surface coverage.

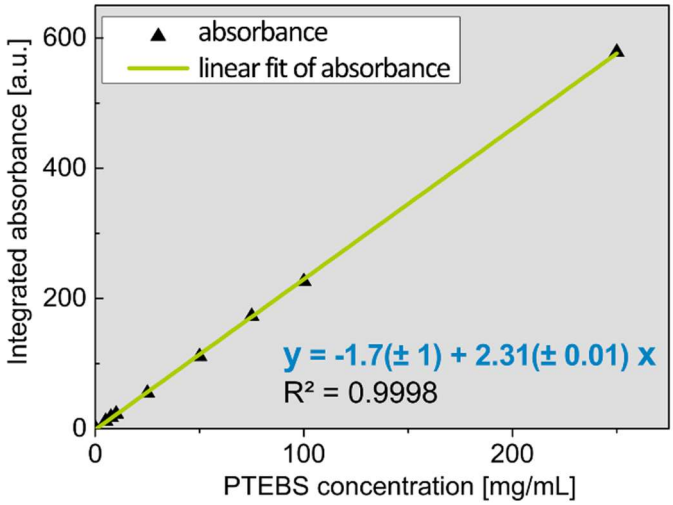


**Figure S3.2.1.2** Calibration curve for aqueous solution of PTEBS: Integrated absorbance from 310 and 550 nm versus PTEBS concentration.

**Table S3.2.1.2** Quantification of PTEBS adsorbed onto AuNRs using the external calibration curve (Figure S3.2.1.2). Incubation time: 2 h.

| PTEBS concentration [µg/mL] | PTEBS mass –Au surface ratio [mg/m$^2$] | PTEBS in the supernatant [µg/mL] | PTEBS adsorbed onto AuNRs [µg/mL] | Estimated AuNR surface coverage [mg/m$^2$] |
|---|---|---|---|---|
| 250 | 2.8 | 193.5 | 56.5 | 0.6 |
| 500 | 5.6 | 391.7 | 108.3 | 1.1 |
| 600 | 6.7 | 481.1 | 118.9 | 1.2 |
| 800 | 9.0 | 632.7 | 167.3 | 1.7 |
| 1000 | 11.3 | 833.6 | 166.4 | 1.7 |

### *Layer preparation*

AuNR patterns were prepared by depositing 10 µL of the inks (25 mg/mL, 3 wt% gold content, dispersed in a mixture of methanol/water (60/40; v/v)) on a glass substrate. PDMS stencil masks, placed on the substrate and separated 1 mm, were used to define the deposition area. Lines were dried at room temperature overnight to ensure complete drying before performing the electrical tests.

The cartridge of a commercial fountain pen was loaded with sintering-free ink containing 25 mg/mL (3 wt%) of gold dispersed in a mixture of isopropanol/water (10/90; v/v). Glossy paper (for photographic prints) was used as the substrate. A light-emitting diode (LED) and batteries were connected to the circuit with silver paste. Photographs of the writing and the circuit are shown in Figure S3.2.1.3.

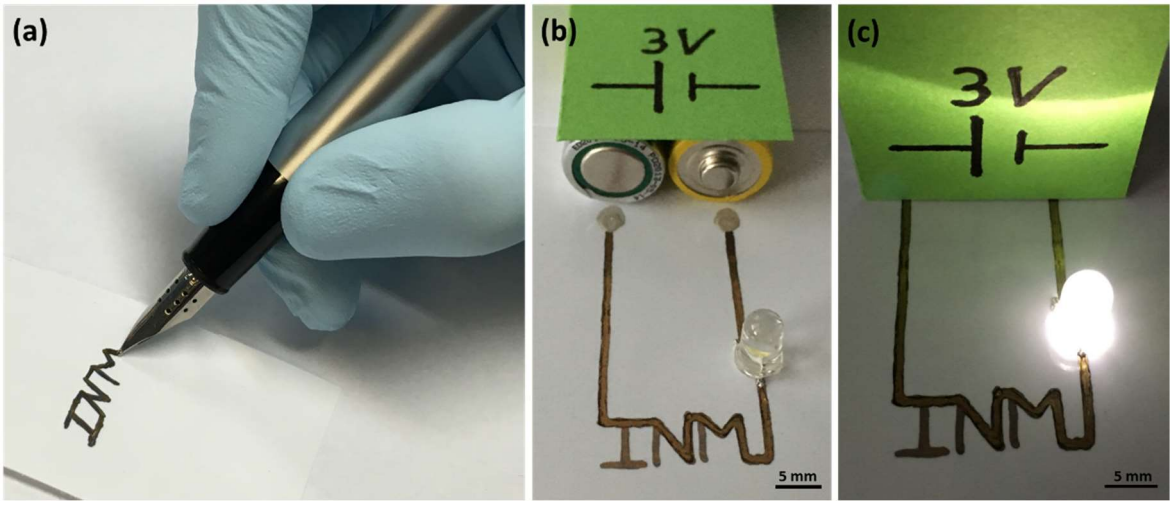


**Figure S3.2.1.3** Photographs of (a) writing, (b) the open circuit, and (c) the closed circuit.

### 3.2.2 Comparison of PTEBS and thiophene adsorbed onto AuNRs

We deposited AuNR@CTAB films, subjected them to $H_2$/Ar plasma for 30 min, and dipped them into pure thiophene for 5 minutes to create AuNR@Thiophene films. Residual thiophene was evaporated at room temperature before the measurement.

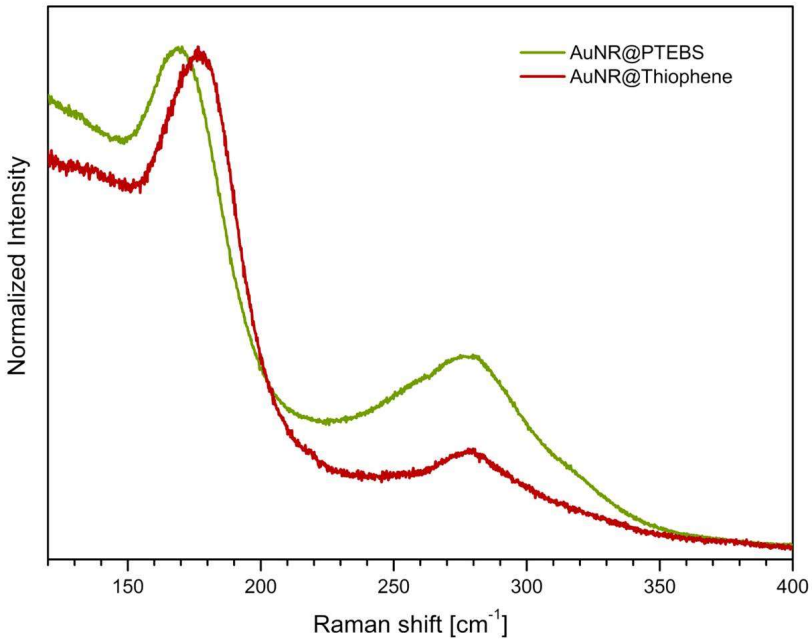


**Figure S3.2.2.4** Normalized Raman spectra of AuNR@PTEBS and AuNR@Thiophene.

### 3.2.3 References

(1) CRC Handbook of Chemistry and Physics; Lide, D. R., Ed.; 84th ed.; CRC Press. Boca Raton, Florida, 2003.

(2) Colle, R.; Grosso, G.; Ronzani, A.; Zicovich-Wilson, C. M. Structure and X-Ray Spectrum of Crystalline poly(3-Hexylthiophene) from DFT-van Der Waals Calculations. Phys. status solidi 2011, 248, 1360–1368.

(3) Zhang, S.; Pelligra, C. I.; Keskar, G.; Jiang, J.; Majewski, P. W.; Taylor, A. D.; Ismail-Beigi, S.; Pfefferle, L. D.; Osuji, C. O. Directed Self-Assembly of Hybrid Oxide/Polymer Core/Shell Nanowires with Transport Optimized Morphology for Photovoltaics. Adv. Mater. 2012, 24, 82–87.

(4) Ye, X.; Zheng, C.; Chen, J.; Gao, Y.; Murray, C. B. Using Binary Surfactant Mixtures to Simultaneously Improve the Dimensional Tunability and Monodispersity in the Seeded Growth of Gold Nanorods. Nano Lett. 2013, 13, 765–771.

(5) Tebbe, M.; Kuttner, C.; Männel, M.; Fery, A.; Chanana, M. Colloidally Stable and Surfactant-Free Protein-Coated Gold Nanorods in Biological Media. ACS Appl. Mater. Interfaces 2015, 7, 5984–5991.

## 3.3 Publication 2: Multivalent bonds in self-assembled bundles of ultrathin gold nanowires

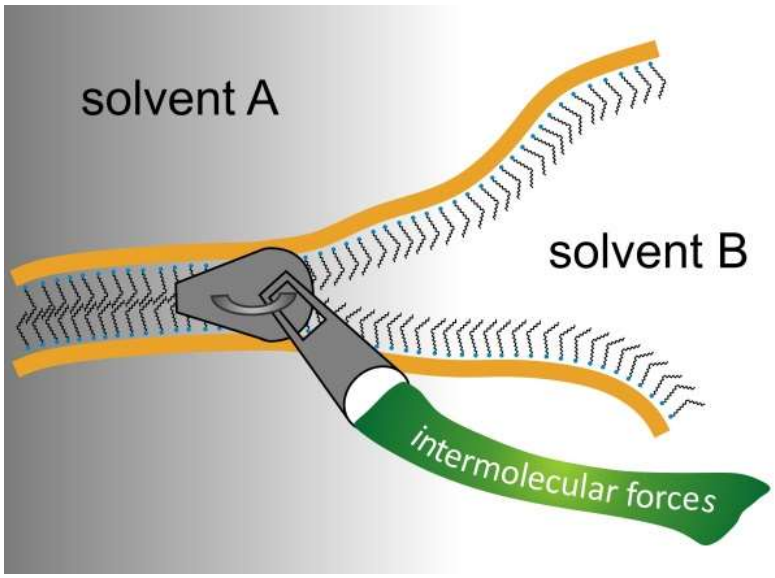


**Reiser, B**.; Gerstner, D.; González-García, L.; Maurer, J. H. M.; Kanelidis, I.; Kraus, T. Multivalent Bonds in Self-Assembled Bundles of Ultrathin Gold Nanowires. *Phys. Chem. Chem. Phys.* **2016**.

Reprinted with permission of all authors. Copyright (2016) Royal Society of Chemistry.[f3]

[f3] Note that Figure, Table and equation numbers as well as section names and numbers have been adapted to ensure consistent labeling and numbering throughout the whole thesis. Some Figures have been rearranged and resized to better fit the format of the thesis.

### 3.3.1 Abstract

Ultrathin gold nanowires are unusual colloidal objects that assemble into bundles with line contacts between parallel wires. Each molecule in the contact line interacts with many ligand and solvent molecules. We used X-ray scattering and electron microscopy to study how these interactions control assembly.

### 3.3.2 State of the art

Ultrathin gold nanowires (AuNW) can be prepared using scalable wet-chemical protocols, which makes them interesting building blocks for functional materials.[1] The wires have already been used as active components for surface-enhanced Raman scattering (SERS) substrates[2], sensors[3], and transparent electronics[4,5] and are promising candidates for nanoscale interconnects.[6] Oleylamine (OAm) that is tethered to the particles' surface serves as a ligand and provides good colloidal stability in organic solvents.[1] The small diameters (below 2 nm) and high aspect ratios (> 1000) of AuNWs lend them high mechanical flexibility.[7] It is possible to coil functionally coated AuNWs into nanosprings that store mechanical energy.[8] The wires can bundle into hexagonal superstructures and adapt to complex shapes[9]; this ability has been exploited to print them as conductive grids.[4]

Self-assembly is an elegant and cost-effective route to fabricate functional particle superstructures.[9] Controlled self-assembly of AuNWs is a realistic way to fabricate hierarchical 3D architectures.[10] They could, for instance, serve as key components in self-assembled electronic circuits.[4,11] Engineering self-assembled superstructures requires a substantiated understanding of nanoparticle interactions. However, the current understanding of the relevant interactions of AuNWs and other nanoparticles with characteristic dimensions in the range of 1-20 nm is limited. The sizes of the stabilizing ligands and the solvent molecules are on the same order of magnitude as the particle cores for such particles. The interactions between their surface ligands can exceed the cores' interactions by far.[12,13] Classical theories of colloidal particle-particle interactions, such as the Derjaguin-Landau-Verwey-Overbeek (DLVO) theory, do not satisfactorily describe the behavior of nanoparticles with diameters below 20 nm; for instance, they do not consider ligand-ligand and ligand-solvent interactions.[14] We believe that such particles are better understood in terms of intermolecular interactions, with the concepts of multi- or polyvalency that are used in biochemistry and supramolecular chemistry.[15,16] Ultrathin nanowires that form line contacts have been

described as polymer analogues.[17] In a figurative sense, the gold core of AuNWs would be the polymer backbone and the ligands the side chains that cause supramolecular interactions.

Because ligands dominate their behavior, the assembly of very small particles can be tuned *via* ligand type[18] and ligand conformation[19] as a step towards the rational design of particle self-assembly. But the choice of ligands that yield anisotropic particles in wet-chemical synthesis is very limited[20] and ligand exchange is often challenging. Recent studies suggest that the solvent, which is relatively easy to exchange, can also influence nanoparticle assembly in dispersion.[18,21] Solvent effects have previously been studied for isotropic particles;[22] here, we study highly anisotropic wires.

We investigated how ligand-solvent interactions affect the superstructure formation of AuNWs in dispersion using small-angle X-ray scattering (SAXS). We demonstrate that the solvent determines whether ordered superstructures form, their formation kinetics, and the wire-wire distance. We found that ligand excess in solution affects the packing density of the superstructures and propose a model based on weak intermolecular interactions to explain the solvent dependence of AuNW bundling. Experiments on AuNW growth in different solvents prove that ligand-solvent interactions also impact the anisotropic particle growth of AuNWs.

### 3.3.3 Results and discussion

Ultrathin AuNWs were synthesized using a protocol adapted from Feng *et al.*[2] that is described in the Supporting information. The synthesis uses oleylamine (OAm) to induce wire growth in *n*-hexane. During synthesis, OAm serves as structure directing agent; it adsorbs on the gold wires with its amine functionality, where it serves as a ligand and provides colloidal stability.

We analyzed as-synthesized AuNW dispersions in the liquid state by SAXS and found wires bundled into hexagonal arrangements with a lattice parameter of 9.2 nm (Figure 3.3.3.1a). Bundles with a lattice parameter of 9.7 nm have previously been described by Loubat *et al.*[23] for 1.7 nm thick wires. Oleylamine has a length of approximately 2 nm in its fully stretched conformation;[24,25] Loubat *et al.* concluded that four OAm molecules separated the gold wires inside a bundle.[23] We find 0.5 nm shorter wire-wire distances that we attribute to stronger OAm interdigitation. The alkane chains of OAm can interlock like the teeth of a zipper as shown in Figure 3.3.3.1c. What determines the extent of interdigitation?

Osmotic pressure exerted by solute molecules is a likely candidate. OAm is used in excess during synthesis, and free OAm may affect the wire-wire distance. We synthesized AuNWs, adjusted the OAm concentration as described in the ESI, and studied the dispersions with SAXS (Figure 3.3.3.1a and 3.3.3.1.1b). All SAXS patterns confirmed hexagonal packing of wires; the Bragg peaks shifted towards larger scattering angles with increasing OAm volume fraction (Figure 3.3.3.1a). The center-to-center distance of the wires was calculated from the scattering angle of the first Bragg peak (10). It decreased monotonously with the total OAm volume fraction in the dispersion (Figure 3.3.3.1b). We believe that the increasing OAm concentration causes an osmotic pressure that drives out solvent molecules from inside of the bundles in order to dilute the free OAm. Interdigitation of the ligand shells thus increases with free OAm concentration as shown in Figure 3.3.3.1c.

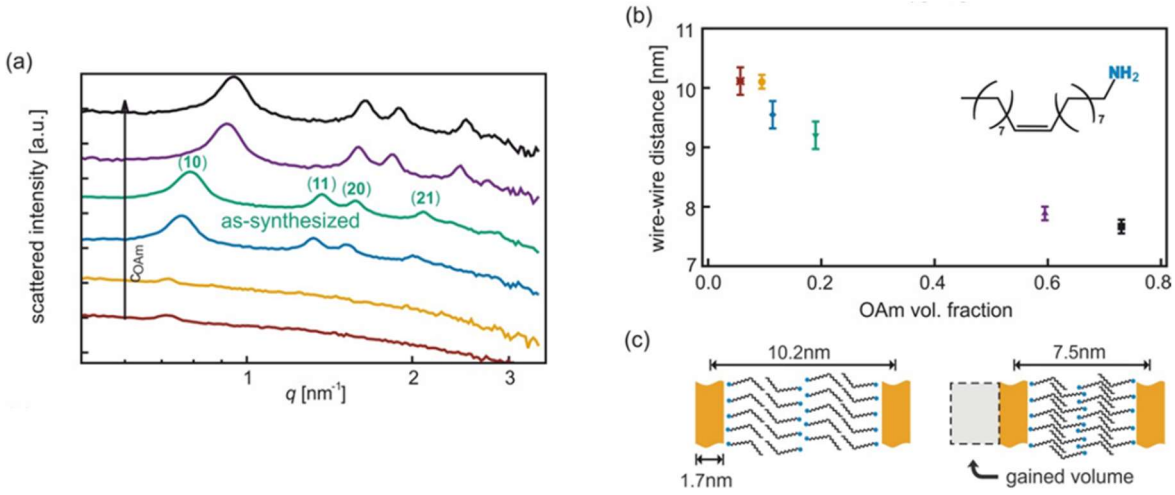


**Figure 3.3.3.1** (a) Normalized SAXS patterns of as-synthesized AuNWs dispersed at different volume fractions of OAm. (b) Wire-wire distance depending on free OAm volume fraction in solution. Inset: skeletal formula of OAm. (c) Schematic illustration of OAm interdigitation for the closest and the least close wire-packing observed and of the difference in solvent volume enclosed between two wires for both cases.

London dispersion interactions between the alkane chains of the tethered OAm molecules become stronger with increasing interdigitation.[12,26] This explains the increasing intensity of the Bragg peaks with increasing OAm volume fraction (Figure 3.3.3.1a): The denser the packing of the OAm is between the wires, the stronger are the multivalent interactions between them, and the greater is the fraction of ordered bundles in the overall dispersion. Similarly variable interdigitation of alkane chains has already been observed for phospholipids in water. A phase transition from a separated to an interdigitated bilayer phase is induced when increasing ethanol concentration.[27]

To reduce the OAm concentration while keeping the AuNW concentration constant, we washed as-synthesized AuNWs by repeated precipitation with ethanol and redispersion in the same volume of a fresh solvent. This procedure removed excess OAm and reduced the lattice parameter of the hexagonal bundles from 9.2 nm to 5.5 nm as previously reported by Moutet *et al.*[28] The reduced spacing is consistent with a wire-wire separation of two OAm molecules as visualized in Figure 3.3.3.2a. We assume that the washing procedure removed all OAm that was not directly tethered to the gold surfaces. The two remaining OAm monolayers interdigitate like a zipper in 3 dimensions. The resulting superlattice reminds of the inverted hexagonal phase of lipids in water[29] although the formation is driven not by hydrogen bonds (as for the lipids in water) but by dispersive interactions.

Bundling occurred slowly after redispersion in *n*-hexane (Figure 3.3.3.2b). The evolution of the first SAXS Bragg peak (10) was analyzed over time (Figure 3.3.3.2b inset) and its peak height, relative to the maximum peak height observed, was used as a measure for bundle formation. Peaks appeared after a few minutes; equilibrium was reached after 140 min, when the peak heights remained constant. Other solvents led to different bundling behavior. We exchanged the solvent after washing and followed the assembly of the AuNWs in three different solvent classes: *n*-alkanes, cycloalkanes, and arenes.

SAXS patterns were recorded 24 h after redispersion in the new solvent to ensure equilibrium. Figure 3.3.3.2c illustrates the effects of the different solvents. Gold nanowires that were redispersed in *n*-hexane and *n*-octane formed hexagonal bundles with a lattice parameter of 5.5 nm. Cyclohexane and cyclooctane prevented ordered assembly entirely; the SAXS patterns of AuNW in these solvents were dominated by the form factor of the wires (further information can be found in section 3.4.2). Dispersions of wires in arenes contained hexagonal superstructures; the AuNWs were packed tighter in arenes than in *n*-alkanes, with wire-wire distances of 5.2 - 5.3 nm.

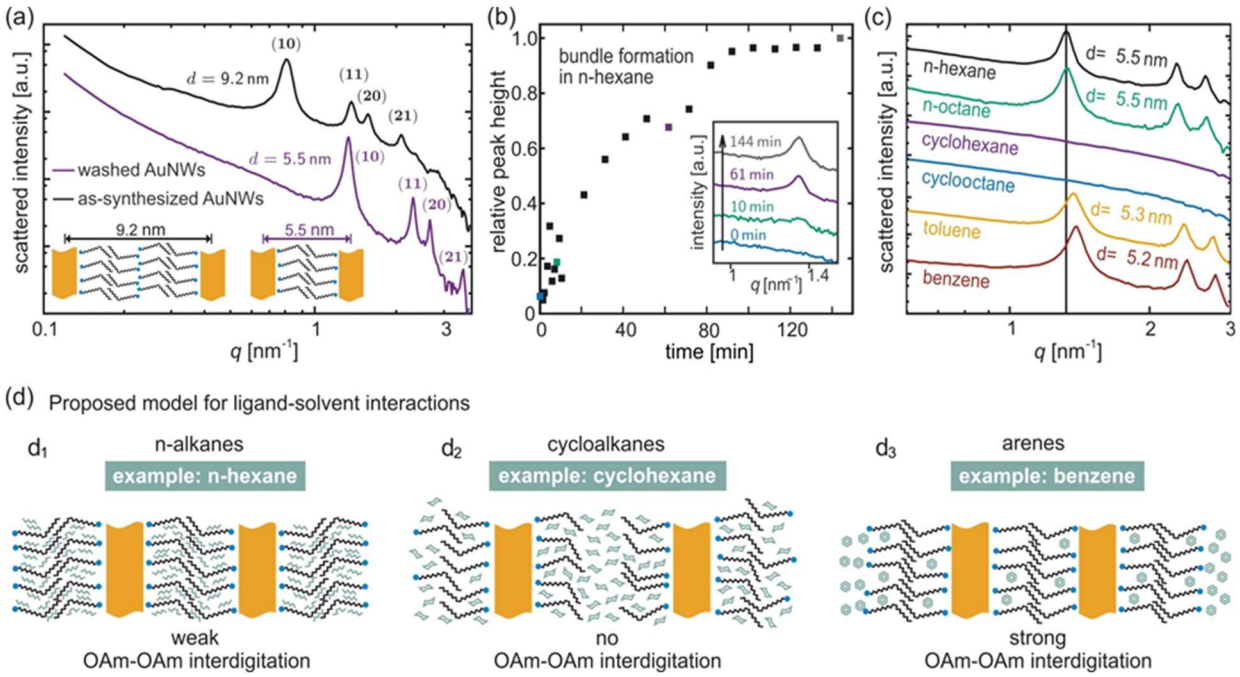


**Figure 3.3.3.2** (a) SAXS patterns of as-synthesized AuNWs and washed nanowires dispersed in *n*-hexane. Inset: Schematic depiction of the ligand layer between two bundled wires. (b) Evolution of the first Bragg peak for washed AuNWs over time when redispersed in *n*-hexane. Inset: SAXS patterns at selected times. (c) SAXS patterns of washed AuNWs recorded 24 h after redispersion in different solvents. (d) Schematic illustration of our model for the arrangement of solvents in the OAm ligand layer of AuNWs and its influence on bundling.

After redispersion vigorous shaking was required to yield a stable colloidal dispersion of AuNWs in arenes, and the dispersion contained bundles immediately after shaking. Shaking probably dispersed small bundles of wires rather than dispersing individual wires that self-assemble subsequently.

The effects of solvents discussed above support our hypothesis that weak intermolecular ligand-ligand and ligand-solvent interactions dominate the AuNW-assembly behavior, similar to assembly in supramolecular chemistry.[30,31] We propose a model for assembly that is based on the balance between an enthalpic term (intermolecular forces) and mixing entropy. London dispersion forces between AuNW-tethered OAm molecules are not specific; they will act between all solvent and ligand molecules. The entropic gain always favors mixing of different molecules; it is the enthalpic contribution that determines whether AuNWs bundle. Solvent molecules will readily intercalate into the ligand shell if ligand-ligand and solvent-solvent interactions are not considerably stronger than ligand-solvent interactions. The intercalating solvent will influence the structure of the ligand shell.[32,33] Our hypothesis is that

wires bundle when the solvent efficiently intercalates neighboring ligand shell or when most solvent is expelled from touching ligand shells.

Short-chained *n*-alkanes such as *n*-hexane have sufficient conformational flexibility to intercalate an ordered OAm ligand layer and to maximize ligand-solvent interactions.[18] Two wires with ordered ligand layers bundle to close the “OAm-teeth” of the “zipper” (Figure 3.3.3.2d1).

Cycloalkanes such as cyclohexane have less conformational flexibility. The energetically favorable "chair"-conformation of cyclohexane cannot intercalate into OAm ligand layers without disturbing their order (Figure 3.3.3.2d2). Disordered OAm layers interact less strongly with the OAm layers of other wires, and bundling becomes less likely.

Arenes have little conformational flexibility, but we did observe bundles in benzene and toluene. We believe that the relatively strong π-π-interactions between the solvent molecules[34] reduced the intercalations of solvents into the OAm ligand shell. This explains both the difficulty encountered when dispersing wires in arenes and the closer packing of the wire bundles when compared to *n*-alkanes. Little arene molecules remain in the tightly packed OAm bilayer (Figure 3.3.3.2d3).

Our interpretation is inspired by earlier models that highlight the role of the solvent’s molecular shape and the solvent-solute interactions in supramolecular assembly.[35] The solvent effects are so strong that we suspected them to affect the formation of AuNW during synthesis, too. Although the exact mechanism of AuNW growth is still under discussion, it is accepted that OAm plays a crucial role in the AuNWs’ anisotropic growth.[23,36] It is also known that solvents affect the polydispersity of spherical gold nanoparticles formed with OAm.[32]

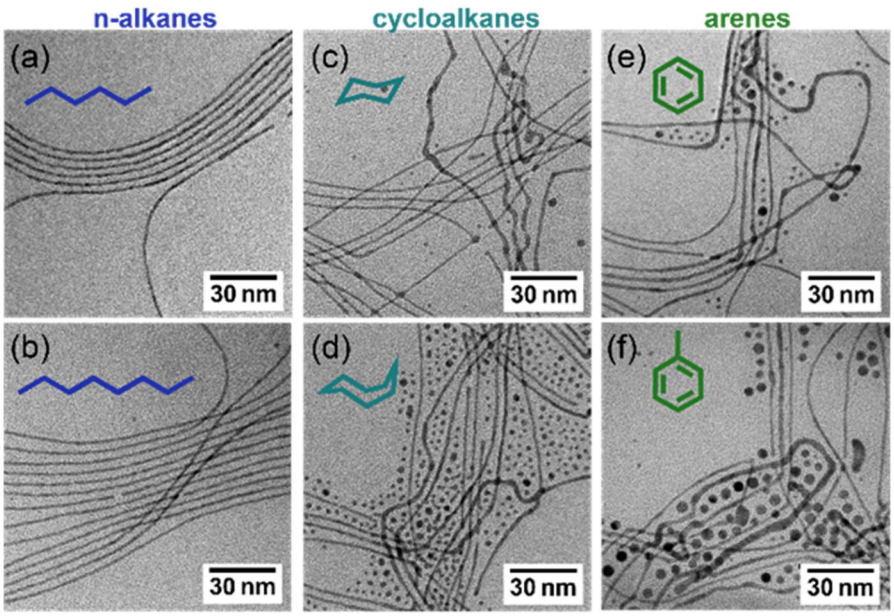


**Figure 3.3.3.3** TEM images of as-synthesized AuNWs in (a) *n*-hexane, (b) *n*-octane, (c) cyclohexene, (d) cyclooctane, e) benzene and (f) toluene. Skeletal formulas of the respective solvents are given as insets.

To test whether ligand-solvent interactions affect AuNW growth, we used the solvents introduced above for wire synthesis while leaving all other parameters unchanged. Figure 3.3.3.3 shows representative TEM images of the resulting wires (more TEM images can be found in the Supporting Information, Figure S3.4.3.1 - S3.4.3.6). *N*-alkanes, most commonly used for AuNW synthesis, yielded large fractions of wires and some small spheres. Cycloalkanes and arenes led to much higher contents of spheres and irregularly shaped wires. Less suitable solvents apparently impair wire growth, but they do not entirely prevent it. This is compatible with the hypothesis of a soft template such as OAm micelles[37] guiding anisotropic growth. The interactions between the soft templates may be affected by the solvent in a way similar to the wire-wire interactions discussed above. Anisotropic micelles, their interactions, and their assembly are well-understood in water,[29] but little is known about the prerequisites for their formation and their dynamics in unpolar solvents. Standard techniques for the analysis of aqueous micelles like SAXS are not suitable for OAm in hexane and many similar systems. Neutron scattering studies with and without metal cores could provide further insight into the dynamics of those templates.

### 3.3.4 Conclusion

In summary, we demonstrated that the intermolecular forces dominate the assembly of AuNWs that are strongly affected by solvents. Although the individual forces are weak, the synergy of bonds along the contact lines between wires increases their collective strength,

similar to the mechanisms responsible for biochemical processes like protein folding.[38] The qualitative thermodynamic model we propose here explains the role of solvents in AuNW superstructure formation and the packing density of the assemblies. It is a first step towards a detailed understanding of the ternary system of metal colloids, their ligand shells, and the dispersant. Our results suggest that the assembly of ultrathin nanowires can be exquisitely controlled through the ligand-solvent interplay. This will facilitate the assembly of AuNW building blocks into functional materials for photonic and electronic applications.

### 3.3.5 References

(1) Cademartiri, L.; Ozin, G. A. Ultrathin Nanowires-A Materials Chemistry Perspective. Adv. Mater. 2009, 21, 1013–1020.

(2) Feng, H.; Yang, Y.; You, Y.; Li, G.; Guo, J.; Yu, T.; Shen, Z.; Wu, T.; Xing, B. Simple and Rapid Synthesis of Ultrathin Gold Nanowires, Their Self-Assembly and Application in Surface-Enhanced Raman Scattering. Chem. Commun. (Camb). 2009, 1984–1986.

(3) Kisner, A.; Heggen, M.; Mayer, D.; Simon, U.; Offenhäusser, A.; Mourzina, Y. Probing the Effect of Surface Chemistry on the Electrical Properties of Ultrathin Gold Nanowire Sensors. Nanoscale 2014, 6, 5146–5155.

(4) Maurer, J. H. M.; González-García, L.; Reiser, B.; Kanelidis, I.; Kraus, T. Templated Self-Assembly of Ultrathin Gold Nanowires by Nanoimprinting for Transparent Flexible Electronics. Nano Lett. 2016, 16, 2921–2925.

(5) Gong, S.; Zhao, Y.; Yap, L. W.; Shi, Q.; Wang, Y.; Bay, J. A. P. B.; Lai, D. T. H.; Uddin, H.; Cheng, W. Fabrication of Highly Transparent and Flexible NanoMesh Electrode via Self-Assembly of Ultrathin Gold Nanowires. Adv. Electron. Mater. 2016, 2, 1600121.

(6) Roy, A.; Pandey, T.; Ravishankar, N.; Singh, A. K. Single Crystalline Ultrathin Gold Nanowires: Promising Nanoscale Interconnects. AIP Adv. 2013, 3, 32131.

(7) Wang, L.; Liu, P.; Guan, P.; Yang, M.; Sun, J.; Cheng, Y.; Hirata, A.; Zhang, Z.; Ma, E.; Chen, M.; et al. In Situ Atomic-Scale Observation of Continuous and Reversible Lattice Deformation beyond the Elastic Limit. Nat. Commun. 2013, 4, 2413.

(8) Xu, J.; Wang, H.; Liu, C.; Yang, Y.; Chen, T.; Wang, Y.; Wang, F.; Liu, X.; Xing, B.; Chen, H. Mechanical Nanosprings: Induced Coiling and Uncoiling of Ultrathin Au Nanowires. J. Am. Chem. Soc. 2010, 132, 11920–11922.

(9) Cademartiri, L.; Bishop, K. J. M. Programmable Self-Assembly. Nat. Mater. 2015, 14, 2–9.

(10) Ozin, G. A.; Hou, K.; Lotsch, B. V; Cademartiri, L.; Puzzo, D. P.; Scotognella, F.; Ghadimi, A.; Thomson, J. Nanofabrication by Self-Assembly. Mater. Today 2009, 12, 12–23.

(11) Wang, M. C. P.; Gates, B. D. Directed Assembly of Nanowires. Mater. Today 2009, 12, 34–43.

(12) Bishop, K. J. M.; Wilmer, C. E.; Soh, S.; Grzybowski, B. A. Nanoscale Forces and Their Uses in Self-Assembly. Small 2009, 5, 1600–1630.

(13) Landman, U.; Luedtke, W. D. Small Is Different: Energetic, Structural, Thermal, and Mechanical Properties of Passivated Nanocluster Assemblies. Faraday Discuss. 2004, 125, 1–22.

(14) Silvera Batista, C. A.; Larson, R. G.; Kotov, N. A. Nonadditivity of Nanoparticle Interactions. Science (80-. ). 2015, 350, 1242477–1242477.

(15) Fasting, C.; Schalley, C. A.; Weber, M.; Seitz, O.; Hecht, S.; Koksch, B.; Dernedde, J.; Graf, C.; Knapp, E.-W.; Haag, R. Multivalency as a Chemical Organization and Action Principle. Angew. Chemie Int. Ed. 2012, 51, 10472–10498.

(16) Uhlenheuer, D. A.; Petkau, K.; Brunsveld, L. Combining Supramolecular Chemistry with Biology. Chem. Soc. Rev. 2010, 39, 2817–2826.

(17) Yuan, B.; Cademartiri, L. Flexible One-Dimensional Nanostructures: A Review. J. Mater. Sci. Technol. 2015, 31, 607–615.

(18) Hajiw, S.; Schmitt, J.; Impéror-Clerc, M.; Pansu, B. Solvent-Driven Interactions between Hydrophobically-Coated Nanoparticles. Soft Matter 2015, 11, 3920–3926.

(19) Klajn, R.; Bishop, K. J. M.; Grzybowski, B. A. Light-Controlled Self-Assembly of Reversible and Irreversible Nanoparticle Suprastructures. Proc. Natl. Acad. Sci. 2007, 104, 10305–10309.

(20) Jana, N. R.; Gearheart, L.; Murphy, C. J. Seed-Mediated Growth Approach for Shape-Controlled Synthesis of Spheroidal and Rod-like Gold Nanoparticles Using a Surfactant Template. Adv. Mater. 2001, 13, 1389–1393.

(21) Goubet, N.; Richardi, J.; Albouy, P.-A.; Pileni, M.-P. Which Forces Control Supracrystal Nucleation in Organic Media? Adv. Funct. Mater. 2011, 21, 2693–2704.

(22) Cademartiri, L.; Bishop, K. J. M.; Snyder, P. W.; Ozin, G. A. Using Shape for Self-Assembly. Philos. Trans. A. Math. Phys. Eng. Sci. 2012, 370, 2824–2847.

(23) Loubat, A.; Impéror-Clerc, M.; Pansu, B.; Meneau, F.; Raquet, B.; Viau, G.; Lacroix, L.-M. Growth and Self-Assembly of Ultrathin Au Nanowires into Expanded Hexagonal Superlattice Studied by in Situ SAXS. Langmuir 2014, 30, 4005–4012.

(24) Mourdikoudis, S.; Liz-Marzán, L. M. Oleylamine in Nanoparticle Synthesis. Chem. Mater. 2013, 25, 1465–1476.

(25) Borges, J.; Ribeiro, J. A.; Pereira, E. M.; Carreira, C. A.; Pereira, C. M.; Silva, F. Preparation and Characterization of DNA Films Using Oleylamine Modified Au Surfaces. J. Colloid Interface Sci. 2011, 358, 626–634.

(26) London, F. The General Theory of Molecular Forces. Trans. Faraday Soc. 1937, 8–26.

(27) Simon, S. A.; McIntosh, T. J. Interdigitated Hydrocarbon Chain Packing Causes the Biphasic Transition Behavior in Lipid/alcohol Suspensions. Biochim. Biophys. Acta - Biomembr. 1984, 773, 169–172.

(28) Moutet, P.; Lacroix, L.-M.; Robert, A.; Impéror-Clerc, M.; Viau, G.; Ressier, L. Directed Assembly of Single Colloidal Gold Nanowires by AFM Nanoxerography. Langmuir 2015, 31, 4106–4112.

(29) Tresset, G. The Multiple Faces of Self-Assembled Lipidic Systems. PMC Biophys. 2009, 2, 3.

(30) Korevaar, P. A.; Schaefer, C.; de Greef, T. F. A.; Meijer, E. W. Controlling Chemical Self-Assembly by Solvent-Dependent Dynamics. J. Am. Chem. Soc. 2012, 134, 13482–13491.

(31) Jeon, H.-J.; Kim, C.; Song, H. H. Solvent Effects on Self-Assembly and Superstructures of Amide Dendrons. Macromol. Res. 2012, 20, 954–959.

(32) Wu, B.-H.; Yang, H.-Y.; Huang, H.-Q.; Chen, G.-X.; Zheng, N.-F. Solvent Effect on the Synthesis of Monodisperse Amine-Capped Au Nanoparticles. Chinese Chem. Lett. 2013, 24, 457–462.

(33) Herwig, K. W.; Matthies, B.; Taub, H. Solvent Effects on the Monolayer Structure of Long n−Alkane Molecules Adsorbed on Graphite. Phys. Rev. Lett. 1995, 75, 3154–3157.

(34) Hunter, C. A.; Sanders, J. K. M. The Nature of .pi.-.pi. Interactions. J. Am. Chem. Soc. 1990, 112, 5525–5534.

(35) Berrocal, J. A.; Di Meo, F.; García-Iglesias, M.; Gosens, R. P. J.; Meijer, E. W.; Linares, M.; Palmans, A. R. A. Consequences of Conformational Flexibility in Hydrogen-Bond-Driven Self-Assembly Processes. Chem. Commun. 2016, 3–6.

(36) Yu, Y.; Cui, F.; Sun, J.; Yang, P. Atomic Structure of Ultrathin Gold Nanowires. Nano Lett. 2016, 16, 3078–3084.

(37) Wang, C.; Hu, Y.; Lieber, C. M.; Sun, S. Ultrathin Au Nanowires and Their Transport Properties. J. Am. Chem. Soc. 2008, 130, 8902–8903.

(38) Dill, K. A. Dominant Forces in Protein Folding. Biochemistry 1990, 29, 7133–7155.

## 3.4 Supporting Information: Multivalent bonds in self-assembled bundles of ultrathin gold nanowires

### 3.4.1 Experimental section

#### *Chemicals*

All chemicals were used without further purification:

Oleylamine (technical grade, 70%) was purchased from Sigma-Aldrich (Germany).

Triisopropylsilane (98%) was purchased ABCR (Germany).

*N*-hexane (99 %) was purchased from ABCR (Germany).

Ethanol (99.8 %) was purchased from Sigma-Aldrich (Germany).

*N*-octane (98 %) was purchased from Sigma-Aldrich (Germany).

Cyclohexane (99 %) was purchased from Sigma-Aldrich (Germany).

Cyclooctane (99 %) was purchased from Sigma-Aldrich (Germany).

Benzene (99 %) was purchased from Sigma-Aldrich (Germany).

Toluene (99.5 %) was purchased from Sigma-Aldrich (Germany).

#### *Synthesis*

Ultrathin gold nanowires were synthesized using a protocol adapted from Feng and coworkers.[1] Briefly, $HAuCl_4$ (10 mM) was dissolved in a oleylamine:n-hexane mixture (8:27, v/v) to result in a dark yellow solution. Triisopropylsilane (1.2 M) was added and the solution was stirred vigorously for 30 s. Afterwards the reaction mixture was flushed with argon and kept undisturbed at 20°C for 16 h.

#### *Variation of the OAm volume fraction of the dispersion*

As-synthesized AuNWs were mixed with *n*-hexane or oleylamine (OAm) to adjust the volume fraction from 5 to 73 vol.% (as-synthesized AuNWs: 18 vol.%). After mixing the resulting dispersions were immediately analyzed by SAXS and all SAXS patterns were normalized to the gold content of as-synthesized wires.

#### *Washing and solvent exchange*

As-synthesized AuNWs were washed by repeated precipitation through the addition of ethanol. The supernatant was carefully removed and the wires were redispersed in the desired organic solvent. The washing step was repeated for a second time. All dispersions were kept at 4°C until further use.

### 3.4.2 Characterization

#### *TEM experiments*

1 µl of as-synthesized AuNWs was left to dry on a 400-mesh carbon coated copper grid (Plano, Germany) and then characterized by Transmission Electron Microscopy using a JEM 2010, JEOL, Germany, operating at 200 kV.

#### *SAXS experiments*

We employed a laboratory scale SAXS setup, the XEUSS 2.0 from XENOCS SA (France) equipped with a CuK$\alpha$ X-ray source and a PILATUS3 R 1M (DECTRIS, Switzerland) X-ray area detector, to record the SAXS data. All measurements were performed at room temperature, 24 hours after solvent exchange, using capillaries with an inner diameter of 1 mm. Scattering patterns of regular superlattices exhibit peaks with spacing that corresponds to the distance between planes of the (super)lattice. Given the Miller indices *h* and *k*, the maxima's positions in *q* space and the distance between single scatterers of a 2D hexagonal lattice are related by[2]:

$$q(h,k) = \frac{4\pi}{\sqrt{3}*d}\sqrt{h^2+k^2} \qquad \text{(eq. 3.4.2.1)}$$

#### *Further information extracted from SAXS data*

The SAXS pattern of AuNWs in cyclohexane (Figure S3.4.2.1) did not show any structure peaks, hence the pattern was dominated by the form factor of the wires. The minimum of scattered intensity was fit with the form factor of a cylinder[3] using the ''SASfit'' software package[4] and yielded a wire-radius of 0.85 ± 0.08 nm, which is in good agreement with TEM.

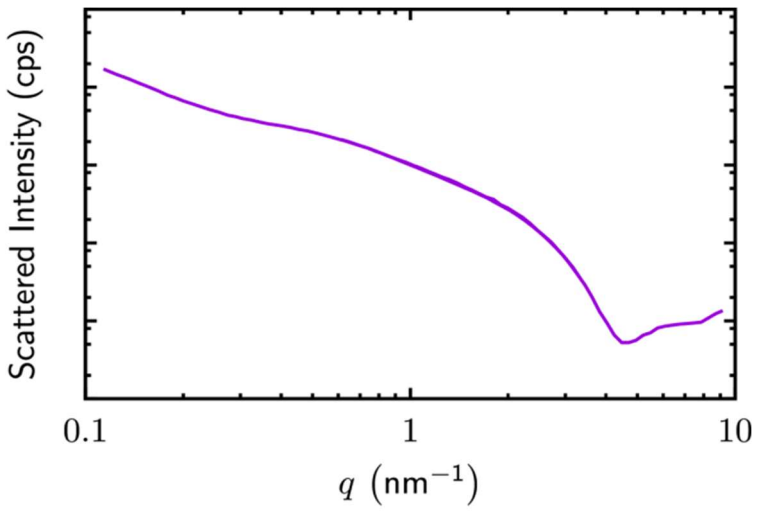


**Figure S3.4.2.1** Small-angle X-ray scattering of AuNWs in cyclohexane

### 3.4.3 Supplementary figures

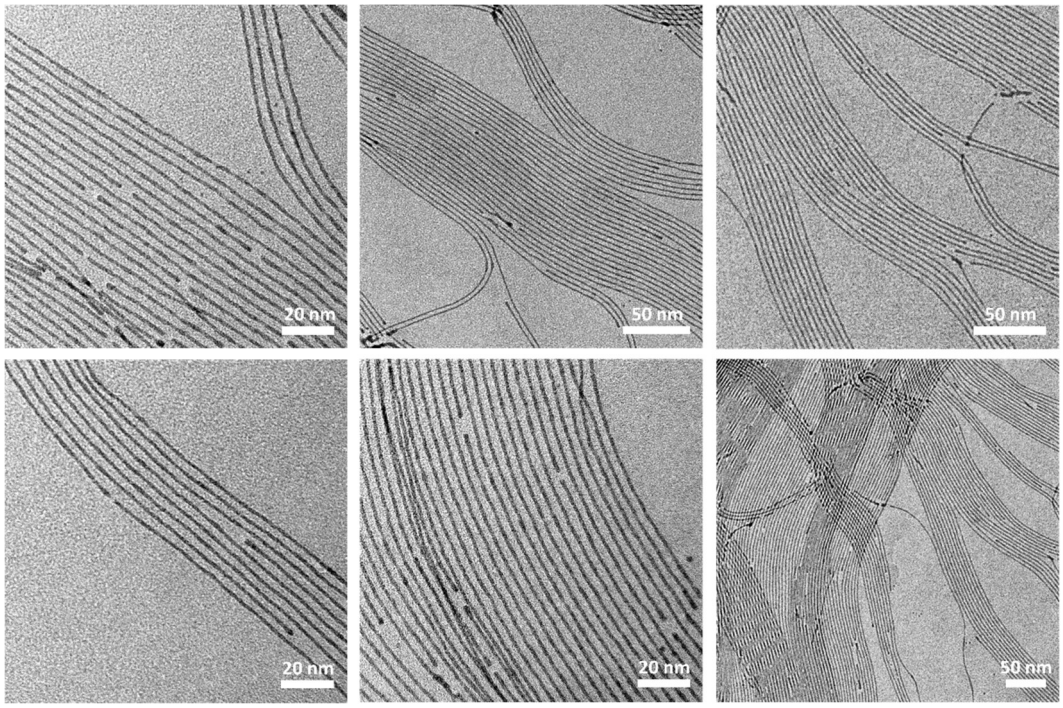


**Figure S3.4.3.2** Representative TEM images of AuNWs synthesized in *n*-hexane.

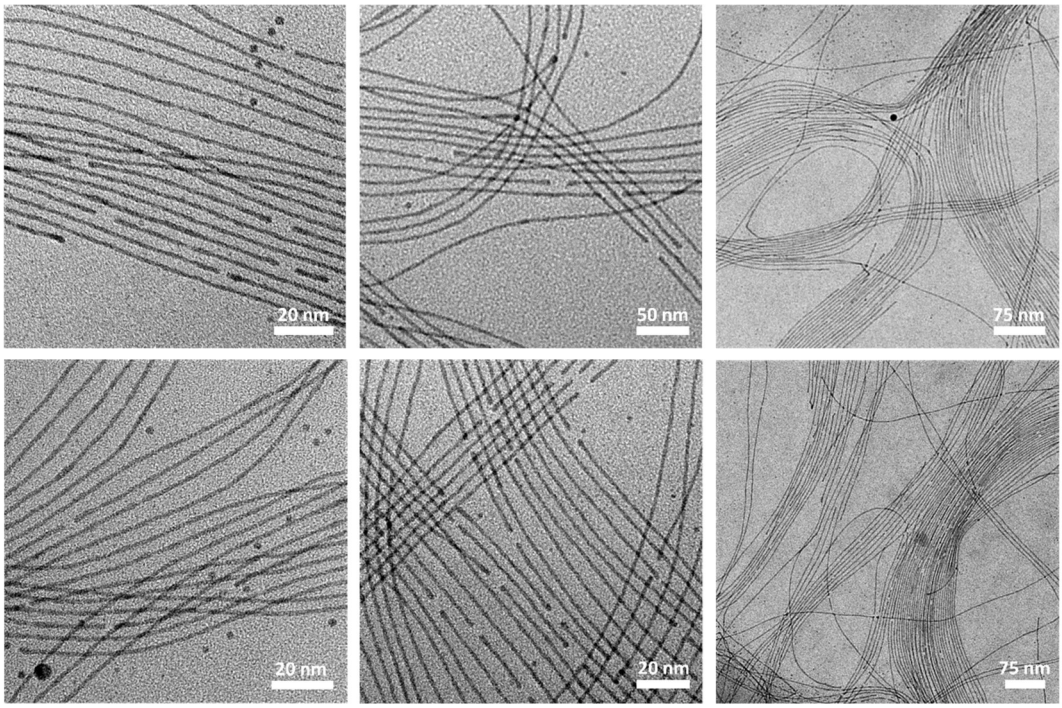


**Figure S3.4.3.3** Representative TEM images of AuNWs synthesized in *n*-octane.

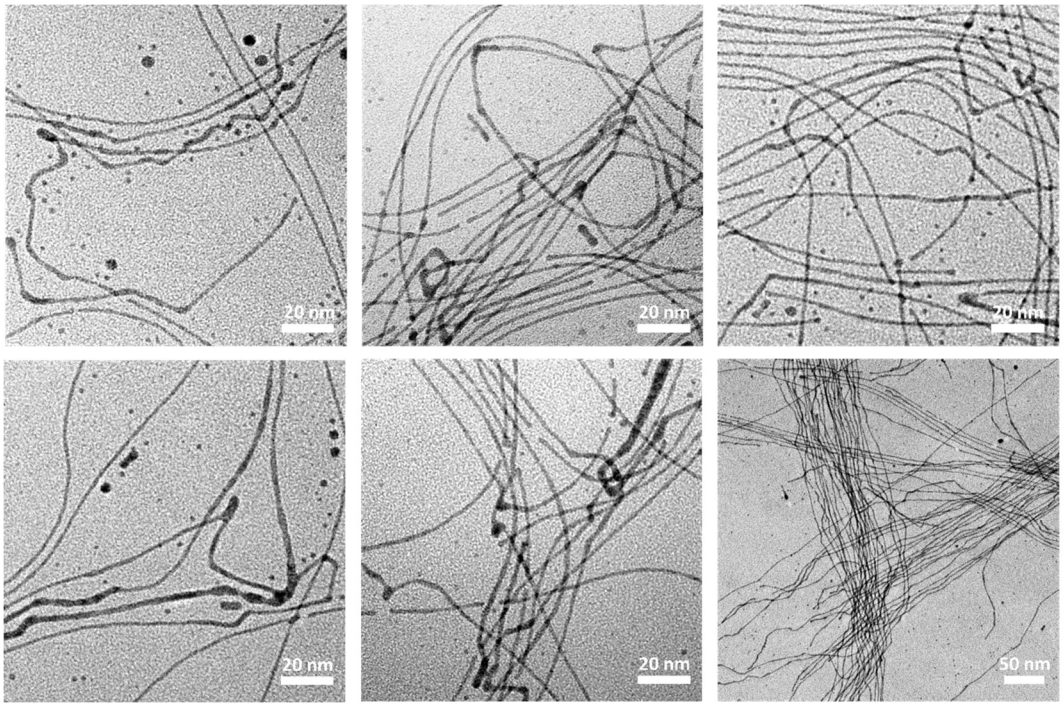


**Figure S3.4.3.4** Representative TEM images of AuNWs synthesized in cyclohexane.

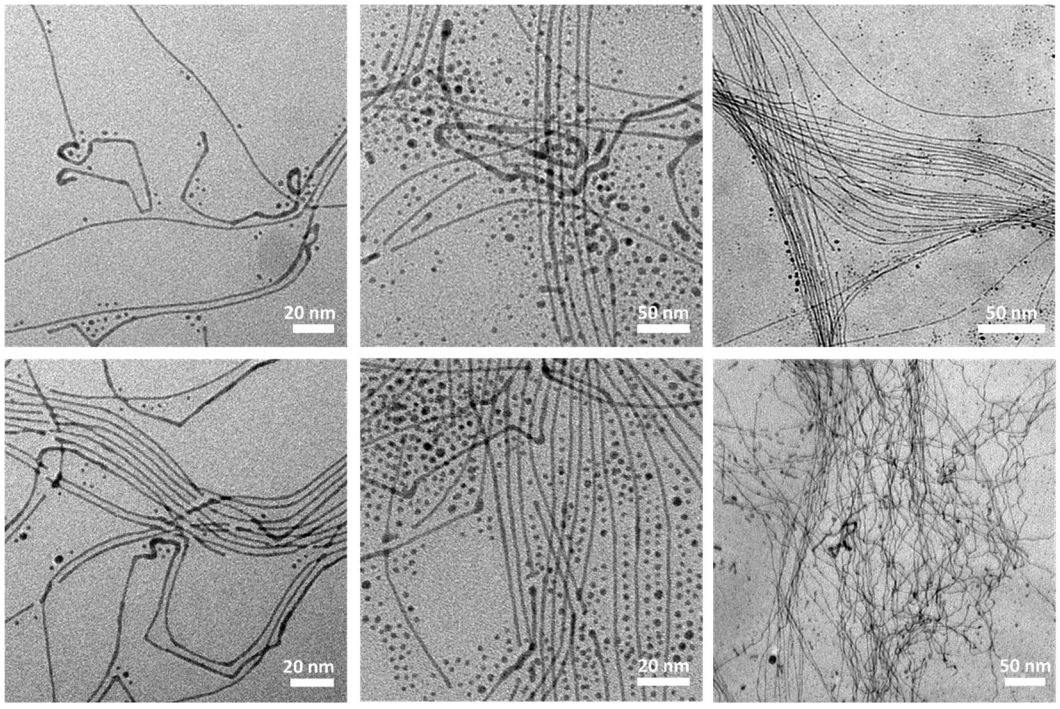


**Figure S3.4.3.5** Representative TEM images of AuNWs synthesized in cyclooctane.

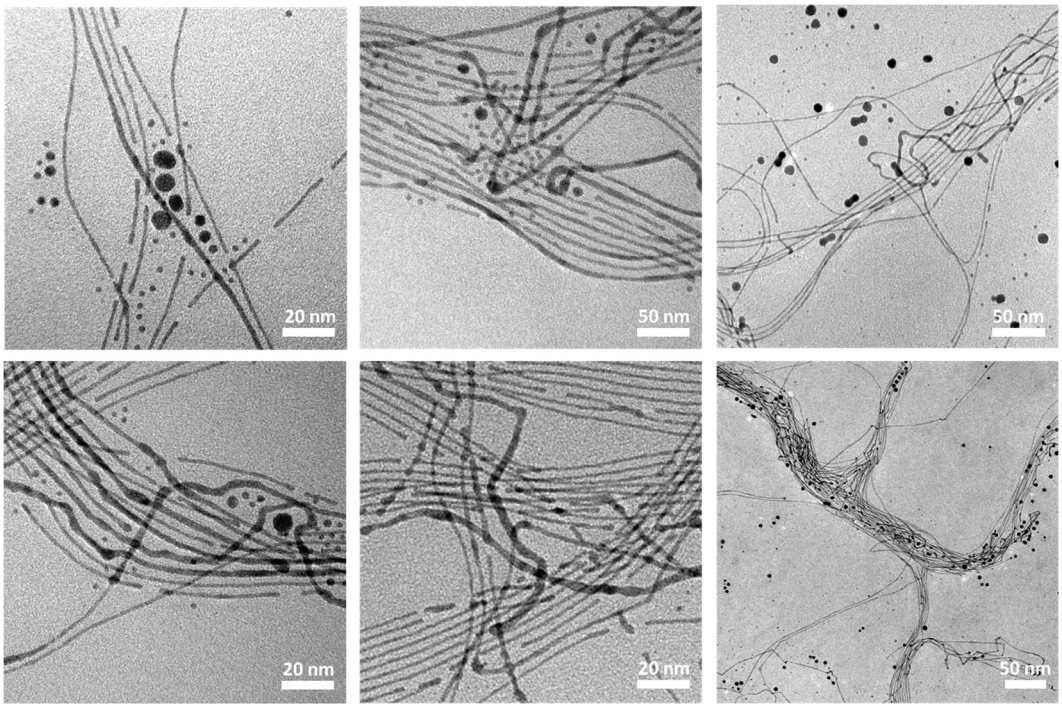


**Figure S3.4.3.6** Representative TEM images of AuNWs synthesized in benzene.

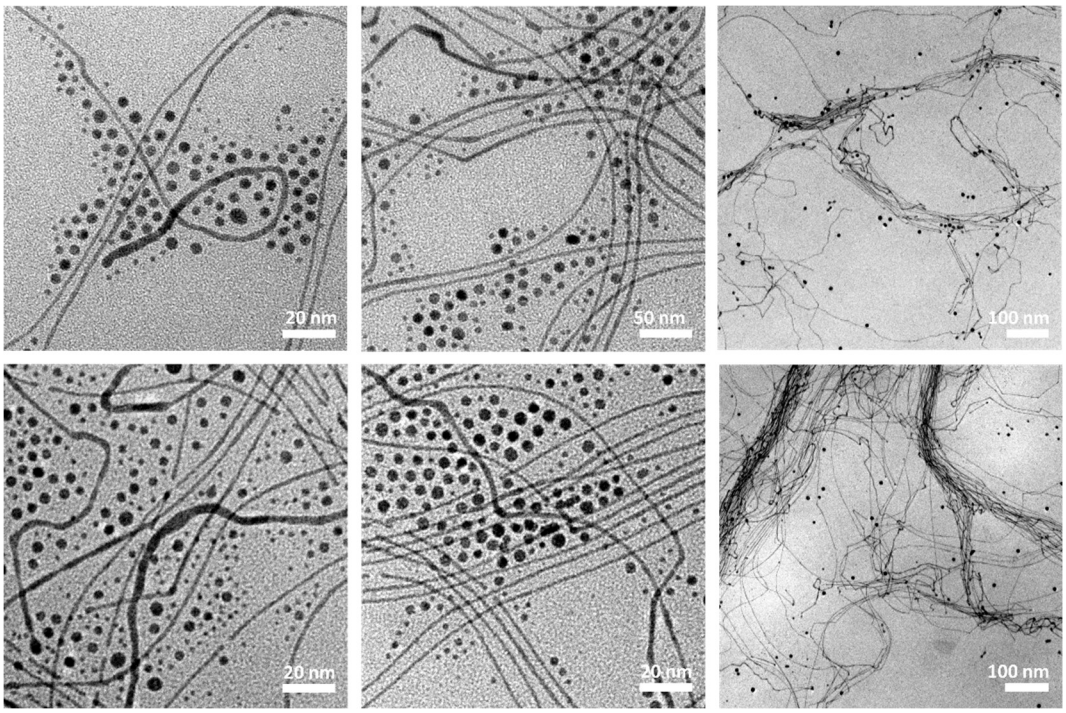


**Figure S3.4.3.7** Representative TEM images of AuNWs synthesized in toluene.

### 3.4.4 References

(1) Feng, H.; Yang, Y.; You, Y.; Li, G.; Guo, J.; Yu, T.; Shen, Z.; Wu, T.; Xing, B. Simple and Rapid Synthesis of Ultrathin Gold Nanowires, Their Self-Assembly and Application in Surface-Enhanced Raman Scattering. Chem. Commun. (Camb). 2009, 1984–1986.

(2) Förster, S.; Timmann, A.; Konrad, M.; Schellbach, C.; Meyer, A.; Funari, S. S.; Mulvaney, P.; Knott, R. Scattering Curves of Ordered Mesoscopic Materials. J. Phys. Chem. B 2005, 109, 1347–1360.

(3) G. Fournet. Fonctions de Diffusion Pour Des Formes Geometriques. Bull. la Société Française Minéralogie Crystallogr. 1951, 74, 39.

(4) I. Breßler, J. Kohlbrecher, and A. F. Thünemann. SASfit: A comprehensive tool for small-angle scattering data analysis. arXiv:1506.02958 [physics.data-an]. June 2015.

## 3.5 Publication 3: Spinning hierarchical gold nanowire microfibers by shear alignment and intermolecular self-assembly

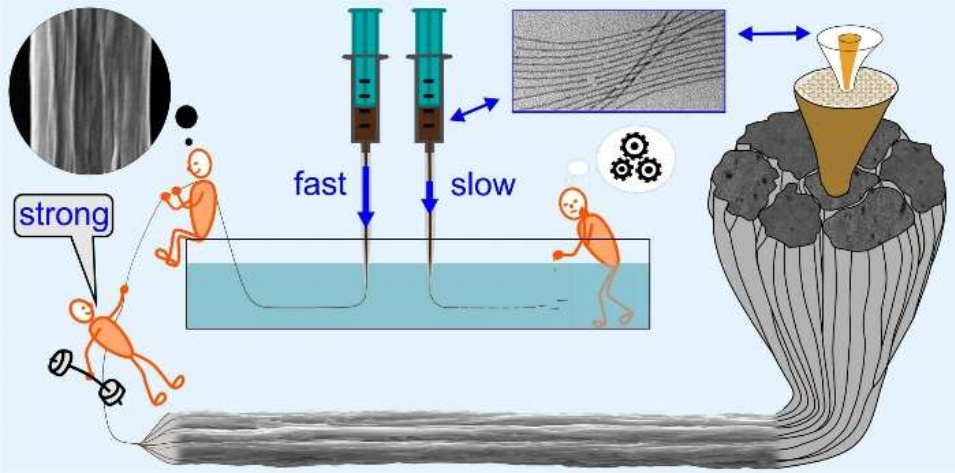


**Reiser, B.**; Gerstner, D.; Gonzalez-Garcia, L.; Maurer, J. H. M.; Kanelidis, I.; Kraus, T. Spinning Hierarchical Gold Nanowire Microfibers by Shear Alignment and Intermolecular Self-Assembly. *ACS Nano* **2017**.

Reprinted with permission of all authors. Copyright (2017) American Chemical Society.[f4]

[f4] Note that Figure, Table and equation numbers as well as section names and numbers have been adapted to ensure consistent labeling and numbering throughout the whole thesis. Some Figures have been rearranged and resized to better fit the format of the thesis. Furthermore, the reference to supporting videos has been changed.

### 3.5.1 Abstract

Hierarchical structures lend strength to natural fibers made of soft nanoscale building blocks. Intermolecular interactions connect the components at different levels of hierarchy, distribute stresses, and guarantee structural integrity under load. Here, we show that synthetic ultrathin gold nanowires with interacting ligand shells can be spun into biomimetic, free-standing microfibers. A solution spinning process first aligns the wires, then lets their ligand shells interact, and finally converts them into a hierarchical superstructure. The resulting fiber contained 80 vol.% organic ligand but was strong enough to be removed from the solution, dried, and mechanically tested. Fiber strength depended on the wire monomer alignment. Shear in the extrusion nozzle was systematically changed to obtain process-structure-property relations. The degree of nanowire alignment changed breaking stresses by a factor of 1.25 and the elongation at break by a factor of 2.75. Plasma annealing of the fiber to form a solid metal shell decreased the breaking stress by 65%.

### 3.5.2 State of the art

Many natural materials are hierarchically structured composites with remarkable properties. Their hierarchical arrangement of small, often anisotropic building blocks distributes loads and inhibits defect propagation.[1] Bamboo, composed of polysaccharides and lignin arranged in at least 7 levels of hierarchy, is highly flexible, yet tough and lightweight.[1–3] Human bone is composed of a collagen matrix that self-organizes into fibrillar structures in which hydroxyapatite crystals are embedded. Its hierarchical structure makes the material fault-tolerant and strong.[3]

Artificially creating complex hierarchical materials by sequential assembly is difficult, in particular if the components are small and simple methods to efficiently tune their interaction forces are unknown.[4,5] Today's commercial composites are structured on one or two levels of hierarchy and otherwise random.[6] This provides considerable gains in strength per weight already,[7] but more levels of hierarchy could further improve perfomance, for example by efficient strain delocalization.[6,8,9] New production techniques that provide improved control over composite structure with limited additional effort are therefore desirable.

Self-assembly is a facile method to produce nano- and microscale hierarchical structures with little effort during material preparation.[10,11] Anisotropic building blocks can direct self-assembly in materials and affect their properties:[12] for example, aligned linear chains of

ultrahigh molecular weight polyethylene drastically increase the yield strength of Dyneema™ fibers.[13] An interesting alternative are highly anisotropic inorganic colloids such as ultrathin gold nanowires (AuNWs) that remind of linear polymers in shape and interactions.[14,15] They can be synthesized on the gram scale through a simple and scalable method that yields wires of several micrometers in length with a 1.6 nm diameter gold core.[16] An oleylamine (OAm) ligand shell around the core lends them good colloidal stability in many organic solvents.[17] These wires are flexible enough to bend reversibly with radii of approximately 25 nm.[18] They were successfully applied in the fields of surface-enhanced Raman scattering (SERS),[19] sensing,[20,21] catalysis,[22] and transparent electronics.[23,24]

Ultrahin gold nanowires interact in dispersion mainly through highly multivalent interactions between their OAm shells.[14] Dispersed wires tend to self-assemble into hexagonal superstructures (bundles)[14,25] that can be used to build miniaturized electronic circuits[23,26] or form nanoscale interconnects.[27] We have shown that multivalent interactions between OAm ligand shells of AuNWs can be tuned by solvent choice. Cycloalkanes lead to weak interaction and dispersion, while, for example, *n*-alkanes lead to the formation of bundles.[14] Cademartiri *et al*. demonstrated that ultrathin $Bi_2S_3$ nanowires can be chemically cross-linked by injection into a solution of bidentate ligands to form fiber-like assemblies.[28] The bidentate ligands form covalent connections between adjacent wires.

Here, we exploit the intermolecular, non-covalent interactions between AuNWs to induce their self-assembly into free-standing, hierarchical fibers. Our wire assembly process is similar to polymer solution spinning, where a “spinning dope” (a polymer solution) is injected into a coagulation bath. This bath contains an anti-solvent that decreases polymer solubility and causes precipitation.[29] Our spinning process exploits similar interactions to assemble ultrathin nanowires rapidly (0.2 m/s) into free-standing, hierarchical microfibers with an organic content of approximately 80% by volume. Their diameter was tuned by adapting the AuNW volume fraction in the spinning dope. The flow rate of the injected spinning dope determined fiber morphology and tensile properties; we introduce a simple model to explain this behavior. Shear alignment was a prerequisite for stable fiber formation; better alignment increased their mechnical strength by 25%. We compared this increase to the effect of a post treatment that converted the outer parts of the fiber into a solid shell and found a 65% reduction in breaking stress compared to the best aligned structure.

## 3.5.3 Results and discussion

### *AuNW structure, assembly, and fiber Spinning*

Ultrathin gold nanowires (AuNWs) were synthesized following a simple and scalable protocol by Feng and coworkers (see details in section 3.5.5).[19] This synthesis uses oleylamine (OAm), which soft-templates wire growth and serves as a ligand for the highly anisotropic nanostructures.[14,30] As-synthesized AuNWs were capped by an OAm double-layer;[14,25] precipitation with ethanol and redispersion in cyclohexane yielded dispersed AuNWs with a single layer of OAm.[14,31] A representative transmission electron microscopy (TEM) image of washed AuNWs is shown in Figure 3.5.3.1a. The characteristic spacing of approximately 2 nm between the 1.6 nm thick AuNWs can be attributed to fully interdigitated OAm ligand layers of neighboring nanowires (Figure 3.5.3.1b).

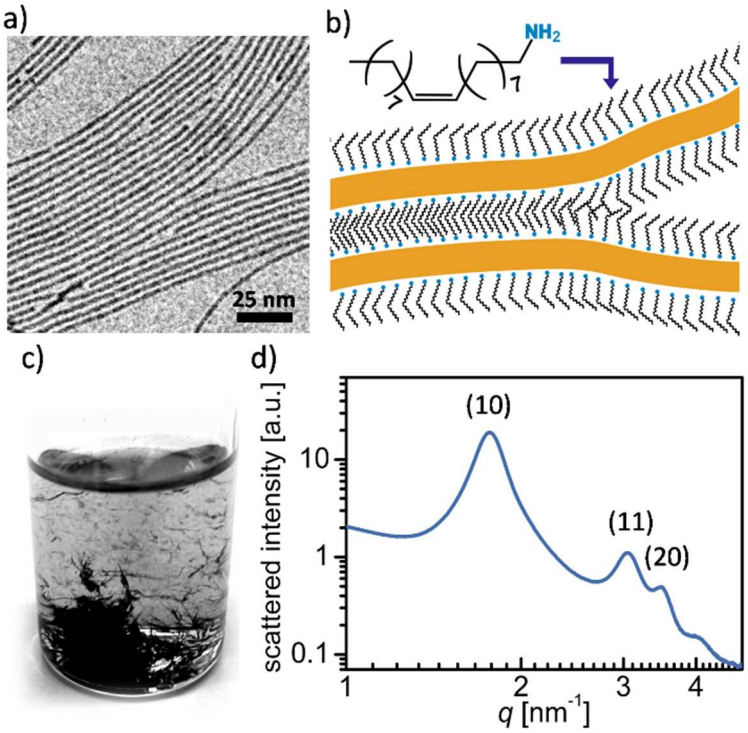


**Figure 3.5.3.1** a) TEM image of washed AuNWs. b) Skeletal formula of OAm and schematic drawing of two AuNWs (1.6 nm diameter) with interacting ligand layers. c) Photograph of AuNWs after precipitation with ethanol. d) SAXS pattern of AuNW-precipitate on polyimide (Kapton™), peaks corresponding to hexagonal packing are indexed.

First, we consider the unconfined precipitation of AuNWs by an anti-solvent like ethanol. The precipitates that are formed when ethanol is added to a dispersion of AuNWs in cyclohexane are displayed in Figure 3.5.3.1c. Note the elongated shape of the agglomerates that form during chaotic mixing of the two liquids. They are very different from globular agglomerates

or networks that would form for spherical particles of similar diameter and composition.[32] Small-angle X-ray scattering (SAXS, Figure 3.5.3.1d) indicated that the precipitate consisted of hexagonally ordered AuNWs, comparable to the structure of bundles reported previously,[14,25] but with a shorter wire-wire (center-to-center) distance of 3.55 nm. The distance corresponds to two fully interdigitated OAm layers (Figure 3.5.3.1b) similar to that of dried wires, while bundling in less polar solvents like arenes or *n*-alkanes leads to typical wire-wire distances of 5.2 nm to 5.5 nm.[14] We conclude that the ethanol-induced wire-wire attraction is stronger than in less polar solvents and induces tighter bundling.

Now we introduce a laminar flow to impress directionality and structure. The setup sketched in Figure 3.5.3.2a injects AuNWs in cyclohexane – dispersed as single wires – (spinning dope) into an ethanol bath through a 75 µm diameter nozzle. The wires form fibers that consist of a loose network of tightly packed AuNW bundles (Figure 3.5.3.2c). When the fibers are pulled through the ethanol-air interface, the loose network is compacted by capillary forces (Figure 3.5.3.2a). Figure 3.5.3.2b shows micrographs of the final product. We used a stagnant spinning bath and moved the nozzle with a constant velocity (see section 3.5.5 for details). Videos of our spinning process and the fiber collection are provided online on the ACS Publications website (Video1 and Video2, see section 3.5.6). A continuous process could use a controlled coaxial flow[33] or collect the precipitate at constant speed during spinning.[29] The velocity of the dispersion in the nozzle was a critical process parameter: fibers could only be spun for mean liquid velocity above 0.4 m/s. The maximal velocity was only capped by the technical limits of our setup.

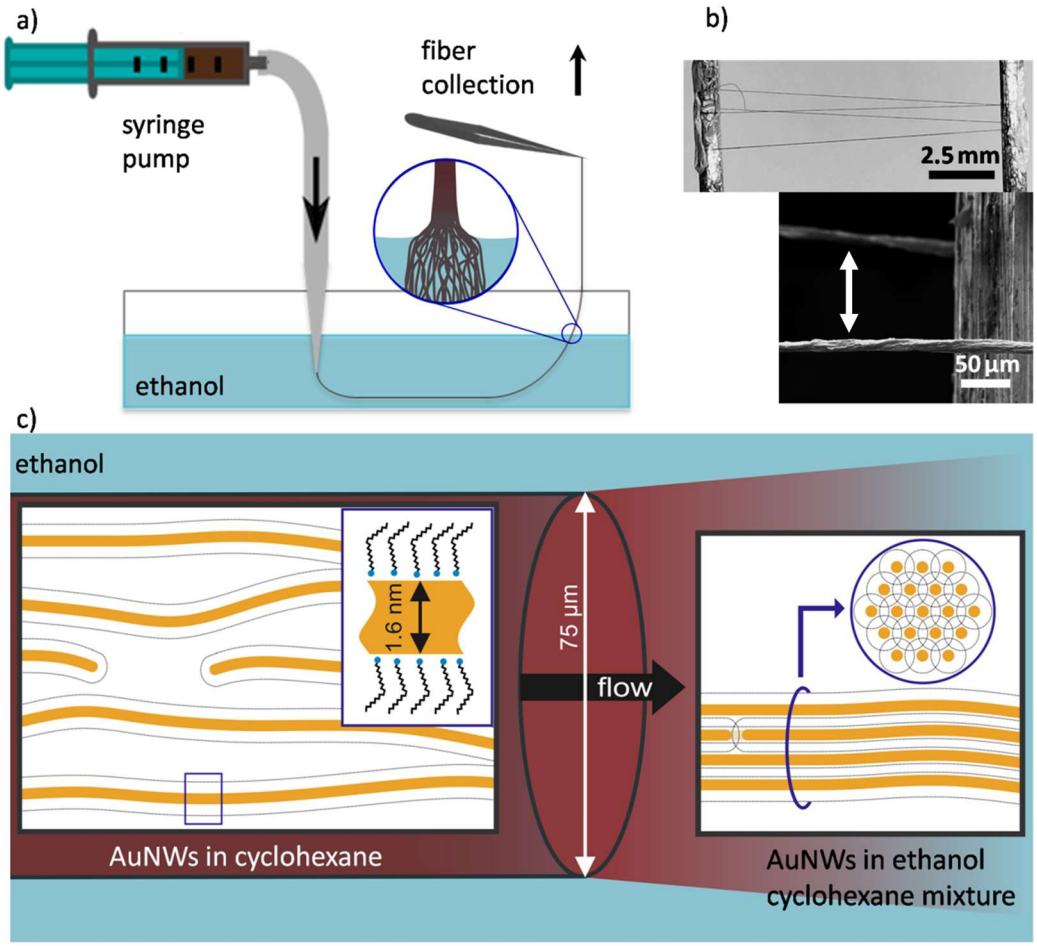


**Figure 3.5.3.2** a) Schematic setup for AuNW fiber spinning: AuNWs dispersed in cyclohexane are injected into an ethanol bath, from which the fibers can then be collected. b) Optical (top) and SEM (bottom) image of free-standing fibers (marked with an arrow). c) Schematic depiction of AuNW injection into ethanol and bundle formation on the single nanowire level.

### *Influence of AuNW concentration on fiber diameter*

Fiber diameters were tuned *via* the AuNW concentration in the spinning dope. We tested AuNW volume fractions between 0.12% and 0.93% at a flow rate of 4 µL/s with nozzle displacement velocities of 0.2 m/s; these parameters reliably led to strong fibers in the entire concentration range. Electron micrographs (Figure 3.5.3.3a) of as-spun fibers revealed increasing fiber diameters for increased AuNW volume fractions of the injected spinning dope. We annealed the fibers with a plasma treatment[34,35] to create a dense metallic shell and facilitate AFM profilometry. Optical microscopy suggests that the fibers did not shrink during plasma sintering. Electron micrographs of as-spun fibers (Figure 3.5.3.3a) appeared similar to micrographs taken after treatment (Figure 3.5.3.3b).

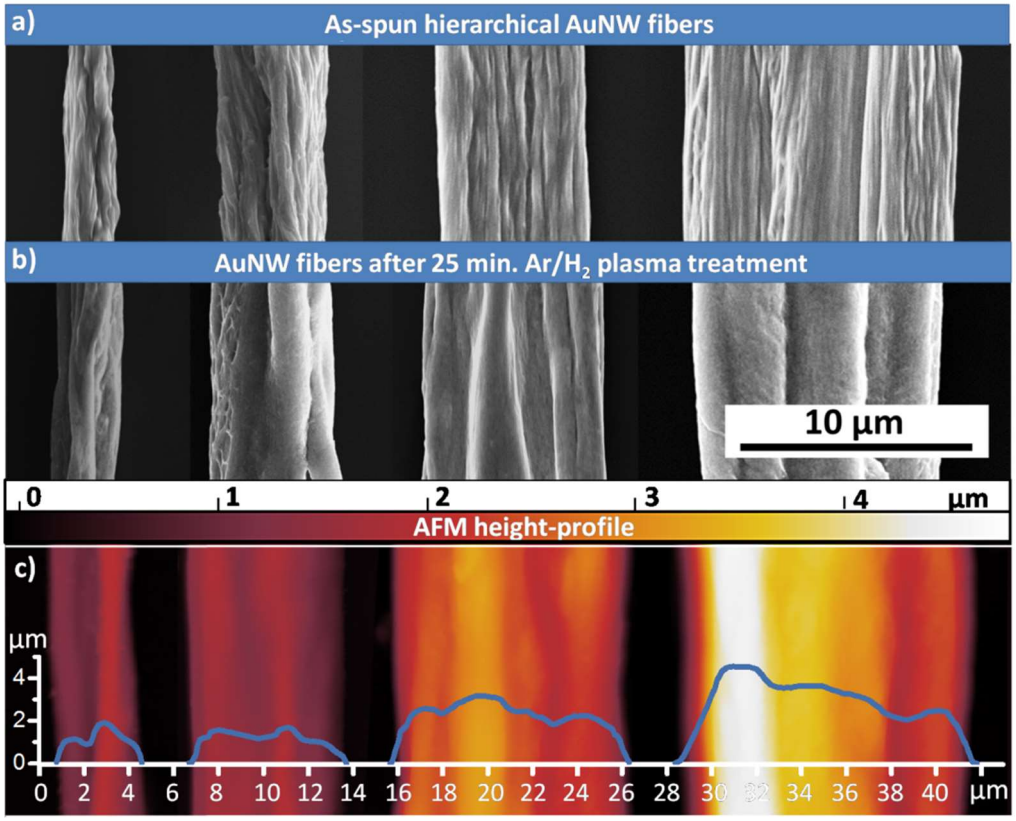


**Figure 3.5.3.3** SEM and AFM images of AuNW fibers spun with different AuNWvolume fractions (left to right: 0.12%, 0.31%, 0.62% and 0.93%); a) SEM images of as-spun fibers, b) SEM images of fibers after plasma treatment. c) AFM measurements of fibers after plasma treatment. Respective profile lines, obtained from the AFM images, are plotted on the corresponding position.

The mean cross-sectional areas given in Table 3.5.3.1 were extracted from atomic force microscopy (AFM) height profiles of plasma treated fibers (Figure 3.5.3.3c). The cross section of the single fibers varied by approximately 3%. The diameter of the spun fibers monotonously increased with the AuNW volume fraction in the spinning dope following:

$$A_{fiber} = \frac{V_{AuNW}}{V_{spinning\ dope}} A_{nozzle}, \qquad \text{(eq. 3.5.3.1)}$$

where A denotes the cross-sectional area and V the volume. Deviations from this proportionality are caused by inaccuracies in the AuNW volume fraction or partial nozzle clogging. Further optimizations should alleviate these issues and provide precise and accurate control of the fiber thickness.

**Table 3.5.3.1** Cross-sectional areas and area fractions of the nozzle of AuNW fibers spun with different volume fractions compared to the theoretical cross-sections derived from equation 3.5.3.1.

| AuNW volume fraction in spinning-dope [%] | 0.12 | 0.31 | 0.62 | 0.93 |
|---|---|---|---|---|
| Mean cross-sectional area from AFM [µm²] | 5.1 | 9.4 | 28 | 35 |
| Standard error of cross-sectional area [%] | 3.0 | 3.7 | 3.2 | 2.4 |
| Theoretical cross-sectional area [µm²] | 5.3 | 14 | 27 | 41 |
| Deviation from the experimental results [%] | 3.8 | 33 | 3.6 | 15 |

### *Influence of AuNW alignment on fiber morphology*

Shear forces in the injection nozzle can align anisotropic objects[36,37] as is well-known for polymer spinning.[33] Colloidal wires align in the flow direction at sufficient shear rates.[38] We analyzed the velocity-dependent alignment of AuNWs in a tube flow of 0.9 mm by *in situ* SAXS (Figure 3.5.3.4b). The 2D scattering patterns of single wires dispersed in cyclohexane (Figure 3.5.3.4a, bottom) and AuNW bundles in *n*-hexane (Figure 3.5.3.4a, top) became clearly anisotropic with increasing flow rates at Reynolds numbers between 1 and 111, all well in the laminar regime. The scattering ring seen for *n*-hexane is caused by the (10) Bragg peak of the wires' hexagonal assembly and does not occur in cyclohexane, which keeps the particles dispersed.[14] The distribution of the detected scattered intensity $I(\varphi)$ along the azimuthal angle $\varphi$ was quantified using the (10) Bragg peak of AuNWs in *n*-hexane (Figure 3.5.3.4a, top). Let $\vartheta$ be the angle between the long axis of an anisotropic scatterer and the average orientation. The probability distribution of this angle, $f(\vartheta)$ (orientational distribution), is connected to the azimuthal distribution of the scattered intensity by[39]

$$I(\varphi) \sim \int f(\vartheta) \mathrm{d}\omega. \qquad \text{(eq. 3.5.3.2)}$$

Since the SAXS pattern $I(\varphi)$ only contains information on the 2D projection of the 3D wire orientational distribution, the angle between the long axis of a scatterer and the X-ray beam $\omega$ has to be taken into account as above. The three angles are connected by

$$\cos\vartheta = \cos\varphi \sin\omega. \qquad \text{(eq. 3.5.3.3)}$$

Without loss of generality, the average direction is $\vartheta = 0°$; $f(\vartheta)$ describes the distribution of angles around it. Assuming a Pseudo-Voigt peak function as a parametrization of $f(\vartheta)$ allows to fit the measured $I(\varphi)$ *via* equation (3.5.3.2) and thereby estimate the true shape of the orientational distribution $f(\vartheta)$; examples are given in Figure 3.5.3.4c (details can be found in section 3.5.5). We assessed the degree of orientation in terms of the nematic order parameter *S* that is often used for liquid crystals[40] and defined as the ensemble average of the second Legendre polynomial of cos $\vartheta$,

$$S = \langle \frac{3\cos^2\vartheta - 1}{2} \rangle. \qquad \text{(eq. 3.5.3.4)}$$

*S* vanishes for isotropic samples and converges to 1 for perfect alignment in the probed volume. Typical values of *S* for nematic liquid crystal phases lie between 0.4 to 0.8.[40] We found increasing *S* that attained values close to 0.8 for the highest flow rates of 100 µL/s that correspond to a mean velocity of 0.16 m/s and a wall shear rate of 7 $\mu s^{-1}$ (Figure 3.5.3.4d). Details on the calculation of *S* can be found in section 3.5.5.

The AuNW alignment in the nozzle turned out to be a prerequisite for the spinning process. We varied the flow speed during fiber spinning process and observed the spinning dope injection with a camera. Continuous fibers were only obtained above a mean liquid velocity of 0.4 m/s; the jet disintegrated into droplets otherwise (Figure 3.5.3.4e). Videos of fiber spinning at 0.45 m/s and at 9 mm/s can be found online on the ACS Publications website (Video1 and Video3, see section 3.5.6). We believe that the alignment in flow increases the interaction strength between the injected fiber constituents. Aligned AuNWs form stronger fibers that do not immediately decompose in the moving liquids.

A simple model explains the strong effects of alignment: *in situ* SAXS indicates that AuNW alignment increases with flow speed. Assume that this alignment is retained partially or completely as the wires are injected into the anti-solvent and rapidly diffuse to maximize contact area. The probability of lateral contact between wires would then increase with flow rate, with the limiting case of fully parallel wires that touch each other along their full lengths. The intermolecular interactions between parallel wires in full lateral contact are greater than in all other contact geometries, and stronger interactions would lead to greater cohesion inside the fiber. Figure 3.5.3.4e schematically depicts this model.

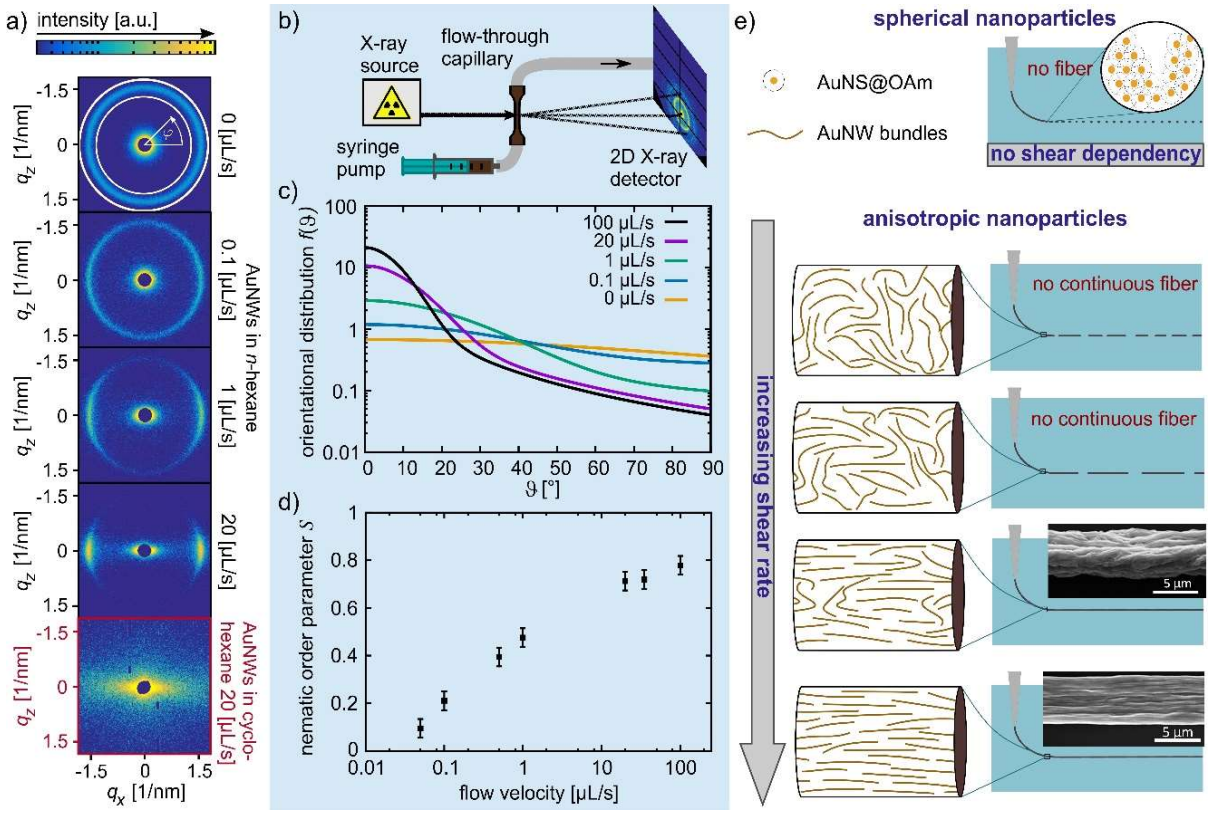


**Figure 3.5.3.4** a) Small-angle X-ray scattering patterns of flowing AuNWs. b) Schematic depiction of the SAXS setup for in situ observation of flowing AuNWs. c) Numerical fits of the orientational distribution for different flow velocities according to equation (2). d) Nematic order parameter of AuNWs in flow as a function of flow velocity. e) Schematic depiction of the impact of anisotropy and alignment on the spinability of AuNW fibers with SEM images of a fiber spun with a flow speed of 2 µL/s (0.45 m/s) and 4 µL/s (0.91 m/s) as insets.

The model was tested by comparing AuNW spinning to the extrusion of nanospheres (3.2 nm diameter) with oleylamine ligands (AuNS@OAm) as spinning dope. A TEM image of the used AuNS@OAm is given in section 3.6.1 (Figure S3.6.1.1). Our aim was to examine whether fiber spinning with 0.3% AuNS@OAm, a volume fraction which is readily spinnable in case of AuNWs, is possible under conditions used for wires. We found that spheres do not form continuous structures at any flow rate (see Figure 3.5.3.4e and Video4, see section 3.5.6). The sphere-sphere contact area (that is three orders of magnitude smaller than for aligned wires) apparently is insufficient to create mechanically stable fibers. This reminds of the lower limit for molecular weight in polymer spinning: polyethylene, for example, can only be spun above approximately 300 kDa,[41] which corresponds to a hydrocarbon chain length of ≈ 3µm and is on the order of the AuNW's length.

The absolute polymer chain length within polymer fibers sets their mechanical strength. Foroughi *et al.*,[42] for instance, reported that polypyrrole fibers increased their ultimate tensile strength by a factor of 5 when increasing the molecular weight of the polymer by a factor of 7-60. They demonstrated that the mechanical strength was further improved by post spinning drawing, a technique that increases molecular alignment and is widely used for polymer fibers. It increases breaking stress while reducing the elongation at break.[42,43] For AuNW fibers, alignment by stretching is impossible, but we find that the alignment in the nozzle is largely retained in the fiber. Electron microscopy (insets Figure 3.5.3.4e and Figure S3.6.1.2) shows preferential alignment of the bundles in flow direction that increased with flow rate. Does this alignment increase mechanical strength as it does for polymers?

### *Mechanical characterization*

We investigated the mechanical properties of AuNW fibers produced at a flow rate of 2 and 4 μL/s ("poorly-" and "well-aligned" fibers) and correlated them with the morphology. Fibers with diameters between 10 and 20 μm were fixed in paper frames to prevent damage prior to uniaxial mechanical testing as depicted in Figure 3.5.3.5a. The frame was cut open once the fiber was fixed inside of the mechanical testing setup, and the fibers were pulled at a constant speed of 0.01 mm/s while the force was measured with a load cell (details on the tensile testing setup can be found in section 3.5.5). Typical stress-strain curves are given in Figure 3.5.3.5b. Well-aligned fibers exhibited a breaking stress of roughly 10 MPa, 25% above that of poorly aligned fibers (8 MPa). The elongations at break of poorly-aligned fibers were 2.75 times that of well-aligned fibers, which is in good agreement with structure-tensile property relations found for polymer fibers.[42,43]

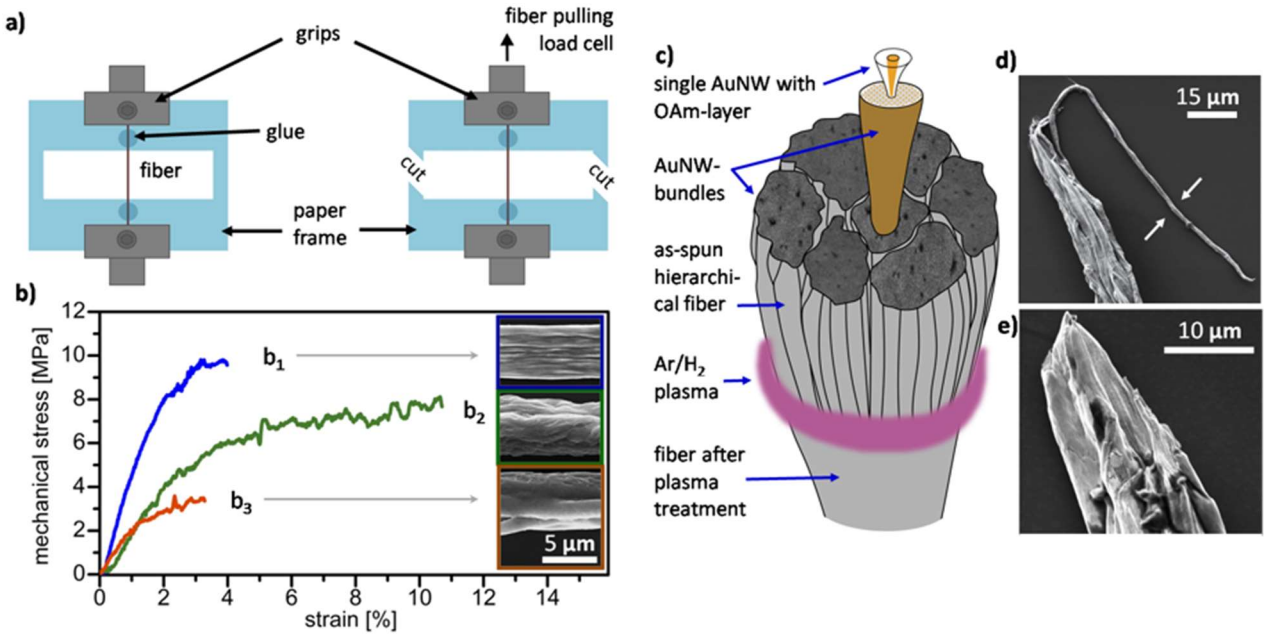


Figure 3.5.3.5 a) Schematic depiction of sample preparation and fiber tensile testing setup. b) Typical stress-strain curves and SEM images of a well-aligned fiber ($b_1$), a poorly-aligned fiber ($b_2$), and a fiber after Ar/$H_2$ plasma treatment ($b_3$). c) Scheme of hierarchical structure of as-spun fibers and fibers after plasma treatment. d) SEM image of as-spun fiber after breaking. e) SEM image of plasma treated fiber after breaking.

The ultimate tensile strength of both fiber types was in the range of wet-spun polypyrrole fibers,[44] non-crosslinked bulk polymers,[45] and thin films of crosslinked polymers,[46] but one order of magnitude below that of bulk gold.[47] The calculated Young's moduli were 530 MPa for well-aligned fibers and 240 MPa for poorly aligned fibers, two orders of magnitude below that of bulk gold.[48] Note, however, that the fibers contained roughly 80% OAm, which is a liquid at room temperature. Surprisingly high mechanical strengths (ultimate tensile strength of 11 MPa) were also reported for membranes of 5.2 nm diameter gold spheres with dodecanethiol ligand layers without cross-linking.[49] The authors assigned the mechanical strength to the interactions between intercalated ligand layers. The membranes were stretched on a support and at 5 % elongation the membranes showed already severe cracks, while our fibers sustained up to 11%.

We believe that the hierarchical fiber structure explains their comparatively high strength. Electron microscopy of failed fibers revealed their internal structure (Figure 3.5.3.5d). The first level of hierarchy, single wires, could not be resolved by our SEM. The second level of hierarchy were AuNW bundles with a typical size of hundreds of nanometers. We believe that they are dense and connected by the intermolecular interactions between intercalating OAm ligand shells. Careful observation of the structure of as-spun fibers (Figure S3.6.1.2) revealed

a fine structure on the fiber surface with intertwined bundle-like structures. This observation suggested that bundles combine into a third level of hierarchy ("super-bundles"). The final fibers (top hierarchical level) are several microns in diameter and exhibit a rough surface. Our hypothesis is that AuNW bundles can be sheared apart upon strain, before the "stronger" multivalent bonds between adjacent wires are sheared apart until failure. The long bundle – or super-bundle – pulled out of the fiber upon failure seen in Figure 3.5.3.5d (marked with arrows) supports this hypothesis. This mechanism would be in accordance with fiber pull-out, a commonly described failure mechanism for fiber-materials.[2] This happens because load can be distributed along the fiber's radial and its longitudinal direction, efficiently using the enhanced contact area between anisotropic fiber features aligned in parallel. It explains why poorly-aligned bundles inside of a fiber reduce breaking stress and Young's modulus of the fiber. The increased elongation at break on the other hand can be explained by uncoiling unaligned bundles prior to bundle and wire pull-out.

We used an $Ar/H_2$ plasma to fuse AuNWs and reduce the number of hierarchical levels. The plasma treatment increased the conductivity of the initally insulating fibers to around 800 S/cm, a value that is approximately 500 times below that of monocrystalline bulk gold,[45] indicative of an interconnected metallic structure. We found no significant difference between the tensile properties of well-aligned and poorly-aligned fibers after the plasma treatment. Surprisingly, treated fibers were weaker than the original fibers (Figure 3.5.3.5b) with a breaking stress of 3.5 MPa, an elongation at break of 3%, and a Young's modulus of 220 MPa. The plasma treatment apparently disrupts the hierarchical fiber structure and causes the reduced fracture strength (but does not significantly change elastic behavior). Focused ion beam (FIB) cross-sections of plasma treated fibers (Figure 3.5.3.6) revealed an outer shell that appears to be organic material in backscattering images (section 3.6, Figure S3.6.1.3). Inside an approximately 600 nm thick gold shell of moderate porosity was found (also see Figure S3.6.1.4). The core appears to contain unsintered, or incompletely sintered, OAm-covered gold wires with a number of pores.

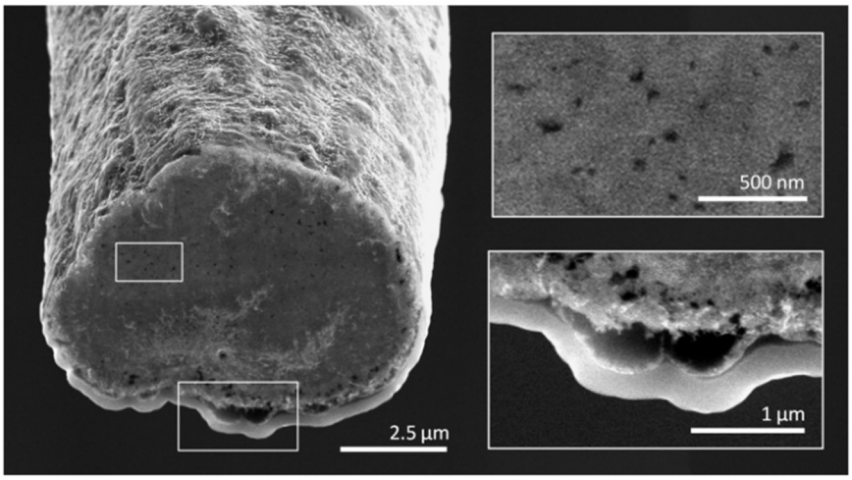


**Figure 3.5.3.6** SEM image of a FIB-cut through a fiber after 25 min $Ar/H_2$ plasma treatment observed at 52° tilt.

The plasma seems to penetrate roughly 600 nm of the fiber and forms porous gold by OAm removal. A certain amount of OAm from the core flows through the pores and forms an organic shell. It appears that OAm accumulates at the bottom of hanging fibers, driven by gravity. The process destroys the hierarchical structure of the fibers. It is remarkable and highlights the importance of the hierarchical AuNW arrangement that the resulting structure is 65% weaker (in breaking stress) than the original fibers.

### 3.5.4 Conclusion

We introduced a spinning technique that yields continuous free-standing, hierarchical fibers from ultrathin gold nanowires at 0.2 m/s. The fiber mechanical properties depended on the spinning conditions that affected alignment and order in the fibers. We used them to demonstrate how hierarchical assembly of nanoscale building blocks can be used to create functional superstructures and influence their properties through process parameters.

The spinning setup is similar to a system for solution spinning of polymers. Fiber thickness was tuned *via* the AuNW concentration in the spinning dope. The flow rate of spinning dope in the nozzle had to exceed a critical value to enable spinning; it also determined the fiber morphology and tensile strength. We found at least three levels of hierarchy in the fibers; lower flow rates induced disorder on higher hierarchical levels. Disordered fibers displayed greater elongations at break, while well-aligned fibers exhibited higher breaking stresses. Plasma treatment of the fibers generated roughly 600 nm thick, porous, but continuous gold shells by fusing single nanowires and thereby reducing the number of hierarchical levels. The

treatment had detrimental effects on the tensile properties, demonstrating the importance of hierarchy for the mechanical properties of our system.

The method we present here relies on interactions between the colloids' surface chemistry and is therefore not restricted to gold wires. Other nanowires that carry OAm or other ligands with moderate to strong attractive interactions could be spun into hierarchical fibers in the same manner. The resulting fibers would be interesting sensor elements, because they are dominated by interfaces and are easy to contact electrically. We are working on ligand shells that are electrically conductive or can be cross-linked after spinning to further increase the strength of the fibers.

### 3.5.5 Materials and methods

#### *AuNW synthesis*

The synthesis protocol was adapted from Feng and coworkers.[19] Briefly, 200 mg of $HAuCl_4 \cdot 3H_2O$ were dissolved in a mixture of 30.7 mL of *n*-hexane (99%, ABCR, Germany) and 9.3 mL of oleylamine (technical grade, 70%, Sigma-Aldrich, Germany), then 13.1 mL of triisopropylsilane (98%, ABCR, Germany) were added. The solution was kept undisturbed to react under argon atmosphere within 16 h at 20 °C. As-synthesized AuNWs were purified by twofold precipitation with an excess of ethanol (99.8%, Sigma-Aldrich, Germany) and subsequent redispersion in cyclohexane (≥ 99%, Sigma-Aldrich, Germany). After the second precipitation, a volume of cyclohexane equivalent to 1, 0.4, 0.2, 0.13 and 0.1 of the reaction volume was added to obtain volume fractions of 0.12%, 0.31%, 0.62%, 0.93% and 1.24%, respectively. Note that the volume of the surrounding ligand layer was considered for the calculation of the volume fraction.

#### *AuNS synthesis*

Gold nanospheres with a diameter of 3.2 nm were produced using a synthesis adapted from Wu and coworkers.[51] Briefly, 100 mg of $HAuCl_4 \cdot 3H_2O$ were dissolved in a mixture of 8 mL of *n*-pentane (99%, Sigma-Aldrich, Germany) and 8 mL oleylamine. The solution was stirred at 20 °C under Ar for 1 h before 40 mg of *tert*-butylamine borane (97%, ABCR, Germany) dissolved in 2 mL of *n*-pentane and 2 mL of oleylamine, were added. The solution was stirred at 20 °C under Ar for 1 h and subsequently purified by repeated precipitation with an excess of ethanol and subsequent redispersion in cyclohexane to yield a final particle concentration of 5 mg/mL, which corresponds to a particle volume fraction of 0.3%.

AuNW fiber production: AuNW fibers were produced using the setup that is sketched in Figure 3.5.3.2a. An AuNW dispersion in cyclohexane was injected *via* a glass nozzle (hollow round glass capillary ID 0.05mm, OD 0.08mm, CM scientific, United Kingdom) with an inner diameter of approx. 75 µm (determined by optical microscopy) in an ethanol bath. The nozzle tip was immersed at least 7 mm deep into the ethanol bath and kept at least 5 mm above the bottom of the bath. The nozzle was connected to a gas-tight glass syringe (Hamilton, Switzerland) filled with AuNWs in cyclohexane *via* standard HPLC fluorinated ethylene propylene tubing (0.8 mm inner diameter). The flow of AuNWs in cyclohexane was controlled with a syringe pump type "NEMESYS" (Cetoni, Germany) and initiated with the nozzle submerged in the ethanol bath. 10 - 20 s after the flow was started, the nozzle was drawn across the ethanol bath at constant speed using a film applicator (TQC, Germany). The speed was slightly below the average dope flow velocity to avoid fiber tearing. Between experiments, the nozzle was kept in chloroform (≥ 99.8%, Sigma-Aldrich, Germany) to prevent clogging. Fibers were picked up with tweezers and pulled through the ethanol-air interface. They were collected either as free-standing fibers in paper frames or between metal bars, or on silicon wafers or microscopy slides for further investigation.

### *Plasma treatment of as-spun AuNW fibers*

As-spun fibers were treated for 25 min in a 13.56 MHz RF (100 W) PICO plasma system (Diener electronic, Germany) in a 0.3 mbar Ar/$H_2$ (95/5, v/v) atmosphere.

### *Characterization and SAXS data analysis*

0.8 µl of a 0.12 vol.% AuNW dispersion in cyclohexane was left to dry on a 400-mesh carbon coated copper grid (Plano, Germany). The dry sample was then analyzed in a transmission electron microscope type JEM 2010 (JEOL, Germany) operating at 200 kV.

To determine the wire-wire distance in AuNW-bundles formed by precipitation with ethanol, the precipitate was placed on a Kapton™ sheet to be analyzed in a laboratory scale SAXS machine (XEUSS 2.0 from XENOCS SA, France) equipped with a CuK$\alpha$ X-ray source and a PILATUS3 R 1M (DECTRIS, Switzerland) X-ray area detector. Flowing AuNWs and AuNW-bundles were analyzed in situ in a round capillary (0.9 mm inner diameter) mounted in the same machine as schematically depicted in Figure 3.5.3.4b. We used the same syringe pump and tubing for the fiber spinning and to record SAXS patterns. For every measurement, 6 – 50

detector images with an acquisition time of 60 s were summed up and divided by the total acquisition time.

The wire-wire (*d*) distance was extracted from the position of the SAXS Bragg peaks corresponding to the relation of the peak position $q_{max}(h, k)$ in scattering patterns of 2D hexagonal lattices and the Miller indices *(h, k)*[52]

$$q_{\max}(h,k) = \frac{4\pi}{\sqrt{3}d}\sqrt{h^2 + k^2 + hk}\,. \qquad \text{(eq. 3.5.5.1)}$$

2D SAXS patterns were analyzed by means of eq. (3.5.3.2). The orientational distribution of anisotropic scatterers (Figure 3.5.3.4c) was reconstructed by fitting the integral in eq. (3.5.3.2). A Pseudo-Voigt function, which is a weighted sum of a Gaussian and Lorentzian distribution functions, was used to parametrize the orientational distribution $f(\vartheta)$. A Python script used the NumPy package and the lmfit library to find the optimal peak parameters to fit the integral in eq. (3.5.3.2).

The nematic order parameter *S*, defined by eq. (3.5.3.4) and represented in Figure 3.5.3.4d, was calculated from the orientational distribution of anisotropic scatterers $f(\vartheta)$ by performing the average

$$S = \int_0^{\frac{\pi}{2}} f(\vartheta)\,\frac{3\cos^2\vartheta - 1}{2}\sin\vartheta \mathrm{d}\vartheta, \qquad \text{(eq. 3.5.5.2)}$$

where the fitted distribution has been normalized,

$$\int_0^{\frac{\pi}{2}} f(\vartheta) sin\vartheta d\vartheta = 1. \qquad \text{(eq. 3.5.5.3)}$$

Scanning electron micrographs (except the cross-section micrographs) were recorded with a Quanta 400 ESEM (FEI, Germany) in secondary and backscattering mode. The cross-section of plasma treated AuNW-fibers in Figure 3.5.3.6, Figure S3.6.1.3 and Figure S3.6.1.4 were imaged using a Versa 3D DualBeam microscope (FEI, Oregon, USA) after cutting it open with a Focused $Ga^+$ Ion Beam (FIB). We protected one fiber (Figure S3.6.1.4) by a 100 nm platinum layer deposited from the gas phase. A second fiber was left untreated (Figure 3.5.3.6 and Figure S3.6.1.3). A trench was cut into the fibers by a $Ga^+$ ion beam operated at 30 kV with a current of 500 pA. The cut was then polished at 30 kV with a current of 100 pA. SEM images of the

cross-section of both the platinum protected and the unprotected fiber were taken at a tilt-angle of 52°.

AFM images were acquired in the tapping mode using a NanoWizard3 (JPK Instruments, Germany).

Tensile testing was performed with the setup depicted in Figure 3.5.3.5a. According to a standard preparation method[53] fibers were attached to paper frames with a 0.5 cm gauge length, which were then clamped inside of the testing setup, and aligned using a Hexapod H-206 precision alignment system (Physik instrumente, Germany). The paper frame was cut open and the fibers were pulled apart with a constant speed of 0.01 mm/s until fiber breakage while the force was measured using a 0.5 N load cell (ME Messsysteme, Germany) that was manually calibrated prior to use. All tests were performed at 20 °C. The elongation at break was calculated by dividing the length of the fiber in pulling direction when failure occured by the tested fiber length. The breaking stress was derived from the force measured before failure, divided by the fiber cross section area before the measurement. The Young's modulus was extracted from the slope of the linear section of the fiber's stress-strain curve.

### 3.5.6 Associated contents

The following videos are available free of charge on the ACS Publications website at DOI: 10.1021/acsnano.7b01551.

- Video 1: fast fiber spinning, 450 mmps, shown at 25% of its original speed (MPG)
- Video 2: fiber collection (MPG)
- Video 3: spinning at 9 mmps (MPG)
- Video 4: spinning process when injecting spherical nanoparticles into ethanol (MPG)

### 3.5.7 References

(1) Fratzl, P.; Weinkamer, R. Nature's Hierarchical Materials. Prog. Mater. Sci. 2007, 52, 1263–1334.

(2) Habibi, M. K.; Lu, Y. Crack Propagation in Bamboo's Hierarchical Cellular Structure. Sci. Rep. 2014, 4, 5598.

(3) Wegst, U. G. K.; Bai, H.; Saiz, E.; Tomsia, A. P.; Ritchie, R. O. Bioinspired Structural Materials. Nat. Mater. 2014, 14, 23–36.

(4) Bishop, K. J. M.; Wilmer, C. E.; Soh, S.; Grzybowski, B. A. Nanoscale Forces and Their Uses in Self-Assembly. Small 2009, 5, 1600–1630.

(5) Sanchez, C.; Belleville, P.; Popall, M.; Nicole, L. Applications of Advanced Hybrid Organic–inorganic Nanomaterials: From Laboratory to Market. Chem. Soc. Rev. 2011, 40, 696–753.

(6) Gorbatikh, L.; Wardle, B. L.; Lomov, S. V. Hierarchical Lightweight Composite Materials for Structural Applications. MRS Bull. 2016, 41, 672–677.

(7) Mallick, P. K. Fiber-Reinforced Composites: Materials, Manufacturing, and Design; 3rd ed.; CRC Press, 2007.

(8) Cheng, J.; Lee, S.-H. Development of New Smart Materials and Spinning Systems Inspired by Natural Silks and Their Applications. Front. Mater. 2016, 2, 1–16.

(9) Meijer, H. E. H.; Govaert, L. E. Mechanical Performance of Polymer Systems: The Relation between Structure and Properties. Prog. Polym. Sci. 2005, 30, 915–938.

(10) Cademartiri, L.; Bishop, K. J. M. Programmable Self-Assembly. Nat. Mater. 2015, 14, 2–9.

(11) Vogel, N.; Retsch, M.; Fustin, C.-A.; Del Campo, A.; Jonas, U. Advances in Colloidal Assembly: The Design of Structure and Hierarchy in Two and Three Dimensions. Chem. Rev. 2015, 115, 6265–6311.

(12) Cademartiri, L.; Bishop, K. J. M.; Snyder, P. W.; Ozin, G. A. Using Shape for Self-Assembly. Philos. Trans. A. Math. Phys. Eng. Sci. 2012, 370, 2824–2847.

(13) Capaccio, G.; Ward, I. M. Preparation of Ultra-High Modulus Linear Polyethylenes; Effect of Molecular Weight and Molecular Weight Distribution on Drawing Behaviour and Mechanical Properties. Polymer (Guildf). 1974, 15, 233–238.

(14) Reiser, B.; Gerstner, D.; González-García, L.; Maurer, J. H. M.; Kanelidis, I.; Kraus, T. Multivalent Bonds in Self-Assembled Bundles of Ultrathin Gold Nanowires. Phys. Chem. Chem. Phys. 2016, 18, 27165–27169.

(15) Yuan, B.; Cademartiri, L. Flexible One-Dimensional Nanostructures: A Review. J. Mater. Sci. Technol. 2015, 31, 607–615.

(16) Pazos-Pérez, N.; Baranov, D.; Irsen, S.; Hilgendorff, M.; Liz-Marzán, L. M.; Giersig, M. Synthesis of Flexible, Ultrathin Gold Nanowires in Organic Media. Langmuir 2008, 24, 9855–9860.

(17) Cademartiri, L.; Ozin, G. A. Ultrathin Nanowires-A Materials Chemistry Perspective. Adv. Mater. 2009, 21, 1013–1020.

(18) Xu, J.; Wang, H.; Liu, C.; Yang, Y.; Chen, T.; Wang, Y.; Wang, F.; Liu, X.; Xing, B.; Chen, H. Mechanical Nanosprings: Induced Coiling and Uncoiling of Ultrathin Au Nanowires. J. Am. Chem. Soc. 2010, 132, 11920–11922.

(19) Feng, H.; Yang, Y.; You, Y.; Li, G.; Guo, J.; Yu, T.; Shen, Z.; Wu, T.; Xing, B. Simple and Rapid Synthesis of Ultrathin Gold Nanowires, Their Self-Assembly and Application in Surface-Enhanced Raman Scattering. Chem. Commun. (Camb). 2009, 1984–1986.

(20) Kisner, A.; Heggen, M.; Mayer, D.; Simon, U.; Offenhäusser, A.; Mourzina, Y. Probing the Effect of Surface Chemistry on the Electrical Properties of Ultrathin Gold Nanowire Sensors. Nanoscale 2014, 6, 5146–5155.

(21) Muratova, I. S.; Mikhelson, K. N.; Ermolenko, Y. E.; Offenhäusser, A.; Mourzina, Y. Chemiresistors Based on Ultrathin Gold Nanowires for Sensing Halides, Pyridine and Dopamine. Sensors Actuators B Chem. 2016, 232, 420–427.

(22) Leelavathi, A.; Madras, G.; Ravishankar, N. Ultrathin Au Nanowires Supported on rGO/TiO2 as an Efficient Photoelectrocatalyst. J. Mater. Chem. A 2015, 3, 17459–17468.

(23) Maurer, J. H. M.; González-García, L.; Reiser, B.; Kanelidis, I.; Kraus, T. Templated Self-Assembly of Ultrathin Gold Nanowires by Nanoimprinting for Transparent Flexible Electronics. Nano Lett. 2016, 16, 2921–2925.

(24) Gong, S.; Zhao, Y.; Yap, L. W.; Shi, Q.; Wang, Y.; Bay, J. A. P. B.; Lai, D. T. H.; Uddin, H.; Cheng, W. Fabrication of Highly Transparent and Flexible NanoMesh Electrode via Self-Assembly of Ultrathin Gold Nanowires. Adv. Electron. Mater. 2016, 2, 1600121.

(25) Loubat, A.; Impéror-Clerc, M.; Pansu, B.; Meneau, F.; Raquet, B.; Viau, G.; Lacroix, L.-M. Growth and Self-Assembly of Ultrathin Au Nanowires into Expanded Hexagonal Superlattice Studied by in Situ SAXS. Langmuir 2014, 30, 4005–4012.

(26) Wang, M. C. P.; Gates, B. D. Directed Assembly of Nanowires. Mater. Today 2009, 12, 34–43.

(27) Roy, A.; Pandey, T.; Ravishankar, N.; Singh, A. K. Single Crystalline Ultrathin Gold Nanowires: Promising Nanoscale Interconnects. AIP Adv. 2013, 3, 032131.

(28) Cademartiri, L.; Scotognella, F.; Brien, P. G. O.; Lotsch, B. V; Thomson, J.; Petrov, S.; Kherani, N. P.; Ozin, G. A. Cross-Linking Bi2S3 Ultrathin Nanowires: A Platform for Nanostructure Formation and Biomolecule Detection. Nano Lett. 2009, 9, 1482–1486.

(29) Foroughi, J.; Spinks, G. M.; Wallace, G. G. Conducting Polymer Fibers. In Handbook of Smart Textiles; Tao, X., Ed.; Springer, 2015; pp. 31–62.

(30) Wang, C.; Hu, Y.; Lieber, C. M.; Sun, S. Ultrathin Au Nanowires and Their Transport Properties. J. Am. Chem. Soc. 2008, 130, 8902–8903.

(31) Moutet, P.; Lacroix, L.-M.; Robert, A.; Impéror-Clerc, M.; Viau, G.; Ressier, L. Directed Assembly of Single Colloidal Gold Nanowires by AFM Nanoxerography. Langmuir 2015, 31, 4106–4112.

(32) Born, P.; Kraus, T. Ligand-Dominated Temperature Dependence of Agglomeration Kinetics and Morphology in Alkyl-Thiol-Coated Gold Nanoparticles. Phys. Rev. E 2013, 87, 062313.

(33) Haynl, C.; Hofmann, E.; Pawar, K.; Förster, S.; Scheibel, T. Microfluidics-Produced Collagen Fibers Show Extraordinary Mechanical Properties. Nano Lett. 2016, 16, 5917–5922.

(34) Cademartiri, L.; Ghadimi, A.; Ozin, G. A. Nanocrystal Plasma Polymerization: From Colloidal Nanocrystals to Inorganic Architectures. Acc. Chem. Res. 2008, 41, 1820–1830.

(35) Maurer, J. H. M.; González-García, L.; Reiser, B.; Kanelidis, I.; Kraus, T. Sintering of Ultrathin Gold Nanowires for Transparent Electronics. ACS Appl. Mater. Interfaces 2015, 7, 7838–7842.

(36) Sekar, S.; Lemaire, V.; Hu, H.; Decher, G.; Pauly, M. Anisotropic Optical and Conductive Properties of Oriented 1D-Nanoparticle Thin Films Made by Spray-Assisted Self-Assembly. Faraday Discuss. 2016, 191, 373–389.

(37) Trebbin, M.; Steinhauser, D.; Perlich, J.; Buffet, A.; Roth, S. V; Zimmermann, W. Anisotropic Particles Align Perpendicular to the Flow Direction in Narrow Microchannels. Proc. Natl. Acad. Sci. 2013, 110, 6706–6711.

(38) Butler, P. Shear Induced Structures and Transformations in Complex Fluids. Curr. Opin. Colloid Interface Sci. 1999, 4, 214–221.

(39) Oldenbourg, R.; Wen, X.; Meyer, R. B.; Caspar, D. L. D. Orientational Distribution Function in Nematic Tobacco-Mosaic-Virus Liquid Crystals Measured by X-Ray Diffraction. Phys. Rev. Lett. 1988, 61, 1851–1855.

(40) de Gennes, P. G. The Physics of Liquid Crystals; Oxford University Press, Inc., 1974.

(41) Smith, P.; Lemstra, P. J.; Pijpers, J. P. L. Tensile Strength of Highly Oriented Polyethylene. II. Effect of Molecular Weight Distribution. J. Polym. Sci. Polym. Phys. Ed. 1982, 20, 2229–2241.

(42) Foroughi, J.; Spinks, G. M.; Wallace, G. G. Effect of Synthesis Conditions on the Properties of Wet Spun Polypyrrole Fibres. Synth. Met. 2009, 159, 1837–1843.

(43) Song, Z.; Hou, X.; Zhang, L.; Wu, S. Enhancing Crystallinity and Orientation by Hot-Stretching to Improve the Mechanical Properties of Electrospun Partially Aligned Polyacrylonitrile (PAN) Nanocomposites. 2011, 4, 621–632.

(44) Lovinger, A. J.; Williams, M. L. Tensile Properties and Morphology of Blends of Polyethylene and Polypropylene. J. Appl. Polym. Sci. 1980, 25, 1703–1713.

(45) Lovinger, A. J.; Williams, M. L.; Telephone, B. Polyethylene and Polypropylene. 1980, 25, 1703–1713.

(46) Chung, J. Y.; Lee, J.; Beers, K. L.; Stafford, C. M. Stiffness, Strength, and Ductility of Nanoscale Thin Films and Membranes: A Combined Wrinkling–Cracking Methodology. Nano Lett. 2011, 11, 3361–3365.

(47) CRC Handbook of Chemistry and Physics; Lide, D. R., Ed.; 84th ed.; CRC Press. Boca Raton, Florida, 2003.

(48) Wu, B.; Heidelberg, A.; Boland, J. J. Mechanical Properties of Ultrahigh-Strength Gold Nanowires. Nat. Mater. 2005, 4, 525–529.

(49) Wang, Y.; Kanjanaboos, P.; Barry, E.; Mcbride, S.; Lin, X.-M.; Jaeger, H. M. Fracture and Failure of Nanoparticle Monolayers and Multilayers. Nano Lett. 2014, 14, 826–830.

(50) Seyedin, M. Z.; Razal, J. M.; Innis, P. C.; Wallace, G. G. Strain-Responsive Polyurethane/PEDOT:PSS Elastomeric Composite Fibers with High Electrical Conductivity. Adv. Funct. Mater. 2014, 24, 2957–2966.

(51) Wu, B.-H.; Yang, H.-Y.; Huang, H.-Q.; Chen, G.-X.; Zheng, N.-F. Solvent Effect on the Synthesis of Monodisperse Amine-Capped Au Nanoparticles. Chinese Chem. Lett. 2013, 24, 457–462.

(52) Förster, S.; Timmann, A.; Konrad, M.; Schellbach, C.; Meyer, A.; Funari, S. S.; Mulvaney, P.; Knott, R. Scattering Curves of Ordered Mesoscopic Materials. J. Phys. Chem. B 2005, 109, 1347–1360.

(53) ASTM D3379-75, Standard Test Method for Tensile Strength and Young's Modulus for High-Modulus Single-Filament Materials (Withdrawn 1996), ASTM International, West Conshohocken, PA, 1975.

## 3.6 Supporting Information: Spinning hierarchical gold nanowire microfibers by shear alignment and intermolecular self-assembly

### 3.6.1 Supplementary figures

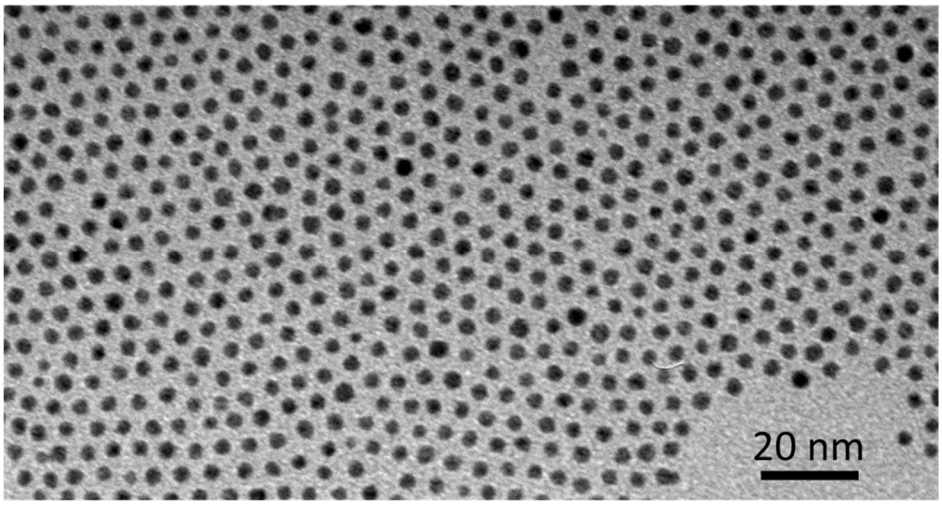


**Figure S3.6.1.1** Transmission electron micrograph of oleylamine-capped gold nanospheres (AuNS@OAm).

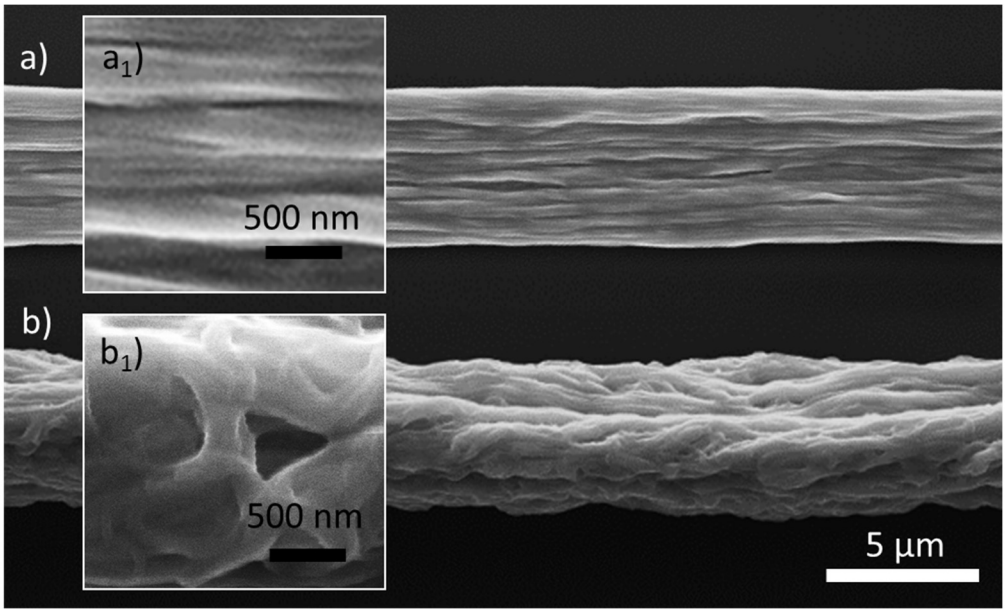


**Figure S3.6.1.2** Scanning electron micrographs of AuNW fibers spun at flow speeds of a) 4 µL/s and b) 2 µL/s.

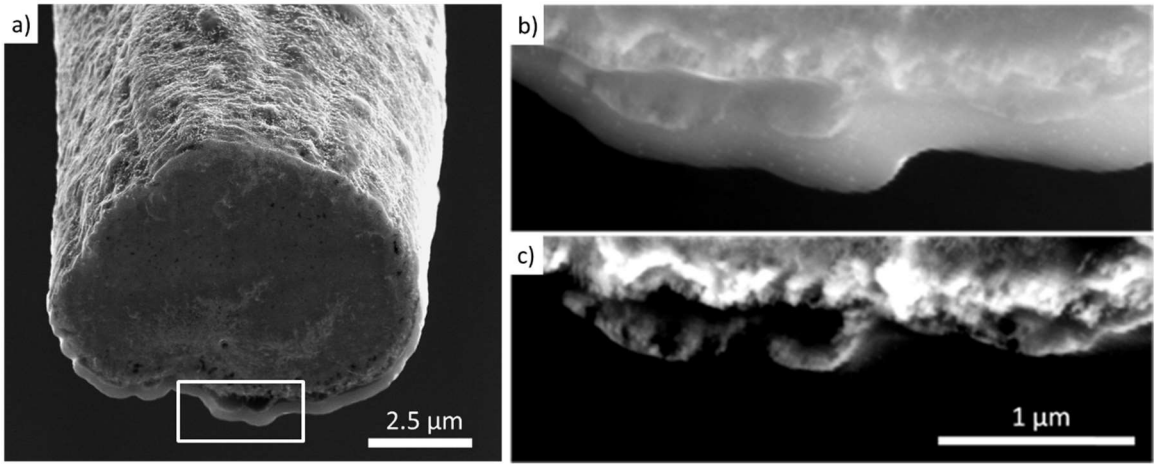


**Figure S3.6.1.3** a) Scanning electron micrographs of a fiber cross-section after 25 min of $Ar/H_2$ plasma treatment. a) Overview image taken at 52° tilt. Detail images taken at 32° tilt: b) secondary electron detector image and c) backscattering detector image.

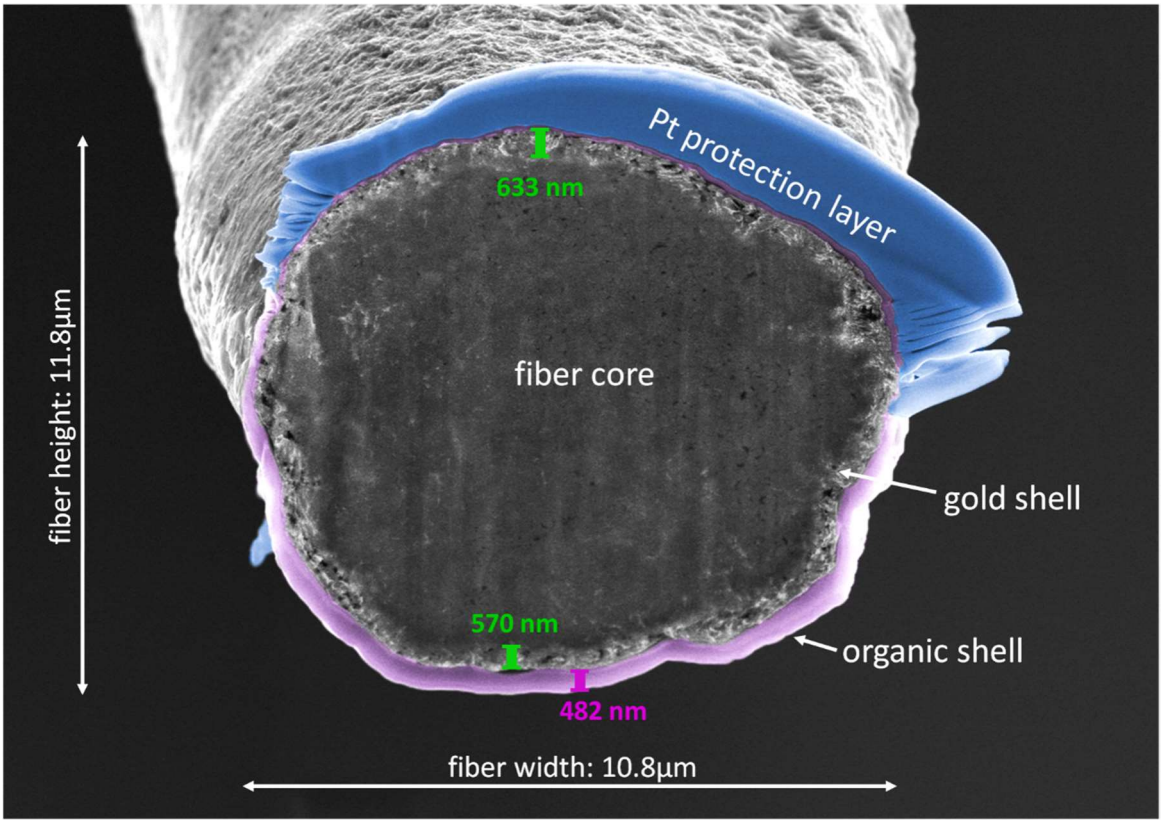


**Figure S3.6.1.4** False-color scanning electron micrograph of a cross-section obtained by Focused Ion Beam (FIB) milling of a gold nanowire-fiber after 25 min $Ar/H_2$ plasma treatment. Size measurements in the image are corrected for the tilting angle (52°).

# 4 Contribution to the state of the art

This thesis demonstrates the bottom-up fabrication of hybrid nanomaterials by colloidal self-assembly and shows possible ways for the technical implementation of the method. For that purpose, dispersions of gold nano-objects with organic shells – the hybrid inks – were used to achieve solution-based material fabrication. Two chosen cases were implemented: sinter-free conductive hybrid inks for the deposition of conductive paths and fibers spun from hybrid nanowire inks, analogous to solution-spun polymers.

In this thesis, the hybrid approach was beneficial because it allowed tailoring of the material properties in two ways, namely

a) by determining the superstructure formed by processing the ink, because the ligands form the interface between the nano-object and the dispersant medium and therefore can determine colloidal interactions and
b) by forming the (soft) interface between the nano-objects in the dry hybrid material.

Therefore it was possible to make hybrid materials with very different properties from the same inorganic core material simply by adapting the ligand shell. To exploit this approach,

I. colloidal stabilization and controlled destabilization as a result of the ligand/solvent interaction was studied and controlled;
II. material fabrication from inks was achieved based on these studies, and
III. the influence of the ligand shell on material properties was investigated and tailored.

The contribution of this work to each of these three aspects is explained in detail in the following:

I. With the hybrid approach chosen in this thesis, colloidal stabilization and destabilization can be controlled by the ligand/solvent interaction. This offers two different possibilities to tune colloidal stability, adapting the ligand shell to a certain solvent, and adapting the solvent to a given ligand. Both approaches have been successfully employed in this work.

   The first option was exploited by systematic ligand exchange to attach the optimal ligand to colloidal gold nanorods to create water-based, sinter-free conductive inks. Their synthesis via a well-established protocol providing good control over size and shape dispersity uses a ligand which is unsuitable for the desired

application. However, a subsequent ligand exchange step enabled adjustment of colloidal stability, ligand binding strength and the electrical conductivity of the final material. These properties needed to be improved to create an ink for printing conductive lines and structures that – unlike current state-of-the-art systems – does not require any sintering step. A conjugated polythiophene-derivative with a sulfonate group in its side chain was identified as a suitable ligand, which was confirmed by a series of experiments. The experiments proved the ligand's excellent resistance to detachment due to its multidentate binding motif, while the sulfonate group in the side chain provided very good colloidal stability in polar solvents and solvent mixtures. Colloidal stabilization was good enough to stabilize high mass fractions of colloids in water – with or without the addition of non-aqueous co-solvents – and rheology-modifying additives.

The second option to tune the dispersion characteristics, adapting the solvent, was exploited to optimize the bundling behavior of oleylamine (OAm) capped ultrathin gold nanowires (AuNWs). These hybrid nano-objects are characterized by a very high aspect ratio (>1000) and a very high organic volume fraction of approximately 80%. Their unique shape resembles that of linear polymers, and their thick organic shell dominates their assembly behavior. Such ultrathin wires combine strong curvature, leaving room for solvent interpenetration and solvent interaction, with an enhanced contact area on their surface. Enhanced contact area increases the interaction strength along the contact lines between wires interacting in parallel, comparable to a multidentate binding motif. This explains the wires' strong intrinsic tendency to form wire bundles.

It has been one of the aims of this thesis to test how far their behavior can be explained using concepts known from supramolecular chemistry. This has been achieved by investigating their solvent-dependent assembly behavior. As shown, weak intermolecular interactions between ligand and solvent molecules could explain the solvent-dependent bundling behavior and kinetics, which is a strong hint to support the hypothesis that AuNWs behave similar to supramolecular objects. In fact, the observed effect was so strong that supramolecular assemblies were also predicted to influence wire formation. This assumption was confirmed by the occurrence of more shape impurities formed when employing less suitable solvents for wire growth. In summary, I presented the first report on the solvent-dependent assembly behavior of

AuNWs and proposed the concept of supramolecular multivalency to understand the colloidal interactions between nanowires.

II. The insights mentioned in the above paragraph were then used to perform material fabrication from inks. It was the aim to achieve good colloidal stability for the ink during processing. The assembly of the colloids in the ink into the hybrid materials should only either start upon solvent evaporation or upon a designed trigger.

The good colloidal stabilization of the gold nanorods provided by the conjugated polythiophene shell enabled the formulation of processable inkjet inks. According to predictions of jettability based on the *Ohnesorge* number, an ink composition embodiment with adjusted fluid properties was identified as jettable with commercial printing heads. Further on single nano-objects were small enough and well-stabilized enough to avoid agglomeration during printing so that nozzle clogging would not be expected. These criteria could pave the way to producing electrical circuits and other functional structures via well-established inkjet printing.

On the other hand, AuNWs and their supramolecular, solvent-dependent assembly characteristic were used to demonstrate the feasibility of using a colloidal ink for material production by a method that has not yet been used for colloids but exploits their polymer-like behavior: solution spinning. The method exploits the wires' controlled precipitation by rapidly changing the solvent quality for the wires. While wires are readily dispersible in cyclohexane, they tend to form bundles slowly, for instance in *n*-hexane. Rapid bundling is achieved by using ethanol as a solvent or adding an excess of ethanol to a dispersion of wires in cyclohexane or *n*-hexane. Exploiting this behavior, wires dispersed in cyclohexane were injected into an ethanol bath through a 75 µm (inner diameter) nozzle. Hexagonal bundles were formed very quickly, which even allowed the fixation of a previously induced orientation of the ultrathin gold nanowires. This phenomenon could be used for the controlled formation of directional colloidal superstructures. Using a setup inspired by polymer spinning, fibers could be spun at high speeds that were limited only by the technical restrictions of the apparatus built in-house. This resulted in the first hybrid fibers spun from colloidal nano-objects using a setup that mimics an industrial process.

III. In both, the hybrid inkjet ink and the spun hybrid fibers, it was further shown that the organic shell significantly influences the properties of the dry material.

Drying a dispersion of gold nanorods with their organic conjugated polymer, which binds directly to the nanorod with its conjugated polymer backbone – the hybrid ink – led directly to conductive structures, whereas an ink of the same particle core with a shell of a non-conjugated polymer yielded insulating structures. The insulating structures only became conductive after a 30 min $H_2$/Ar plasma treatment, which removed the organic shell. Hence, the polythiophene-AuNR hybrid ink developed in this thesis overcomes the trade-off between colloidal stability and sintering effort because it is stable and requires no sintering. It is the first contribution to use a conjugated polymer/metal nano-object hybrid concept to formulate inkjet printable inks with long-term stability that achieve good conductivities directly after drying.

While the ligand provides an electrical connection in the dry, sinter-free ink, the ligand of the AuNWs provides mechanical interdigitation, which lends the fibers structural integrity. This integrity was also shown to depend on the spinning process parameters. Only above a minimum shear rate in the injection nozzle were continuous fibers obtained. Tensile tests in fiber direction revealed two main findings: first, with increasing wire-ink shear rate during spinning (which increases the degree of wire monomer alignment) fibers resist higher stresses but failure occurs at lower strains. Second, their Young's modulus resembles that of organic materials rather than metals, indicating that the elastic behavior of oleylamine-gold hybrid fibers is dominated by their soft ligand shell. It is the first contribution to describe process-structure-property relations of hybrid materials obtained by colloidal self-assembly and demonstrates the importance of the ligand shell for the mechanical properties of this kind of hybrid materials.

# 5 Conclusion

This thesis deals with several implications of the surface chemistry of colloids in the bottom-up fabrication of mechanically connected and electrically conductive hybrid materials by wet-processing techniques. It shows that, starting from the wet-chemical synthesis of the colloids, the ligands and their interaction with the dispersant medium play an important role. A primary insight is that careful tailoring of the ligand/solvent interface can lead to a high degree of control over colloidal interactions. Hence, for the rational design of the interface, both ligand and solvent are important. This has been shown by two applications implemented for colloidal inks: water-based sinter-free conductive inks and hierarchical fibers spun analogous to solution-spun polymers. In the first case, the ligand was tailored for the solvent composition of choice, and in the second case the solvent was adjusted to control stabilization and destabilization of AuNWs capped by oleylamine.

Inkjet printing is well-established for color inks but is gaining importance in the additive manufacturing of electronic components. Here the trade-off between colloidal stability and ease of forming electrically conductive contacts using metal nano-object inks was addressed by adapting the ligand shell for low-toxicity water-based formulations.

A ligand shell that enables the formation of electrically conductive contacts directly after solvent evaporation eliminated the need for any sintering effort. It is thus an example for the effectiveness of careful design of the ligand/solvent interaction for simple processing of colloidal nano-objects. At the same time, this example showed that the importance of the ligand shell goes beyond processability and has a major impact on material properties.

Gold nanowires assembled into defined fibrous superstructures when exchanging the solvent. External shear stress caused nanowire alignment. A combination of both structure-directing effects was achieved by rapidly injecting a dispersion of nanowires in cyclohexane into ethanol. The dispersed wires aligned in the injection nozzle and were then rapidly precipitated by the ethanol. Based on the understanding of the interaction between ligand and solvent, complex functional hybrid structures were achieved with the simplicity of wet-processing approaches known from commercial polymer spinning. This presents an important step towards the technical implementation of colloidal self-assembly processes.

In both material embodiments obtained by processing colloidal inks, a careful study of the ligand/solvent interaction for a specific application, and improvements made thereupon constituted major improvements to the state of the art.

In both exemplary hybrid materials that were obtained by processing colloidal inks a careful study of the ligand-solvent interplay towards a specific application were demonstrated to constitute major improvements to the state of the art.

# 6 Outlook

It would be highly desirable to adapt the concepts developed in this thesis to other systems and applications. The rod shape and unique optical properties of gold nanorods could be used to deposit aligned rods to minimize particle/particle interfaces while monitoring alignment with an optical on-line analysis setup. Furthermore, the chemical inertness of gold makes the hybrid ink a promising candidate for the circuitry of medical sensing devices that can be applied *in vivo*. It would also be worthwhile to test the applicability of the hybrid concept to other conducting or semi-conducting cores. The concept could, for instance, help to improve the performance of all solution-deposited devices that rely on charge injection- and/or charge extraction-like field effect transistors, photodetectors or solar cells.

Similarly, it would be interesting to try to spin fibers from ultrathin wires of other cores like semiconductors to explore their applicability as sensor elements because of the large surface area accessible on such fibers. From a more fundamental standpoint, it would also be worthwhile to investigate the influence of other ligands on the spinnability and/or the use of ligands that are susceptible to other assembly triggers. One possibility would be the introduction of azobenzene moieties that switch their conformation with the wavelength of light with which they are illuminated. Furthermore, it would be interesting to study the dependence of fiber tensile strength on the type of ligand which mechanically connects the fiber.

More generally speaking, further studies towards understanding ligand shells at a molecular level and predicting colloidal behavior thereupon are highly recommended. These could make simple colloidal self-assembly methods a viable pathway towards a huge variety of hybrid materials with minimal process development effort.

# 7 Appendix

## 7.1 Abbreviations and symbols

| | |
|---|---|
| 2D | 2-dimensional |
| 3D | 3-dimensional |
| *A* | Hamaker constant |
| *a* | Characteristic length |
| AFM | Atomic force microscopy |
| ATR | Attenuated total reflectance |
| AuNR(s) | Gold nanorod(s) |
| AuNR@CTAB | Gold nanorods capped by Cetyltrimethylammonium-bromide (the @ connection is also used for other nano-object/ligand combinations) |
| AuNS | Gold nanospheres |
| AuNW(s) | Ultrathin gold nanowire(s) |
| CNT(s) | Carbon nanotube(s) |
| CTAB | Cetyltrimethylammonium-Bromide |
| *D* | Diameter |
| *d* | Distance |
| DLVO | Derjaguin Landau Verwey Overbeek |
| EDTA | Ethylenediaminetetraacetic acid |
| eq. | Equation |
| *F* | Force |
| $f(\vartheta)$ | Orientational distribution function |
| FIB | Focused ion beam |
| FTIR | Fourier transform infrared |
| $\Gamma$ | Ligand surface grafting density |
| $\gamma$ | Surface tension |
| $G_f$ | Geometrical factor |
| $\eta$ | Viscosity |
| *h, k* | Miller indices |
| HSAB | Hard Soft Acid Base |

| | |
|---|---|
| ICP-MS | Inductively coupled plasma mass spectrometry |
| LED(s) | Light-emitting diode(s) |
| L-LSPR | Longitudinal localized surface plasmon resonance |
| MD | Molecular dynamics |
| OAc | Oleic acid |
| OAm | Oleylamine |
| *Oh* | Ohnesorge number |
| P3HT | Poly-(3-hexylthiophene) |
| PDMS | Polydimethylsiloxane |
| PEDOT:PSS | Poly(3,4-ethylenedioxythiophene) Polystyrene Sulfonate |
| PEG-SH | Thiolated polyethylene glycol / O-[2-(3-mercaptopropionylamino)ethyl]-O'-methylpolyethylene glycol |
| PTEBS | Poly[2-(3-thienyl)-ethyloxy-4-butylsulfonate)] |
| *q* | Scattering vector |
| $\rho$ | Density |
| RFID | Radio frequency identification |
| RI | Refractive index |
| *S* | Nematic order parameter |
| SAM(s) | Self-assembled monolayer(s) |
| SAXS | Small angle X-ray scattering |
| SEM | Scanning electron microscopy |
| SERS | Surface enhanced raman scattering |
| SPR | Surface plasmon resonance |
| TEM | Transmission electron microscopy |
| TGA | Thermogravimetric analysis |
| T-LSPR | Transversal localized surface plasmon resonance |
| UV-vis | Ultraviolet-visible |
| v.d.W. | Van der Waals |

## 7.2 Scientific contributions

### 7.2.1 Peer-reviewed publications

(8) **Spinning Hierarchical Gold Nanowire Microfibers by Shear Alignment and Intermolecular Self-Assembly**
B. Reiser, D. Gerstner, L. González-García, J. H. M. Maurer, I. Kanelidis, and T. Kraus
*ACS Nano*, **2017**, 11, 4934-4942

(7) **Direct nanoimprinting of a colloidal self-organizing nanowire ink for flexible, transparent electronics**
J. H. M. Maurer, L. González-García, I. K. Backes, B. Reiser, S. M. Schlossberg, and T. Kraus
*Adv. Mater. Technol.*, **2017**, 1700034

(6) **Multivalent bonds in self-assembled bundles of ultrathin gold nanowires**
B. Reiser, D. Gerstner, L. Gonzalez-Garcia, J. H. M. Maurer, I. Kanelidis, and T. Kraus
*Phys. Chem. Chem. Phys*., **2016**, 18, 27165-27169

(5) **Ultrathin gold nanowires for transparent electronics: Soft sintering and temperature stability**
J. H. M. Maurer, L. González-García, B. Reiser, I. Kanelidis, and T. Kraus
*Phys. Status Solidi A*, **2016**, 213, 2336–2340

(4) **Templated Self-Assembly of Ultrathin Gold Nanowires by Nanoimprinting for Transparent Flexible Electronics**
J. H. M. Maurer, L. González-García, B. Reiser, I. Kanelidis, and T. Kraus
*Nano Lett.*, **2016,** 16, 2921-2925

(3) **Gold nanorods with conjugated polymer ligands: sintering-free conductive inks for printed electronics**
B. Reiser, L. Gonzalez-Garcia, I. Kanelidis, J. H.M. Maurer, and T. Kraus
*RSC Chem. Sci*., **2016**, 7, 4190-4196

(2) **Ultrathin gold nanowires for transparent electronics: breaking barriers**
L. González-García, J. H. M. Maurer, B. Reiser, I. Kanelidis and T. Kraus
*Procedia Eng.* **2016**, 141, 152–156

(1) **Sintering of ultrathin gold nanowires for transparent electronics**
J. H. M. Maurer, L. González-García, B. Reiser, I. Kanelidis and T. Kraus
*ACS Appl. Mater. Inter.,* **2015**, 7, 7838-7842

### 7.2.2 Patent applications

(2) **Conductive nanocomposites**

Inventors: B. Reiser, T. Kraus, L. González-García, J. H. M. Maurer and I. Kanelidis;
Original Assignee: Leibniz-Institut Für Neue Materialien Gemeinnützige Gmbh;
File reference: WO2017045989A1;
Priority date: 2015-09-15

(1) **Method for producing structured surfaces**

Inventors: J. H. M. Maurer, T. Kraus, L. González-García, B. Reiser, I. Kanelidis, P. W. De Oliveira, J. Kampka, K. Moh;
Original Assignee: Leibniz-Institut Für Neue Materialien Gemeinnützige Gmbh;
File reference: WO2017042094A1;
Priority date: 2015-09-07

### 7.2.3 Non-peer-reviewed publication

(1) **Anisotropic nanoparticles: general discussion**
A. Castelli *et al.*,
*Faraday Discuss.,* **2016**, 191, 229-254

### 7.2.4 Conference presentations

**11.2017** **Particle-Based Materials Symposium, Saarbrücken, Germany**

Poster presentation: "Industrial polymer processing inspired gold nanowire microfiber spinning"

2nd Poster presentation price awarded

**04.2017** **13th Zsigmondy Kolloquium, Saarbrücken, Germany**

Oral presentation: "Spinning of hierarchical hybrid fibers: controlled colloidal assembly"

**03.2017** **5th Multifunctional, Hybrid and Nanomaterials Conference, Lisbon, Portugal**

Oral presentation: "Nanoparticle-polymer hybrid inks for printed electronics"

**09.2016** **30th Conference of the European Colloids and Interface Society, Rome, Italy**

Oral presentation: "Colloidally stable inks of nanoparticle-polymer hybrids for printed electronics"

Poster presentation: "Ligand-solvent interaction driven self-assembly of ultrathin gold nanowires"

**07.2016** **Faraday Discussions on Nanoparticles with Morphological and Functional Anisotropy, Glasgow, UK**

Poster presentation: "Multivalent bonds in self-assembled bundles of ultrathin gold nanowires"

**12.2015** **4th Nano Today Conference, Dubai, UAE**

Oral presentation: "Self-assembly of ultrathin gold nanowires: ligand-solvent interplay"

Poster presentation: "Sintering-free metal colloid inks for printed electronics", supported by Elsevier "student travel award"

**09.2015** **Fall Meeting of the European Materials Research Society, Warsaw, Poland**

Oral presentation: "Bundling and alignment of ultrathin gold nanowires for the production of transparent electronics"

**03.2015** **17th JCF-Frühjahrssymposium, Münster, Germany**

Poster presentation: "Ligand effects on the structure and performance of metal-polymer nanocomposites for transparent electronics"